



# The evolution of Devonian hydrocarbon gases in shallow aquifers of the northern Appalachian Basin: Insights from integrating noble gas and hydrocarbon geochemistry

Thomas H. Darrah<sup>a,\*</sup>, Robert B. Jackson<sup>b,1</sup>, Avner Vengosh<sup>c,2</sup>,  
Nathaniel R. Warner<sup>d,3</sup>, Colin J. Whyte<sup>a,4</sup>, Talor B. Walsh<sup>e,f,5,6</sup>,  
Andrew J. Kondash<sup>c</sup>, Robert J. Poreda<sup>e,7</sup>

<sup>a</sup> Divisions of Solid Earth Dynamics and Water, Climate and the Environment, School of Earth Sciences, The Ohio State University, Columbus, OH 43210, USA

<sup>b</sup> School of Earth, Energy, and Environmental Sciences, Woods Institute for the Environment, and Precourt Institute for Energy, Stanford University, Stanford, CA 94305, USA

<sup>c</sup> Division of Earth and Ocean Sciences, Nicholas School of the Environment, Duke University, Durham, NC 27708, USA

<sup>d</sup> Department of Civil and Environmental Engineering, Pennsylvania State University, University Park, PA 16802, USA

<sup>e</sup> Department of Earth and Environmental Sciences, University of Rochester, Rochester, NY 14627, USA

<sup>f</sup> Department of Earth Sciences, Millersville, PA 17551, USA

Received 22 January 2013; accepted in revised form 14 September 2015; Available online 21 September 2015

## Abstract

The last decade has seen a dramatic increase in domestic energy production from unconventional reservoirs. This energy boom has generated marked economic benefits, but simultaneously evoked significant concerns regarding the potential for drinking-water contamination in shallow aquifers. Presently, efforts to evaluate the environmental impacts of shale gas development in the northern Appalachian Basin (NAB), located in the northeastern US, are limited by: (1) a lack of comprehensive “pre-drill” data for groundwater composition (water and gas); (2) uncertainty in the hydrogeological factors that control the occurrence of naturally present CH<sub>4</sub> and brines in shallow Upper Devonian (UD) aquifers; and (3) limited geochemical techniques to quantify the sources and migration of crustal fluids (specifically methane) at various time scales. To address these questions, we analyzed the noble gas, dissolved ion, and hydrocarbon gas geochemistry of 72 drinking-water wells and one natural methane seep all located  $\gg 1$  km from shale gas drill sites in the NAB. In the present study, we consciously avoided groundwater wells from areas near active or recent drilling to ensure shale gas development would not bias the results. We also intentionally targeted areas with naturally occurring CH<sub>4</sub> to characterize the geochemical signature and geological context of gas-phase hydrocarbons in shallow aquifers of the NAB. Our data display a positive relationship between elevated

\* Corresponding author. Tel.: +1 (614) 688 2132; fax: +1 (614) 292 7688.

E-mail addresses: [darrah.24@osu.edu](mailto:darrah.24@osu.edu) (T.H. Darrah), [rob.jackson@stanford.edu](mailto:rob.jackson@stanford.edu) (R.B. Jackson), [vengosh@duke.edu](mailto:vengosh@duke.edu) (A. Vengosh), [nrw6@psu.edu](mailto:nrw6@psu.edu) (N.R. Warner), [whyte.25@osu.edu](mailto:whyte.25@osu.edu) (C.J. Whyte), [talor.walsh@millersville.edu](mailto:talor.walsh@millersville.edu) (T.B. Walsh), [robert.poreda@rochester.edu](mailto:robert.poreda@rochester.edu) (R.J. Poreda).

<sup>1</sup> Tel.: +1 (919) 660 7408; fax: +1 (919) 684 5833.

<sup>2</sup> Tel.: +1 (919) 681 8050; fax: +1 (919) 684 5833.

<sup>3</sup> Tel.: +1 (814) 865 9423; fax: +1 (814) 863 7304.

<sup>4</sup> Tel.: +1 (614) 688 2132; fax: +1 (614) 292 7688.

<sup>5</sup> Present address.

<sup>6</sup> Tel.: +1 (843) 324 8829; fax: +1 (585) 244 5689.

<sup>7</sup> Tel.: +1 (585) 275 0051; fax: +1 (585) 244 5689.

[CH<sub>4</sub>], [C<sub>2</sub>H<sub>6</sub>], [Cl], and [Ba] that co-occur with high [<sup>4</sup>He]. Although four groundwater samples show mantle contributions ranging from 1.2% to 11.6%, the majority of samples have [He] ranging from solubility levels ( $\sim 45 \times 10^{-6} \text{ cm}^3 \text{ STP/L}$ ) with below-detectable [CH<sub>4</sub>] and minor amounts of tritiogenic <sup>3</sup>He in low [Cl] and [Ba] waters, up to high [<sup>4</sup>He] = 0.4 cm<sup>3</sup> STP/L with a purely crustal helium isotopic end-member (<sup>3</sup>He/<sup>4</sup>He =  $\sim 0.02$  times the atmospheric ratio (*R/R<sub>a</sub>*)) in samples with CH<sub>4</sub> near saturation for shallow groundwater (P(CH<sub>4</sub>) =  $\sim 1$  atmosphere) and elevated [Cl] and [Ba]. These data suggest that <sup>4</sup>He is dominated by an exogenous (i.e., migrated) crustal source for these hydrocarbon gas- and salt-rich fluids. In combination with published inorganic geochemistry (e.g., <sup>87</sup>Sr/<sup>86</sup>Sr, Sr/Ba, Br<sup>-</sup>/Cl<sup>-</sup>), new noble gas and hydrocarbon isotopic data (e.g., <sup>20</sup>Ne/<sup>36</sup>Ar, C<sub>2</sub>+/<sub>1</sub>,  $\delta^{13}\text{C-CH}_4$ ) suggest that a hydrocarbon-rich brine likely migrated from the Marcellus Formation (via primary hydrocarbon migration) as a dual-phase fluid (gas + liquid) and was fractionated by solubility partitioning during fluid migration and emplacement into conventional UD traps (via secondary hydrocarbon migration). Based on the highly fractionated <sup>4</sup>He/CH<sub>4</sub> data relative to Marcellus and UD production gases, we propose an additional phase of hydrocarbon migration where natural gas previously emplaced in UD hydrocarbon traps actively diffuses out into and equilibrates with modern shallow groundwater (via tertiary hydrocarbon migration) following uplift, denudation, and neotectonic fracturing. These data suggest that by integrating noble gas geochemistry with hydrocarbon and dissolved ion chemistry, one can better determine the source and migration processes of natural gas in the Earth's crust, which are two critical factors for understanding the presence of hydrocarbon gases in shallow aquifers.

© 2015 Elsevier Ltd. All rights reserved.

## 1. INTRODUCTION

The extraction of unconventional hydrocarbon resources, which has been enhanced by horizontal drilling and hydraulic fracturing, has rejuvenated American and international domestic energy development (Kerr, 2010; Tour et al., 2010). These new technologies have reduced electricity generation from coal and expanded oil and natural gas production by exploiting previously untapped black shales and tight sands (Kerr, 2010; Tour et al., 2010). Despite these economic benefits, potential risks for drinking-water contamination remain a concern (Molofsky et al., 2011, 2013; Osborn et al., 2011; Jackson et al., 2013; Vidic et al., 2013; Darrah et al., 2014; Vengosh et al., 2014; Heilweill et al., 2015; Siegel et al., 2015; Drollette et al., 2015). Specific environmental concerns include the presence of elevated levels of combustible, thermogenic gases in drinking-water wells <1 km from shale gas drilling sites (Osborn et al., 2011; Jackson et al., 2013; Darrah et al., 2014) in the northern Appalachian Basin (NAB) (Fig. 1).

A lack of information about: (1) comprehensive pre-drill groundwater data; (2) uncertainty in the timing and conditions of geological and hydrogeological migration of hydrocarbon-rich crustal brines and/or natural gas; and (3) a robust set of geochemical techniques that can accurately constrain the source, mechanism, and timing of fluid migration in the Earth's crust, limits our understanding of the environmental impacts of shale gas development, specifically whether the presence of natural gas in drinking-water is natural or anthropogenic (Molofsky et al., 2011, 2013; Osborn et al., 2011; Jackson et al., 2013; Darrah et al., 2014, 2015). In the NAB, geochemical evidence (e.g., Br<sup>-</sup>/Cl<sup>-</sup> and <sup>87</sup>Sr/<sup>86</sup>Sr) suggests that cross-formational pathways may transmit diluted Middle-Devonian (i.e., Marcellus-like) gas-rich brines to shallow aquifers on yet undetermined time scales and by uncertain migration processes (Warner et al., 2012; Vengosh et al., 2014), while a subset of drinking-water wells may have elevated levels of methane because of

the presence of poor gas-well integrity in areas <1 km from drilling (Osborn et al., 2011; Jackson et al., 2013; Darrah et al., 2014). Conversely, natural methane seeps (e.g., Salt Spring State Park, Montrose, PA) provide compelling evidence for natural geological gas migration, unrelated to shale gas development (Molofsky et al., 2011, 2013; Warner et al., 2012; Baldassare et al., 2014; Darrah et al., 2014). In this paper, we focus on understanding the natural mechanisms of migration for the emplacement of hydrocarbon gases into shallow aquifers by studying these processes in the NAB, which is an example of an archetypal unconventional energy basin located in the northeastern United States.

The occurrence, distribution, and composition of hydrocarbons in the Earth's crust, including Devonian hydrocarbon-bearing formations in the NAB (Fig. 1), result from the complex interplay between the tectonic and hydrologic cycles (e.g., Bethke and Marshak, 1990; Cathles, 1990; Ballentine et al., 1991). For example, tectonic processes induce catagenesis (by increasing burial) and drive the migration of hydrocarbons and “deep” crustal brines. Hydrocarbon migration, which is often accompanied by “deep” crustal (“oil field”) brines, typically occurs by two major processes: (1) *primary migration* out of source rocks (e.g., black shales, which constitute modern-day unconventional hydrocarbon reservoir rocks) and (2) *secondary migration*, which transports hydrocarbons away from the hinterland (Oliver, 1986; Allen and Allen, 1990; Bethke and Marshak, 1990), where regional groundwater flow and buoyancy forces emplace them in stratigraphic or tectonically-induced structural traps (Cathles, 1990; Ballentine et al., 1991; Sherwood Lollar and Ballentine, 2009). Following primary and secondary migration, hydrocarbon- and brine-rich fluids may be restricted to deeply buried stratigraphic and structural traps or to “unconnected” fractures, limiting their interaction with the active hydrologic cycle (e.g., Selley, 1998; Engelder, 2012; Holland et al., 2013). For example, at the time of maximum burial, the Marcellus and overlying UD traps in the study area were likely buried 2–6 km below the surface (Evans, 1995).

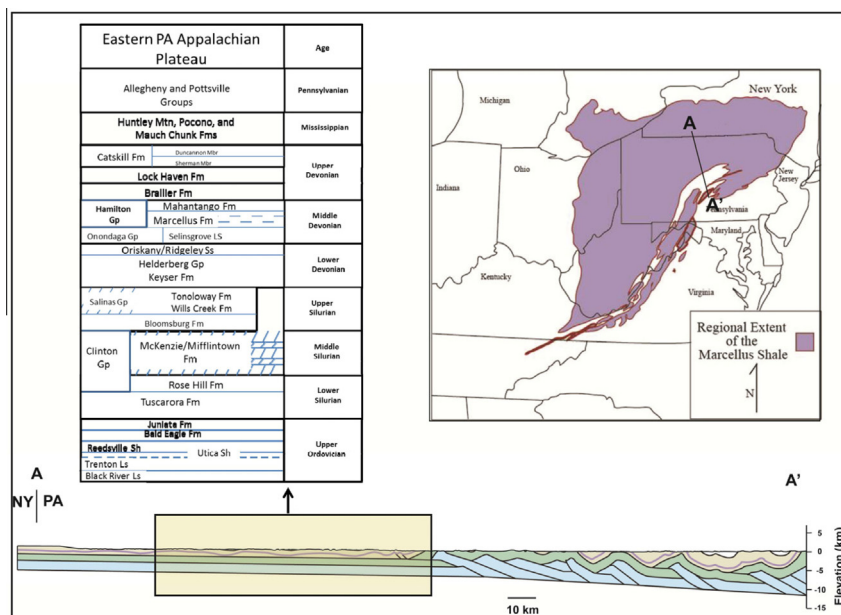


Fig. 1. A generalized stratigraphic column (left), areal extent of the Marcellus Formation (right), and a simplified structural cross-section (reproduced from Sak et al., 2012) of the northern Appalachian Basin (NAB) plateau in northeastern PA and southern NY (bottom, see cross-section A–A' on map). The Marcellus Formation outcrop belt (upper right) is highlighted in red and the areal extent of the Marcellus Formation is shown in purple. The three principal shallow Upper Devonian aquifers include the Catskill and Lock Haven Formations, and Neogene surficial sediment deposits (alluvium). The generalized structural cross-section (bottom) spans from the Appalachian Plateau (to the north and west) to the intensely deformed Valley and Ridge province (southeast) across the Appalachian Structural Front (ASF). Samples in this study were collected within the yellow box at distances ranging from ~20 to 80 km from the ASF. (For interpretation of the references to color in this figure legend, the reader is referred to the web version of this article.)

Throughout geological time, additional tectonic and climatic factors may also induce and/or accelerate subsequent phases of hydrocarbon migration, commonly termed *tertiary migration* (Selley, 1998). For example, the culmination of major orogenic events, such as the Alleghanian orogeny that buried Devonian sediments in the current study area, is followed by tectonic rifting and basin inversion (uplift and denudation), which can induce neotectonic fractures, joints, and faults. These deformational features can reduce the competency of hydrocarbon seals and allow for the subsequent migration of hydrocarbons from conventional structural and stratigraphic traps. Uplift and denudation processes also bring deeply buried, hydrocarbon- and brine-rich formations closer to the surface where they can interact with the active hydrological cycle. Similar episodes of erosion and uplift following glacial events have been observed in the Michigan and Illinois basins (Lerche et al., 1997; Schlegel et al., 2011). Following these late stage deformational processes, the hydrologic cycle can redistribute thermogenic hydrocarbons within shallow aquifers, where they mix with CH<sub>4</sub> produced from *in-situ* biological processes leading to natural gases with hydrocarbon fingerprints of indeterminate origin.

Consequently, numerous questions still remain regarding fluid sources, the extent and mechanism of crustal fluid migration in the NAB as well as other petroliferous foreland basins, and the fate and residence time of organic carbon in the shallow crust. For example, what mechanisms could have driven natural gas and brine migration into the

previously deeply buried modern aquifers? Did fluids migrate exclusively during episodic tectonic events, such as the Alleghanian Orogeny (Oliver, 1986; Bethke and Marshak, 1990; Evans, 1995; Lash and Engelder, 2009), or do these fluids actively migrate today?

In complex tectonic regimes such as the NAB, hydrological, geophysical, and geochemical techniques are all helpful in evaluating the distribution of hydrocarbons in the Earth's crust. One technique that traditionally links these disciplines is the analysis of gas geochemistry, specifically stable isotopic compositions (e.g.,  $\delta^{13}\text{C}$ ,  $\delta^{18}\text{O}$ , and  $\delta^2\text{H}$ ) of hydrocarbon gases or CO<sub>2</sub> (e.g., Craig, 1953; Ballentine et al., 1991; Sherwood Lollar et al., 1994; Gilfillan et al., 2009; Sherwood Lollar and Ballentine, 2009).

Within the context of petroleum geochemistry, natural gases are often classified as thermogenic, biogenic, or “mixed” based on their molecular ratios (e.g., wetness: C<sub>2</sub>+/C<sub>1</sub>) along with C and H isotopic composition (e.g., Bernard, 1978; Schoell, 1980, 1983; Rice and Claypool, 1981; Schoell, 1988; Clayton, 1991). The composition of thermogenic gases evolves as the organic source (i.e., kerogen or liquid hydrocarbons) degrades, producing diagnostic geochemical fingerprints (i.e.,  $\delta^{13}\text{C}$ -CH<sub>4</sub>,  $\delta^2\text{H}$ -CH<sub>4</sub>,  $\delta^{13}\text{C}$ -C<sub>2</sub>H<sub>6</sub>, and C<sub>1</sub>/C<sub>2</sub>+ (e.g., Schoell, 1983)). Conversely, “biogenic” gas forms at a relatively low temperature (<<100 °C) in dysoxic or anoxic conditions from the microbial decomposition of organic matter and/or the reduction of CO<sub>2</sub> (e.g., Schoell, 1980; Rice and Claypool, 1981; Whiticar et al., 1986). Under these conditions, microbes

almost exclusively produce  $\text{CH}_4$  ( $C_1/C_{2+} \geq \sim 5000$ ) with a typically light  $\delta^{13}\text{C}-\text{CH}_4$  between  $-55\%$  and  $-75\%$  (Schoell, 1983; Whiticar et al., 1985). It should be noted that the measurement of multiply substituted isotopologues of methane are now providing additional insights on the formation temperatures of thermogenic and biogenic methane; this approach also helps to distinguish between methane derived from each of these sources (Stolper et al., 2014, 2015).

In addition to these genetic fingerprints, microbial activity (e.g., methanogenesis and methanotrophy), sulfate reduction (thermal or bacterially driven), or post-genetic fractionation (e.g., fractionation during gas transport in the subsurface) can alter the original composition of natural gases or lead to complex mixtures of natural gases from multiple sources. The addition of methane produced by methanogenesis would in theory progressively enrich the natural gas mixture in methane relative to higher aliphatic hydrocarbons (higher  $C_1/C_{2+}$ ) and lead to a more depleted  $\delta^{13}\text{C}-\text{CH}_4$  (Bernard, 1978; Schoell, 1983; Whiticar et al., 1985). By comparison, microbial oxidation or sulfate reduction would similarly increase the  $C_1/C_{2+}$  in the natural gas mixture because higher aliphatic hydrocarbons are oxidized preferentially to methane; however, these reactions would produce a residual natural gas that is more enriched in  $\delta^{13}\text{C}-\text{CH}_4$  and  $\delta^{13}\text{C}-\text{C}_2\text{H}_6$  than the original composition (e.g., Kessler et al., 2006; Pape et al., 2010). Natural gases that migrate can become enriched in  $^{12}\text{C}$  and  $^1\text{H}$  relative to their original composition (Prinzhofer and Huc, 1995; Pape et al., 2010; Xia and Tang, 2012) because of the faster diffusion and/or lower solubility of lower molecular weight compounds (e.g.,  $^{12}\text{C}^1\text{H}_4$  vs.  $^{13}\text{C}^1\text{H}_4$  or  $^{12}\text{C}^1\text{H}_3^2\text{H}$ ). Throughout the last few decades, the potential importance of stable isotope fractionation of hydrocarbon gases by diffusion or solubility partitioning has been discounted by the limited feasibility for kilometer-scale diffusion of hydrocarbons in the crust and minimal evidence for significant fractionation of stable isotopes (e.g.,  $\sim 5\%$ ) within natural gas reservoirs (e.g., Fuex, 1980; Milkov, 2011). As a result, today, many modern workers do not consider post-genetic modification processes other than microbial oxidation or sulfate reduction when interpreting the molecular and isotopic composition of hydrocarbons in groundwater studies.

The elemental and isotopic compositions of noble gases (e.g., helium (He), neon (Ne), argon (Ar)) constitute a set of non-reactive geochemical tracers. Therefore, the original noble gas composition is preserved in shallow groundwater independent of microbial activity, chemical reactions (e.g., sulfate reduction), or changes in oxygen fugacity. The inert nature, low terrestrial abundance, and well-characterized isotopic composition of noble gases in the mantle, crust, hydrosphere, and atmosphere enhance their utility as geochemical tracers of crustal fluids (Ballentine et al., 2002).

The noble gas composition of hydrocarbons and other geological fluids are derived from three primary sources: the mantle, atmosphere, and the crust (Ballentine et al., 2002). While a subset of four samples in the current study contain higher than anticipated helium isotopic values (elevated  $R/Ra$ ) consistent with resolvable mantle

contributions ( $> \sim 1\%$ ), our previous work indicates that mantle noble gases constitute  $< 1\%$  of helium isotopic mixture in the majority of samples in the NAB, specifically in the hydrocarbon-rich end-member (Hunt et al., 2012) (discussed further in the results). Thus, in the majority of samples in our study area, and in most shallow aquifers globally, the noble gas isotopic composition reflects a binary mixture of inert gases from two distinct sources: the atmosphere (air-saturated water (ASW): e.g.,  $^{20}\text{Ne}$ ,  $^{36}\text{Ar}$ ,  $^{38}\text{Ar}$ ,  $^{84}\text{Kr}$ ) and the crust ( $\text{U} + \text{Th} \rightarrow ^4\text{He}$  and  $^{21}\text{Ne}^*$  and  $^{40}\text{K} \rightarrow ^{40}\text{Ar}^*$ , where the \* denotes the proportion derived from radioactive decay) (e.g., Ballentine et al., 2002). The noble gas signatures of crustal fluids only fractionate by well-constrained physical mechanisms such as diffusion and solubility-driven phase partitioning in response to changing fluid conditions (e.g., Gilfillan et al., 2009; Zhou et al., 2012).

Atmospheric noble gases (AIR) dissolve in groundwater when meteoric water equilibrates with the atmosphere prior to groundwater recharge into the subsurface according to Henry's Law solubility (i.e., solubility increases with atomic mass:  $\text{He} < \text{Ne} < \text{Ar} < \text{Kr} < \text{Xe}$ ) (Weiss, 1971a,b). Because the meteoric source for ASW is constant globally, the concentrations of ASW components in groundwater are a well-constrained function of temperature, salinity, and atmospheric pressure (elevation) (Weiss, 1971a,b). The typical composition of shallow groundwater in unconfined aquifers has ASW noble gas composition characterized by near solubility levels of  $[^4\text{He}]$  ( $\sim 40\text{--}45 \times 10^{-6} \text{ cm}^3 \text{ STP/L}$ ),  $[\text{Ne}]$  ( $175\text{--}220 \times 10^{-6} \text{ cm}^3 \text{ STP/L}$ ), and  $[\text{Ar}]$  ( $0.28\text{--}0.49 \text{ cm}^3 \text{ STP/L}$ ) (Weiss, 1971a,b). Isotopically, each gas component is similar to atmospheric compositions (i.e., helium:  $^3\text{He}/^4\text{He} = 1.36 \times 10^{-6}$  or  $\sim 0.985Ra$ , where  $Ra$  is the ratio of a sample relative to the ratio of helium isotopes in AIR =  $1.39 \times 10^{-6}$ , neon:  $^{20}\text{Ne}/^{22}\text{Ne}$  (9.78) and  $^{21}\text{Ne}/^{22}\text{Ne}$  ( $\sim 0.0289$ ), and argon  $^{40}\text{Ar}/^{36}\text{Ar}$  ( $\sim 295.5$ )). Only helium ( $0.985Ra$ ) displays an isotopic effect related to Henry's Law dissolution into meteoric water that is larger than the analytical measurement errors.

Crustal noble gases are produced *in-situ* within the Earth's crust from the decay of U, Th ( $^4\text{He}$  and  $^{21}\text{Ne}^*$ ), and K ( $^{40}\text{Ar}^*$ ) (e.g., Ballentine and Burnard, 2002). As either hydrocarbons or groundwater interact with the Earth's crust, the noble gas composition changes according to the radiogenic nature and geologic history of the rock protolith in which the fluids form and through which they migrate (Ballentine et al., 2002). In black shales, typical ranges for radioactive components are U ( $\sim 1\text{--}30$  ppm), Th ( $\sim 1\text{--}30$  ppm), and  $^{40}\text{K}$  (total K  $\sim 26,000$  ppm, with  $[^{40}\text{K}]/\text{K}$  ratio of  $1.170 \times 10^{-4} = \sim 3$  ppm of  $^{40}\text{K}$  of which 11% decays to  $^{40}\text{Ar}^*$ ), respectively (Taylor and McLennan, 1995). Typical isotopic ratios of crustal noble gases are  $^3\text{He}/^4\text{He} = \sim 0.01\text{--}0.02Ra$ ,  $^{20}\text{Ne}/^{22}\text{Ne}$  ( $\sim 9.6\text{--}10.0$ ),  $^{21}\text{Ne}/^{22}\text{Ne}$  ( $\sim 0.029\text{--}0.060$ ), and  $^{40}\text{Ar}/^{36}\text{Ar}$  ( $\sim 295.5\text{--}1100$ ), respectively (e.g., Ballentine et al., 2002).

Because the mantle acquired significant quantities of primordial  $^3\text{He}$  during the accretion of the Earth (e.g., Ballentine et al., 2002), elevated  $[^3\text{He}]$  and  $R/Ra$  [where  $R/Ra$  is  $(^3\text{He}/^4\text{He}_{\text{sample}})/(^3\text{He}/^4\text{He}_{\text{air}})$  and the  $Ra = 1.39 \times 10^{-6}$ ] measurements can be used to distinguish the presence

and/or proportion of relatively small contributions ( $\sim 1\%$ ) from mantle-derived components in shallow groundwater or other crustal fluids (Oxburgh et al., 1986; Poreda et al., 1986). Mantle helium isotopic end-members can range from  $\sim 2$  to  $8Ra$  for MORB-like contributions common in extensional regimes up to  $>30Ra$  near mantle plumes (e.g., Yellowstone, Hawaii, Iceland). In addition to the  $R/Ra$  value, the relative abundance of helium and other heavier noble gases (e.g., neon) can provide important insights on the source of fluids (Hilton, 1996; Ballentine and Hall, 1999; Saar et al., 2005). Air-saturated water and excess atmospheric air have relatively low He/Ne that range from 0.219 to 0.247 and  $\sim 0.288$ , respectively. By comparison, mantle- and crustal-derived fluids typically have He/Ne of  $>1000$  or more (e.g., Craig et al., 1978; Hilton, 1996).

When paired with hydrocarbon composition, noble gases can provide valuable insights into the source, migrational history, and residence time of crustal fluids (e.g., Ma et al., 2005, 2009b; Zhou and Ballentine, 2006; Gilfillan et al., 2009; Sherwood Lollar and Ballentine, 2009; Darrah et al., 2014). Here, we demonstrate that noble gases in combination with hydrocarbon and dissolved ion geochemistry provide a geochemical framework that can help to constrain the geological history of “background” hydrocarbon gases naturally present in shallow aquifers in the NAB and potentially in other unconventional energy basins in the future. Additionally, by understanding the geochemical signatures imparted on a fluid as it migrates through the crust, we present a more robust geochemical framework for differentiating hydrocarbon gases found naturally compared to those that may arise from anthropogenic fugitive natural gas release related to natural gas drilling, gas storage fields, or carbon sequestration.

## 2. BACKGROUND

### 2.1. Geological background

The NAB is an archetypal energy-producing foreland basin located in the northeastern United States (Fig. 1). In the eastern part of the NAB (northeastern Pennsylvania and southeastern New York), oil and gas production occurs within various lithologies throughout the northern Appalachian Plateau physiographic province, but is largely confined to two genetic groups: (1) migrated gases sourced from Ordovician shales and hosted in Ordovician/Silurian hydrocarbon traps and (2) Middle Devonian source/reservoir “tight gas” black shales of the Marcellus Group (Jenden et al., 1993; Engelder et al., 2009). More complete descriptions of relevant Appalachian geology and hydrocarbon potential are available elsewhere (Rast, 1989; Jenden et al., 1993; Laughrey and Baldassare, 1998; Engelder et al., 2009; Lash and Engelder, 2009; Burruss and Laughrey, 2010), but a brief summary is included below.

The structural architecture of the NAB evolved throughout the Taconic, Acadian, and Alleghanian orogenies, which deposited and deformed the sedimentary rocks throughout the basin (Faill, 1997a,b; Scanlin and Engelder,

2003; Sak et al., 2012). Today, the complex depositional and structural history of this area is exposed within the northern section of the Appalachian Plateau physiographic province, whose gently dipping strata are broadly folded due to salt-core detachment folds, and further deformed by layer parallel shortening, reverse faults, and fracturing (Davis and Engelder, 1985; Scanlin and Engelder, 2003; Lash et al., 2004; Sak et al., 2012).

Select lithologies of interest in this study area include: the Middle Ordovician Trenton/Black River Group, the Upper Silurian Salina Formation, the Middle Devonian Hamilton Group, and the Upper Devonian Brallier, Lock Haven, and Catskill Formations (Fig. 1). The interbedded limestones and shales of the Trenton/Black River Group and the overlying organic-rich Utica shale represent detrital sediments from the Taconic Orogeny (Milici and Witt, 1988; Burruss and Laughrey, 2010). The Salina Formation consists of interbedded shales, dolomites, and salt deposits that act as the regional decollement for Alleghanian structures (Frey, 1973; Scanlin and Engelder, 2003). As a result, structural folds and faults above the decollement (i.e., Devonian and younger stratigraphic units) bear little resemblance in deformation style or hydraulic connectivity to those present beneath the Salina Formation (Frey, 1973; Scanlin and Engelder, 2003).

The Hamilton Group is a wedge of marine sediments that is thicker to the east and south and includes the organic- and siliciclastic-rich, hydrocarbon-producing Marcellus subgroup at its base (Ryder et al., 1996; Straeten et al., 2011). Rb–Sr age-dating suggests that the deposition of the Marcellus Formation occurred from approximately  $384 \pm 9$  to  $377 \pm 11$  Ma (Bofinger and Compston, 1967). The Upper Devonian formations consist of thick, coarsening upward synorogenic deposits of deltaic and marine shale, siltstone, sandstone, and conglomerate with interbedded carbonates including the Brallier, Lock Haven, and Catskill Formations (Fig. 1). The latter two formations constitute the two primary lithologies that serve as bedrock aquifers in northeastern PA and southeastern NY, along with the overlying glacial and sedimentary alluvium (Taylor, 1984).

The Hamilton Group and other formations above the Salina were deformed by stably sliding along the weak Salina layer as part of the Appalachian Plateau detachment sheet (Davis and Engelder, 1985; Scanlin and Engelder, 2003). Deformation within the Appalachian Plateau detachment sheet is significantly less intense than the Valley and Ridge Province and shows a combination of layer parallel shortening and folding that leads to the broad anticline/syncline sequences, duplex/thrust faulting structures, and jointing (Scanlin and Engelder, 2003; Engelder and Whitaker, 2006; Lash and Engelder, 2009). Each of these deformation features is present and observable within our study area. A combination of thrust-load-induced subsidence, clastic loading, and Alleghanian deformation led to the onset of thermal maturation and eventually catagenesis of the Marcellus Formation (Evans, 1995; Lash and Engelder, 2009). In the NAB, the Alleghanian deformation also leads to large-scale migration of “hot”, “deep” formational brines away from the hinterland and into the

foreland (i.e., Appalachian Plateau) (Oliver, 1986; Bethke and Marshak, 1990; Evans, 1995).

Rifting of the Atlantic Ocean began in the Mesozoic, as seen in the Triassic basalts of Connecticut and New Jersey, accelerated in the Miocene, and continues today. This process has led to rapid basin inversion (exhumation/unloading), erosion, and neotectonic jointing (often termed  $J_3$ ) in at least the top  $\sim 0.5$  km of the crust (Engelder, 2008). The major Triassic rift basins in the Appalachian Basin occur in the Gettysburg-Newark lowland and offshore.

Pleistocene glacial cycles have also influenced the permeability of aquifer lithologies within our study area. Ice loading and retreat led to an additional cycle of shallow crustal compaction, glacial isostatic rebound, and likely additional neotectonic fracturing throughout the last 12,000 yr. As a result of both tectonic and glacial processes, previously deeply buried lithologies such as the Catskill and Lock Haven Formations are much closer to the surface today (by at least  $\sim 1.5$ – $5$  km) (Blackmer et al., 1994; Evans, 1995) and often serve as highly naturally fractured, dual permeability aquifers for drinking water supplies in our study area (Taylor, 1984; Williams et al., 1998; Williams, 2010). The major stratigraphic sequences above the Upper Devonian Catskill Formation in our study area have eroded away and therefore are not discussed for brevity. More complete reviews of Carboniferous Age deposition in the NAB are available elsewhere (Faill, 1997b).

## 2.2. Hydrogeological background

Detailed descriptions of potable groundwater resources in the NAB, including the three principal aquifers discussed here, were provided previously (e.g., Lohman, 1937, 1939; Taylor, 1984; Williams et al., 1998). More detailed characteristics of domestic well construction and well productivity are summarized using a larger and more complete dataset in Taylor (1984) (Table 1); our data ( $n = 72$ ) are a statistically similar representation of homeowner-reported depths and yields with a range between 35 and 90 m.

The groundwater systems in the current study area include alluvium and Lock Haven and Catskill bedrock aquifers. In general, the depth to groundwater is shallower in the valleys with median depths of 7.6 m, while 32.9 m is the median for domestic wells located on hilltops (Taylor, 1984). All three aquifers generally contain good-quality water of Ca-HCO<sub>3</sub> water type, however, select wells, commonly located in local valley bottoms, yield water with iron or manganese at higher concentrations and either Na-CO<sub>3</sub> or Na-Cl type water, which was discussed in detail

elsewhere (Williams et al., 1998; Williams, 2010; Warner et al., 2012; Llewellyn, 2014).

Several shallow unconsolidated and unconfined glacial outwash and riverine alluvium deposits, consisting of cobbles, sands, silts, and clays, constitute the alluvium aquifers. The alluvium deposits are thickest ( $>10$  m) in the valleys and either absent or only thin covers on the ridge tops. Domestic drinking-water wells drilled into the alluvium typically have steel casings that penetrate nearly to the bottom of the entire well (Lohman, 1937, 1939; Taylor, 1984; Williams et al., 1998; Williams, 2010).

Beneath the alluvium are the UD bedrock aquifers of the Catskill and Lock Haven Formations (geology described above). These aquifer units are typically locally recharged, nested, unconfined to semi-confined, highly naturally fractured (neotectonic), dual permeability systems (Lohman, 1937, 1939; Taylor, 1984; Williams et al., 1998; Williams, 2010). Water bearing zones are generally provided from secondary porosity (fractures) for both formations and are typically less than 60 m below ground surface, but some domestic wells penetrate as deep as 179 m (Taylor, 1984). The potentiometric surface of the water table in these bedrock aquifers typically mimics the localized (on the scale of individual ridge (hill top)-valley systems) ground surface with flow sub-laterally from the recharge areas, which are dominated by shallow vertical fractures and/or porous sediments in the local hilltops, towards discharge points in the local valleys or hillslope (Lohman, 1937, 1939; Taylor, 1984; Williams et al., 1998; Williams, 2010). Bedrock wells that are drilled into either the Catskill or Lock Haven Formations typically have much shorter casings (10–15 m) or open holes for the majority of the well bore.

## 3. MATERIALS AND METHODS

### 3.1. Sample selection

We examine the noble gas, hydrocarbon (molecular and stable isotopic ( $\delta^{13}\text{C-CH}_4$  and  $\delta^2\text{H-CH}_4$ )), and dissolved ion (e.g., Cl, Ba) compositions of 72 domestic groundwater wells and one natural methane seep within an eight county area of Pennsylvania, USA (PA) (Bradford, Lycoming, Sullivan, Susquehanna, and Wayne counties) and New York, USA (NY) (Broome, Delaware and Sullivan counties). These samples constitute the subset of samples  $\gg 1$  km away from active or historical natural gas drill sites in Darrah et al. (2014) in an attempt to minimize any potential impacts of anthropogenic activity. In this study, we intentionally include a subset of water wells known to have

Table 1  
Summary of domestic drinking-water well characteristics for the three principal aquifers sampled during this study that were also sampled by Taylor (1984).

| Formation  | Well depth (m) | Number (n) | Casing depth (m) | Number (n) | Depth to water (m) | Number (n) | Reported well yield (l/m) | Number (n) | Specific capacity (l/min/m) | Number (n) |
|------------|----------------|------------|------------------|------------|--------------------|------------|---------------------------|------------|-----------------------------|------------|
| Alluvium   | 17.1           | 56         | 17.4             | 54         | 5.5                | 45         | 68.1                      | 56         | 0.9                         | 10         |
| Catskill   | 60.4           | 950        | 12.8             | 918        | 16.8               | 737        | 45.4                      | 931        | 0.6                         | 352        |
| Lock Haven | 43.3           | 213        | 15.2             | 211        | 14                 | 165        | 37.9                      | 211        | 0.2                         | 34         |

elevated methane  $\gg 1$  km from drill sites along with other nearby domestic wells in order to characterize the hydrogeological context of naturally elevated methane (and diluted brines) throughout the study area. As a result, our study design does not provide any information on the probability of finding elevated methane in shallow drinking-water aquifers in the region.

The study area is within the NAB Plateau region underlain by the Marcellus Shale ( $\sim 800$ – $2200$  m depth) (Figs. 1 and 2). The typical depth of shallow drinking-water wells in our study was 35–90 m. We integrate our noble gas, hydrocarbon gas (i.e., molecular and isotopic composition of natural gas), and dissolved inorganic constituent (i.e., Cl, Ba) data with previous work on the principal aquifers of the region (Alluvium, Catskill, and Lock Haven). Previous work in this area focused on the salt composition (i.e., Cl, Br), inorganic isotopic composition (e.g.,  $^{87}\text{Sr}/^{86}\text{Sr}$ ) and hydrocarbon molecular and isotopic composition (e.g.,  $\delta^{13}\text{C}\text{-CH}_4$ ) in groundwater from UD aquifers (Baldassare et al., 2014; Darrah et al., 2014; Llewellyn, 2014; Osborn et al., 2011; Revesz et al., 2010; Warner et al., 2012).

We present data from this study with color-coded symbols, while data from previous studies are identified by gray symbols. Within all figures, the abundance of methane is preserved using a color intensity scale, where methane concentrations of  $0\text{ cm}^3\text{ STP/L}$  are blue and range up to red for  $[\text{CH}_4] > 40\text{ cm}^3\text{ STP/L}$ . To preserve geographic location, we present data from each county using different shapes. The symbols are as follows: Bradford (square), Lycoming (triangle), Sullivan (diamond), Susquehanna (inverted triangle), and Wayne (circle) counties in PA and NY (hexagon) (including Broome, Delaware and Sullivan counties). We place these data, and some available data from natural gas production wells (Jenden et al., 1993; Laughrey and Baldassare, 1998; Burruss and Laughrey, 2010; Osborn and McIntosh, 2010; Hunt et al., 2012) within the geological history of the NAB.

### 3.2. Sampling and analysis

Although 35 of 73 samples were analyzed for dissolved ion composition and strontium isotope chemistry as part

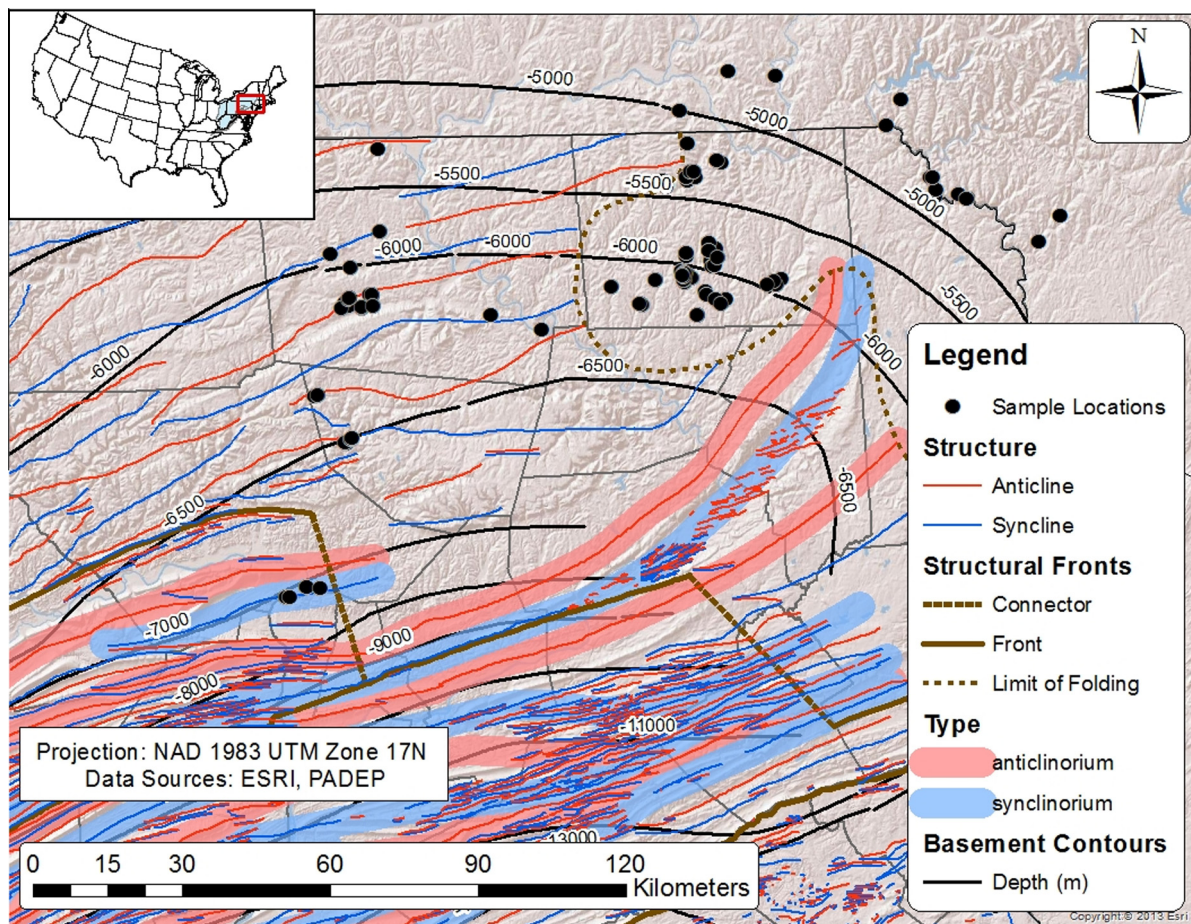


Fig. 2. Digital elevation map of groundwater samples ( $n = 72$ ) and the Salt Spring at Salt Spring State Park, Montrose, PA. Shaded pink areas represent anticlines, while the blue areas demark synclines. All samples from this study were collected at distances  $>1$  km from active shale gas development at the time of sample collection across five counties in Pennsylvania (PA) (Bradford, Lycoming, Sullivan, Susquehanna, Wayne) and three counties in New York (NY) (Delaware, Sullivan, Broome). Previous work identifies increasing  $[\text{CH}_4]$  and salt concentrations in valley bottoms (Molofsky et al., 2011; Warner et al., 2012) related to the cores of eroded anticlines. (For interpretation of the references to color in this figure legend, the reader is referred to the web version of this article.)

Table 2a

The hydrocarbon, noble gas, and atmospheric gases and chlorine (Cl) and barium (Ba) concentrations of drinking-water samples in northeastern PA and southeastern NY.

| Sample                            | CH <sub>4</sub><br>(cm <sup>3</sup> /L) | C <sub>2</sub> H <sub>6</sub><br>(cm <sup>3</sup> /L) | N <sub>2</sub><br>(cm <sup>3</sup> /L) | O <sub>2</sub><br>(cm <sup>3</sup> /L) | Ar<br>(cm <sup>3</sup> /L) | <sup>4</sup> He<br>(10 <sup>-6</sup> cc/L) | <sup>20</sup> Ne<br>(10 <sup>-6</sup> cc/L) | Ne (total)<br>(10 <sup>-6</sup> cc/L) | <sup>36</sup> Ar<br>(10 <sup>-6</sup> cc/L) | Cl<br>(mg/L) | Ba<br>(μg/L) | C <sub>1</sub> /C <sub>2</sub> | C <sub>2</sub> /C <sub>1</sub> | N <sub>2</sub> /Ar | CH <sub>4</sub> / <sup>36</sup> Ar | <sup>4</sup> He/CH <sub>4</sub><br>(×10 <sup>6</sup> ) |
|-----------------------------------|---|---|--|--|----------------------------|--|---|---------------------------------------|---|--------------|--------------|--------------------------------|--------------------------------|--------------------|------------------------------------|--|
| <i>Pennsylvania</i>               |   |   |  |  |                            |  |   |                                       |   |              |              |                                |                                |                    |                                    |  |
| <i>Susquehanna county</i>         |   |   |  |  |                            |  |   |                                       |   |              |              |                                |                                |                    |                                    |  |
| DPA-1                             | 0.97                                    | 1.5E-04   | 12.0                                   | 0.09                                   | 0.31                       | 5261                                       | 273   | 302                                   | 1053  | 13           | 385          | 6420                           | 1.56E-04                       | 38.5               | 920                                | 5428   |
| DPA-2                             | 1.32                                    | 1.8E-04   | 14.1                                   | 0.17                                   | 0.33                       | 11,662                                     | 318   | 352                                   | 1098  | 60           | 529          | 7530                           | 1.33E-04                       | 43.3               | 1202                               | 8835   |
| DPA-3                             | 0.01                                    | bdl   | 12.6                                   | 0.07                                   | 0.33                       | 3599                                       | 225   | 248                                   | 1098  | 24           | 55           |                                |                                | 38.9               | 9                                  | 359,938  |
| DPA-4                             | 2.34                                    | 4.0E-04   | 14.0                                   | 0.04                                   | 0.27                       | 6233                                       | 403   | 446                                   | 916   | 59           | 765          | 5850                           | 1.71E-04                       | 51.6               | 2556                               | 2664   |
| DPA-5                             | 0.01                                    | bdl   | 15.3                                   | 0.07                                   | 0.39                       | 84   | 194   | 214                                   | 1308  | 2            | 60           |                                |                                | 39.4               | 8                                  | 8446   |
| DPA-6                             | 0.01                                    | bdl   | 13.1                                   | 0.09                                   | 0.32                       | 5792                                       | 183   | 203                                   | 1084  | 15           | 73           |                                |                                | 40.7               | 9                                  | 579,190  |
| DPA-7                             | 3.56                                    | 1.7E-02   | 13.6                                   | 0.01                                   | 0.34                       | 5632                                       | 253   | 280                                   | 1149  | 623          | 378          | 210                            | 4.76E-03                       | 40.1               | 3102                               | 1581   |
| DPA-9                             | 0.01                                    | bdl   | 13.6                                   | 0.02                                   | 0.36                       | 158  | 260   | 287                                   | 1233  | 2            | 57           |                                |                                | 37.3               | 8                                  | 15,788   |
| DPA-10                            | 0.01                                    | bdl   | 14.2                                   | 0.01                                   | 0.32                       | 66   | 161   | 178                                   | 1086  | 5            | 151          |                                |                                | 44.1               | 9                                  | 6563   |
| DPA-13                            | 0.08                                    | bdl   | 11.6                                   | 0.02                                   | 0.28                       | 159  | 230   | 255                                   | 960   | 13           | 61           |                                |                                | 40.7               | 83                                 | 1985   |
| DPA-14                            | 0.01                                    | bdl   | 15.6                                   | 0.01                                   | 0.43                       | 148  | 351   | 388                                   | 1444  | 6            | 57           |                                |                                | 36.6               | 7                                  | 14,787   |
| DPA-21                            | 0.01                                    | bdl   | 17.1                                   | 0.05                                   | 0.47                       | 84   | 307   | 340                                   | 1602  | 2            |              |                                |                                | 36.1               | 6                                  | 8447   |
| DPA-22                            | 0.01                                    | bdl   | 19.5                                   | 0.02                                   | 0.50                       | 88   | 230   | 254                                   | 1688  | 3            |              |                                |                                | 38.9               | 6                                  | 8836   |
| DPA-26                            | 0.01                                    | bdl   | 13.9                                   | 0.01                                   | 0.34                       | 111  | 384   | 425                                   | 1133  | 15           | 49           |                                |                                | 41.5               | 9                                  | 11,083   |
| DPA-27                            | 0.01                                    | bdl   | 12.8                                   | 0.04                                   | 0.27                       | 25   | 107   | 118                                   | 912   | 3            |              |                                |                                | 47.2               | 11                                 | 2480   |
| DPA-39                            | 3.4                                     | 4.3E-04   | 15.7                                   | 0.00                                   | 0.30                       | 9874                                       | 544   | 602                                   | 1017  | 22           |              | 7977                           | 1.25E-04                       | 52.0               | 3373                               | 2879   |
| DPA-41                            | 0.05                                    | bdl   | 17.0                                   | 0.08                                   | 0.40                       | 1505                                       | 306   | 338                                   | 1348  | 2            | 84           |                                |                                | 42.5               | 34                                 | 32,985   |
| DPA-42                            | 0.00                                    | bdl   | 10.2                                   | 0.41                                   | 0.26                       | 38   | 151   | 167                                   | 865   | 2            |              |                                |                                | 39.7               | 4                                  | 10,964   |
| DPA-74                            | 0.01                                    | bdl   | 14.8                                   | 0.08                                   | 0.38                       | 73   | 190   | 210                                   | 1270  | 3            | 67           |                                |                                | 39.3               | 5                                  | 12,272   |
| DPA-81                            | 0.02                                    | bdl   | 16.2                                   | 0.05                                   | 0.43                       | 1118                                       | 290   | 321                                   | 1455  | 9            |              |                                |                                | 37.7               | 15                                 | 50,578   |
| DPA-82                            | 0.02                                    | bdl   | 21.4                                   | 0.03                                   | 0.54                       | 221  | 311   | 343                                   | 1833  | 2            | 64           |                                |                                | 39.4               | 9                                  | 12,999   |
| DPA-85                            | 0.08                                    | bdl   | 16.9                                   | 0.18                                   | 0.45                       | 1219                                       | 284   | 314                                   | 1518  | 7            |              |                                |                                | 37.6               | 53                                 | 15,233   |
| DPA-212                           | 0.00                                    | bdl   | 14.9                                   | 0.52                                   | 0.39                       | 63   | 198   | 219                                   | 1321  | 1            | 38           |                                |                                | 38.1               | 3                                  | 15,493   |
| DPA-213                           | 0.01                                    | bdl   | 16.3                                   | 0.29                                   | 0.40                       | 57   | 200   | 221                                   | 1337  | 2            | 55           |                                |                                | 41.3               | 5                                  | 8423   |
| DPA-214                           | 0.01                                    | bdl   | 18.8                                   | 1.64                                   | 0.66                       | 197  | 395   | 436                                   | 2234  |              | 64           |                                |                                | 28.5               | 4                                  | 21,538   |
| DPA-215                           | 1.77                                    | 2.6E-04   | 16.5                                   | 0.54                                   | 0.44                       | 3694                                       | 662   | 732                                   | 1477  | 17           | 417          | 6743                           | 1.48E-04                       | 37.7               | 1198                               | 2087   |
| DPA-216                           | 0.31                                    | bdl   | 14.6                                   | 0.35                                   | 0.41                       | 5613                                       | 296   | 328                                   | 1385  |              | 257          |                                |                                | 35.6               | 224                                | 18,105   |
| DPA-217                           | 0.47                                    | 1.5E-04   | 16.5                                   | 0.66                                   | 0.45                       | 9694                                       | 379   | 418                                   | 1520  | 15           | 250          | 3133                           | 3.19E-04                       | 36.7               | 309                                | 20,626   |
| DPA-218                           | 1.34                                    | 2.1E-04   | 16.8                                   | 0.13                                   | 0.31                       | 16,338                                     | 522   | 576                                   | 1047  | 17           | 468          | 6390                           | 1.56E-04                       | 54.3               | 1279                               | 12,192   |
| DPA-219                           | 0.01                                    | bdl   | 11.8                                   | 0.04                                   | 0.30                       | 1514                                       | 345   | 382                                   | 1026  | 17           | 87           |                                |                                | 38.8               | 6                                  | 238,470  |
| DPA-220                           | 2.02                                    | 3.2E-04   | 14.9                                   | 0.00                                   | 0.35                       | 27,803                                     | 546   | 604                                   | 1182  | 24           | 522          | 6400                           | 1.56E-04                       | 42.6               | 1708                               | 13,764   |
| DPA-221                           | 0.03                                    | bdl   | 14.4                                   | 0.00                                   | 0.42                       | 1608                                       | 181   | 201                                   | 1419  | 7            | 61           |                                |                                | 34.3               | 23                                 | 49,892   |
| DPA-222                           | 0.15                                    | bdl   | 16.2                                   | 0.00                                   | 0.31                       | 2045                                       | 241   | 266                                   | 1047  | 15           | 190          |                                |                                | 52.4               | 146                                | 13,367   |
| DPA-223                           | 1.18                                    | 5.0E-04   | 13.9                                   | 0.00                                   | 0.31                       | 8602                                       | 292   | 323                                   | 1047  | 17           | 343          | 3976                           | 2.52E-04                       | 44.9               | 1122                               | 7319   |
| DPA-224                           | 6.80                                    | 9.6E-04   | 14.6                                   | 0.01                                   | 0.34                       | 16,508                                     | 828   | 915                                   | 1155  | 59           | 482          | 7096                           | 1.41E-04                       | 42.6               | 5885                               | 2428   |
| DPA-225                           | 37.8                                    | bdl   | 17.0                                   | 0.01                                   | 0.34                       | 37   | 174   | 192                                   | 1145  | 2            | 57           | 38,000                         | 2.63E-05                       | 50.0               | 33,005                             | 1.0  |
| <i>Salt Spring (Montrose, PA)</i> |   |   |  |  |                            |  |   |                                       |   |              |              |                                |                                |                    |                                    |  |
| DPA-8                             | 40.8                                    | 2.2E-01<br>1.9E+02                                    | 12.8                                   | 0.00                                   | 0.30                       | 79,372                                     | 312   | 345                                   | 1017  | 3973         | 83,700       | 183                            | 5.46E-03                       | 42.4               | 40,122                             | 1945   |

*Bradford county*

|         |      |         |      |      |      |         |      |      |      |      |        |        |          |      |        |        |
|---------|------|---------|------|------|------|---------|------|------|------|------|--------|--------|----------|------|--------|--------|
| DPA-34  | 0.01 | bdl     | 12.6 | 0.10 | 0.32 | 185     | 174  | 192  | 1089 | 3    | 52     |        |          | 39.1 | 9      | 18,546 |
| DPA-36  | 0.01 | bdl     | 11.3 | 0.04 | 0.30 | 223     | 131  | 144  | 1025 | 6    | 67     |        |          | 37.2 | 10     | 22,266 |
| DPA-102 | 0.01 | bdl     | 27.3 | 1.08 | 0.62 | 385     | 547  | 604  | 2092 | 6    | 36     |        |          | 44.1 | 5      | 38,495 |
| DPA-103 | 23.3 | 3.9E-03 | 14.2 | 0.82 | 0.33 | 28,266  | 817  | 903  | 1115 | 71   | 1474   | 5909   | 1.69E-04 | 43.0 | 20,899 | 1213   |
| DPA-105 | 0.49 | bdl     | 18.3 | 0.98 | 0.39 | 514     | 405  | 448  | 1318 | 14   |        |        |          | 46.9 | 372    | 1049   |
| DPA-106 | 30.8 | 3.7E-03 | 15.3 | 0.66 | 0.32 | 42,416  | 914  | 1010 | 1078 | 1412 | 19,380 | 8323   | 1.20E-04 | 47.9 | 28,544 | 1379   |
| DPA-107 | 39.7 | 8.6E-03 | 11.1 | 0.01 | 0.31 | 169,761 | 1141 | 1261 | 1044 | 1003 | 2497   | 4062   | 2.46E-04 | 35.8 | 38,030 | 4276   |
| DPA-226 | 4.40 | 6.6E-04 | 25.2 | 0.01 | 0.46 | 55,365  | 524  | 579  | 1541 | 191  | 3498   | 6655   | 1.50E-04 | 55.3 | 2856   | 12,583 |
| DPA-227 | 29.1 | 4.8E-03 | 15.8 |      | 0.35 | 93,500  |      |      | 1166 | 143  | 4363   | 6053   | 1.65E-04 | 45.7 | 24,967 | 3213   |
| DPA-228 | 21.2 | 2.0E-03 | 17.9 | 0.01 | 0.41 | 79,633  | 889  | 983  | 1385 | 66   | 1490   | 10,733 | 9.32E-05 | 43.6 | 15,327 | 3751   |

*Wayne county*

|         |      |         |      |      |      |         |      |      |      |     |      |        |          |      |        |        |
|---------|------|---------|------|------|------|---------|------|------|------|-----|------|--------|----------|------|--------|--------|
| DPA-52  | 5.04 | 3.4E-04 | 20.1 | 0.15 | 0.40 | 29,967  | 480  | 530  | 1345 | 197 | 1340 | 14,800 | 6.76E-05 | 50.6 | 3746   | 5950   |
| DPA-53  | 5.39 | 4.9E-04 | 26.3 | 0.02 | 0.40 | 23,969  | 473  | 523  | 1355 | 54  | 190  | 11,011 | 9.08E-05 | 65.6 | 3979   | 4447   |
| DPA-54  | 3.05 | 2.4E-04 | 22.1 | 0.03 | 0.39 | 21,325  | 1021 | 1128 | 1331 | 45  | 690  | 12,667 | 7.89E-05 | 56.2 | 2289   | 7000   |
| DPA-241 | 39.8 | 3.3E-03 | 26.3 | 0.15 | 0.59 | 403,035 | 1754 | 1939 | 1993 | 993 | 5120 | 11,354 | 8.81E-05 | 44.5 | 19,967 | 10,127 |

*Sullivan county*

|         |      |         |      |      |      |        |     |     |      |     |     |      |          |      |      |        |
|---------|------|---------|------|------|------|--------|-----|-----|------|-----|-----|------|----------|------|------|--------|
| DPA-200 | 0.0  | bdl     | 12.0 | 0.16 | 0.34 | 39     | 168 | 186 | 1154 | 1   |     |      |          | 35.1 | 9    | 3888   |
| DPA-201 | 0.42 | 7.7E-05 | 11.6 | 0.01 | 0.27 | 2528   | 389 | 429 | 912  | 56  | 213 | 5473 | 1.83E-04 | 43.0 | 460  | 6019   |
| DPA-202 | 0.61 | 3.5E-03 | 14.3 | 0.01 | 0.31 | 1363   | 639 | 706 | 1047 | 128 | 427 | 175  | 5.71E-03 | 46.1 | 582  | 2234   |
| DPA-203 | 2.75 | 3.4E-04 | 15.3 | 0.01 | 0.29 | 28,411 | 413 | 456 | 980  | 145 | 967 | 8159 | 1.23E-04 | 52.8 | 2807 | 10,331 |
| DPA-204 | 0.01 | bdl     | 18.2 | 0.01 | 0.43 | 62     | 200 | 221 | 1463 | 2   | 41  |      |          | 41.9 | 7    | 6150   |
| DPA-205 | 0.01 | bdl     | 12.8 | 0.01 | 0.36 | 38     | 163 | 180 | 1206 |     | 29  |      |          | 35.8 | 8    | 3830   |
| DPA-206 | 0.01 | bdl     | 15.6 | 0.01 | 0.45 | 47     | 201 | 222 | 1530 |     | 48  |      |          | 34.4 | 7    | 4720   |
| DPA-207 | 0.01 | bdl     | 11.1 | 0.01 | 0.38 | 74     | 177 | 196 | 1287 | 4   | 34  |      |          | 29.2 | 8    | 7390   |
| DPA-208 | 0.01 | bdl     | 15.9 | 0.01 | 0.42 | 62     | 153 | 169 | 1432 | 9   | 67  |      |          | 37.5 | 7    | 6176   |
| DPA-209 | 0.98 | 1.0E-04 | 16.4 | 0.01 | 0.31 | 56     | 153 | 169 | 1061 | 5   | 28  | 9800 | 1.02E-04 | 52.3 | 924  | 57     |

*Lycoming county*

|         |      |         |      |      |      |        |     |     |      |    |     |        |          |      |        |      |
|---------|------|---------|------|------|------|--------|-----|-----|------|----|-----|--------|----------|------|--------|------|
| DPA-210 | 17.1 | 5.0E-04 | 21.4 | 0.01 | 0.35 | 189    | 156 | 173 | 1193 | 7  | 28  | 34,260 | 2.92E-05 | 60.5 | 14,364 | 11   |
| DPA-211 | 15.7 | 5.0E-04 | 19.5 | 0.01 | 0.35 | 164    | 162 | 179 | 1182 | 9  | 57  | 31,460 | 3.18E-05 | 55.7 | 13,303 | 10   |
| DPA-58  | 2.28 | 3.1E-04 | 14.6 | 0.57 | 0.34 | 15,239 | 501 | 554 | 1149 | 16 | 314 | 7321   | 1.37E-04 | 42.8 | 1985   | 6684 |

*New York**Sullivan county*

|         |      |     |      |      |      |    |     |     |      |   |    |  |  |      |   |      |
|---------|------|-----|------|------|------|----|-----|-----|------|---|----|--|--|------|---|------|
| DNY239  | 0.01 | bdl | 15.0 | 0.63 | 0.41 | 60 | 215 | 238 | 1383 | 9 | 89 |  |  | 36.6 | 9 | 4973 |
| DNY-240 | 0.01 | bdl | 13.1 | 0.00 | 0.38 | 42 | 174 | 192 | 1298 | 7 | 67 |  |  | 34.0 | 8 | 3787 |

*Delaware county*

|         |      |         |      |      |      |         |      |      |      |     |      |        |          |      |        |        |
|---------|------|---------|------|------|------|---------|------|------|------|-----|------|--------|----------|------|--------|--------|
| DNY-236 | 24.7 | 1.8E-03 | 21.0 | 0.56 | 0.51 | 181,906 | 1491 | 1648 | 1733 | 269 | 1930 | 13,650 | 7.33E-05 | 41.0 | 14,239 | 7374   |
| DNY-238 | 22.5 | 1.7E-03 | 19.6 | 0.69 | 0.50 | 142,433 | 1585 | 1751 | 1687 | 161 | 910  | 13,065 | 7.65E-05 | 39.3 | 13,317 | 6341   |
| DNY-242 | 0.02 | bdl     | 18.2 | 0.48 | 0.43 | 851     | 267  | 295  | 1467 | 6   | 40   |        |          | 41.8 | 12     | 48,381 |

*Broome county*

|         |      |         |      |      |      |         |     |     |      |     |      |        |          |      |        |        |
|---------|------|---------|------|------|------|---------|-----|-----|------|-----|------|--------|----------|------|--------|--------|
| DNY-243 | 37.5 | 2.8E-03 | 12.7 | 0.31 | 0.36 | 120,953 | 895 | 990 | 1199 | 250 | 1710 | 13,421 | 7.45E-05 | 35.8 | 31,243 | 3228   |
| DNY-244 | 0.00 | bdl     | 12.5 | 0.03 | 0.31 | 41      | 187 | 207 | 1062 | 7   | 90   |        |          | 39.9 | 3      | 13,157 |
| DNY-245 | 3.39 | 1.8E-04 | 16.1 | 0.02 | 0.35 | 14,539  | 320 | 354 | 1166 | 51  | 241  | 18,461 | 5.42E-05 | 46.8 | 2910   | 4287   |
| DNY-246 | 0.03 | bdl     | 18.9 | 0.61 | 0.49 | 762     | 357 | 394 | 1654 | 2   | 70   |        |          | 38.7 | 16     | 28,505 |

Table 2b

Stable carbon and hydrogen isotope ratios of methane and helium, neon, and argon isotope measurements in drinking-water samples in northeastern PA and southeastern NY.

| Sample                            | $\delta^{13}\text{C-C}_1$<br>(per mil) | $\delta^2\text{H-C}_1$<br>(per mil) | $^3\text{He}/^4\text{He}$ ( <i>R/Ra</i> )<br>( $\pm 1\sigma$ ) | $\frac{^{20}\text{Ne}}{^{22}\text{Ne}}$<br>( $\pm 1\sigma$ ) | $\frac{^{21}\text{Ne}}{^{22}\text{Ne}}$<br>( $\pm 1\sigma$ ) | $\frac{^{38}\text{Ar}}{^{36}\text{Ar}}$<br>( $\pm 1\sigma$ ) | $\frac{^{40}\text{Ar}}{^{36}\text{Ar}}$<br>( $\pm 1\sigma$ ) | $\frac{^{20}\text{Ne}}{^{36}\text{Ar}}$<br>( $\pm 1\sigma$ ) | $\frac{^4\text{He}}{^{20}\text{Ne}}$ | $\frac{^4\text{He}}{\text{Ne}}$ | $\frac{^4\text{He}}{^{36}\text{Ar}}$ | $^3\text{H}$<br>T.U. | Aquifer |       |       |      |      |          |
|-----------------------------------|--|-------------------------------------|--|--|--|--|--|--|--------------------------------------|---------------------------------|--------------------------------------|----------------------|---------|-------|-------|------|------|----------|
| <i>Pennsylvania</i>               |  |                                     |  |  |  |  |  |  |                                      |                                 |                                      |                      |         |       |       |      |      |          |
| <i>Susquehanna county</i>         |  |                                     |  |  |  |  |  |  |                                      |                                 |                                      |                      |         |       |       |      |      |          |
| DPA-1                             | −43.3                                  | −199.6                              | 0.03   | 0.000  | 9.78   | 0.079  | 0.0288   | 0.0003   | 0.1919                               | 0.0014                          | 295.0                                | 3.5                  | 0.26    | 19.2  | 17.4  | 5.0  | 0.4  | Alluvium |
| DPA-2                             | −42.9                                  | −180.4                              | 0.09   | 0.000  | 9.94   | 0.083  | 0.0288   | 0.0003   | 0.1873                               | 0.0019                          | 306.6                                | 2.4                  | 0.29    | 36.7  | 33.2  | 10.6 | 5.2  | Alluvium |
| DPA-3                             |  |                                     | 0.15   | 0.001  | 9.92   | 0.076  | 0.0292   | 0.0004   | 0.2051                               | 0.0016                          | 301.1                                | 2.3                  | 0.20    | 16.0  | 14.5  | 3.3  | 3.9  | Alluvium |
| DPA-4                             |  |                                     | 0.04   | 0.000  | 9.83   | 0.075  | 0.0287   | 0.0002   | 0.1895                               | 0.0021                          | 305.3                                | 2.4                  | 0.44    | 15.5  | 14.0  | 6.8  | 0.4  | Alluvium |
| DPA-5                             |  |                                     | 0.62   | 0.003  | 9.87   | 0.088  | 0.0287   | 0.0003   | 0.1969                               | 0.0016                          | 307.1                                | 1.9                  | 0.15    | 0.4   | 0.4   | 0.06 | 8.9  | Catskill |
| DPA-6                             |  |                                     | 0.12   | 0.001  | 9.89   | 0.097  | 0.0286   | 0.0003   | 0.1915                               | 0.0008                          | 300.8                                | 1.7                  | 0.17    | 31.6  | 28.6  | 5.3  | 5.1  | Catskill |
| DPA-7                             | −45.8                                  | −243.0                              | 0.02   | 0.000  | 9.80   | 0.096  | 0.0291   | 0.0003   | 0.1858                               | 0.0011                          | 304.8                                | 1.9                  | 0.22    | 22.2  | 20.1  | 4.9  | 2.4  | Catskill |
| DPA-9                             |  |                                     | 0.56   | 0.003  |  |  |  |  | 0.1854                               | 0.0014                          | 299.9                                | 2.2                  | 0.21    | 0.6   | 0.5   | 0.13 | 3.4  | Catskill |
| DPA-10                            |  |                                     | 1.32   | 0.007  |  |  |  |  | 0.1873                               | 0.0016                          | 295.4                                | 1.9                  | 0.15    | 0.4   | 0.4   | 0.06 | 1.1  | Catskill |
| DPA-13                            | −55.9                                  | −237.0                              | 0.24   | 0.001  |  |  |  |  | 0.1876                               | 0.0013                          | 296.5                                | 2.2                  | 0.24    | 0.7   | 0.6   | 0.17 | 0.6  | Alluvium |
| DPA-14                            |  |                                     | 0.75   | 0.003  |  |  |  |  | 0.1898                               | 0.0011                          | 296.0                                | 1.9                  | 0.24    | 0.4   | 0.4   | 0.10 | 1.4  | Catskill |
| DPA-21                            |  |                                     | 1.10   | 0.003  | 9.84   | 0.096  | 0.0289   | 0.0002   | 0.1906                               | 0.0013                          | 299.5                                | 2.2                  | 0.19    | 0.3   | 0.2   | 0.05 | 3.7  | Catskill |
| DPA-22                            |  |                                     | 0.80   | 0.004  | 9.78   | 0.078  | 0.0284   | 0.0003   | 0.1876                               | 0.0015                          | 297.0                                | 2.6                  | 0.14    | 0.4   | 0.3   | 0.05 |      | Catskill |
| DPA-26                            |  |                                     | 1.26   | 0.005  | 10.03  | 0.098  | 0.0299   | 0.0002   | 0.1939                               | 0.0011                          | 300.6                                | 1.4                  | 0.34    | 0.3   | 0.3   | 0.10 | 5.2  | Catskill |
| DPA-27                            |  |                                     | 1.10   | 0.005  |  |  |  |  | 0.1928                               | 0.0011                          | 309.5                                | 1.9                  | 0.12    | 0.2   | 0.2   | 0.03 | 5.0  | Catskill |
| DPA-39                            | −44.1                                  | −196.5                              | 0.03   | 0.000  |  |  |  |  |                                      |                                 |                                      |                      | 0.54    | 18.1  | 16.4  | 9.7  |      | Catskill |
| DPA-41                            |  |                                     | 0.09   | 0.000  | 9.76   | 0.096  | 0.0289   | 0.0002   | 0.1998                               | 0.0012                          | 296.7                                | 1.1                  | 0.23    | 4.9   | 4.5   | 1.1  |      | Catskill |
| DPA-42                            |  |                                     | 0.99   | 0.004  | 9.79   | 0.096  | 0.0300   | 0.0002   | 0.1984                               | 0.0010                          | 298.2                                | 1.9                  | 0.17    | 0.3   | 0.2   | 0.04 | 3.1  | Catskill |
| DPA-74                            |  |                                     | 1.01   | 0.004  | 9.66   | 0.094  | 0.0294   | 0.0001   | 0.1919                               | 0.0015                          | 297.6                                | 2.3                  | 0.15    | 0.4   | 0.3   | 0.06 | 8.8  | Catskill |
| DPA-81                            |  |                                     | 0.11   | 0.000  | 9.95   | 0.094  | 0.0286   | 0.0003   | 0.1897                               | 0.0015                          | 295.5                                | 2.2                  | 0.20    | 3.9   | 3.5   | 0.77 |      | Catskill |
| DPA-82                            |  |                                     | 0.51   | 0.002  | 9.99   | 0.094  | 0.0290   | 0.0002   | 0.1928                               | 0.0015                          | 300.3                                | 1.6                  | 0.17    | 0.7   | 0.6   | 0.12 | 2.6  | Catskill |
| DPA-85                            |  |                                     | 0.10   | 0.000  | 9.88   | 0.096  | 0.0281   | 0.0002   | 0.1878                               | 0.0013                          | 294.3                                | 1.9                  | 0.19    | 4.3   | 3.9   | 0.8  | 2.4  | Catskill |
| DPA-212                           |  |                                     | 1.22   | 0.007  | 9.86   | 0.078  | 0.0291   | 0.0003   | 0.1909                               | 0.0015                          | 294.0                                | 2.2                  | 0.15    | 0.3   | 0.3   | 0.05 | 11.7 | Catskill |
| DPA-213                           |  |                                     | 1.07   | 0.004  | 9.94   | 0.096  | 0.0287   | 0.0003   | 0.1932                               | 0.0019                          | 299.0                                | 1.4                  | 0.15    | 0.3   | 0.3   | 0.04 | 5.0  | Catskill |
| DPA-214                           |  |                                     | 0.59   | 0.002  | 9.76   | 0.085  | 0.0289   | 0.0003   | 0.1912                               | 0.0019                          | 298.9                                | 2.3                  | 0.18    | 0.5   | 0.5   | 0.09 |      | Catskill |
| DPA-215                           | −43.1                                  |                                     | 0.06   | 0.000  | 9.90   | 0.098  | 0.0284   | 0.0002   | 0.1890                               | 0.0021                          | 295.1                                | 2.6                  | 0.45    | 5.6   | 5.0   | 2.5  |      | Catskill |
| DPA-216                           |  |                                     | 0.97   | 0.004  | 10.01  | 0.120  | 0.0291   | 0.0003   | 0.1860                               | 0.0014                          | 297.3                                | 2.3                  | 0.21    | 18.9  | 17.1  | 4.1  | 1.0  | Catskill |
| DPA-217                           | −53.9                                  |                                     | 1.04   | 0.004  |  |  |  |  | 0.1907                               | 0.0019                          | 294.7                                | 1.7                  | 0.25    | 25.6  | 23.2  | 6.4  | 5.3  | Catskill |
| DPA-218                           | −56.7                                  | −168.4                              | 0.05   | 0.000  |  |  |  |  | 0.1917                               | 0.0015                          | 303.4                                | 2.4                  | 0.50    | 31.3  | 28.3  | 15.6 |      | Catskill |
| DPA-219                           |  |                                     | 0.48   | 0.002  |  |  |  |  |                                      |                                 | 304.6                                | 2.4                  | 0.34    | 4.4   | 4.0   | 1.5  |      | Catskill |
| DPA-220                           | −59.5                                  | −171.3                              | 0.05   | 0.000  |  |  |  |  | 0.1859                               | 0.0018                          | 298.7                                | 2.9                  | 0.46    | 50.9  | 46.0  | 23.5 |      | Catskill |
| DPA-221                           |  |                                     | 0.17   | 0.001  |  |  |  |  |                                      |                                 |                                      |                      | 0.13    | 8.9   | 8.0   | 1.1  | 0.2  | Catskill |
| DPA-222                           | −54.3                                  | −164.9                              | 0.22   | 0.001  |  |  |  |  |                                      |                                 |                                      |                      | 0.23    | 8.5   | 7.7   | 2.0  | 0.1  | Catskill |
| DPA-223                           | −54.4                                  | −165.2                              | 0.07   | 0.000  |  |  |  |  | 0.1881                               | 0.0019                          | 314.1                                | 2.9                  | 0.28    | 29.5  | 26.7  | 8.2  |      | Catskill |
| DPA-224                           | −36.7                                  | −146.0                              | 0.02   | 0.000  |  |  |  |  |                                      |                                 |                                      |                      | 0.72    | 19.9  | 18.0  | 14.3 |      | Catskill |
| DPA-225                           | −68.3                                  | −312.4                              | 1.01   | 0.004  | 9.83   | 0.098  | 0.0284   | 0.0003   | 0.1880                               | 0.0005                          | 294.7                                | 2.9                  | 0.15    | 0.2   | 0.2   | 0.03 | 5.2  | Catskill |
| <i>Salt Spring (Montrose, PA)</i> |  |                                     |  |  |  |  |  |  |                                      |                                 |                                      |                      |         |       |       |      |      |          |
| DPA-8                             | −45.8                                  | −243.0                              | 0.02   | 0.000  | 10.02  | 0.084  | 0.0293   | 0.0002   | 0.2007                               | 0.0020                          | 304.8                                | 1.4                  | 0.31    | 254.1 | 229.9 | 78.1 | 2.5  | Catskill |

|                          |       |        |      |       |       |       |        |        |        |        |       |     |      |       |       |       |     |            |
|--------------------------|-------|--------|------|-------|-------|-------|--------|--------|--------|--------|-------|-----|------|-------|-------|-------|-----|------------|
| <i>Bradford county</i>   |       |        |      |       |       |       |        |        |        |        |       |     |      |       |       |       |     |            |
| DPA-34                   |       |        | 0.18 | 0.001 | 9.87  | 0.083 | 0.0287 | 0.0003 | 0.1912 | 0.0015 | 298.0 | 1.8 | 0.16 | 1.1   | 1.0   | 0.17  | 0.7 | Lock Haven |
| DPA-36                   |       |        | 0.17 | 0.000 | 9.84  | 0.085 | 0.0286 | 0.0003 | 0.1960 | 0.0015 | 297.5 | 2.2 | 0.13 | 1.7   | 1.5   | 0.22  |     | Lock Haven |
| DPA-102                  |       |        | 0.55 | 0.002 | 10.00 | 0.088 | 0.0289 | 0.0002 | 0.1897 | 0.0027 | 295.6 | 1.9 | 0.26 | 0.7   | 0.6   | 0.18  |     | Lock Haven |
| DPA-103                  | -41.7 | -195.0 | 0.10 | 0.000 | 10.01 | 0.085 | 0.0286 | 0.0002 | 0.1900 | 0.0028 | 296.1 | 2.1 | 0.73 | 34.6  | 31.3  | 25.4  | 0.2 | Lock Haven |
| DPA-105                  | -66.5 |        | 0.91 | 0.004 | 9.90  | 0.084 | 0.0289 | 0.0003 | 0.1959 | 0.0015 | 298.6 | 2.0 | 0.31 | 1.3   | 1.1   | 0.39  | 5.3 | Lock Haven |
| DPA-106                  | -56.0 | -204.9 | 0.02 | 0.000 | 9.92  | 0.088 | 0.0287 | 0.0003 | 0.1891 | 0.0013 | 307.1 | 2.7 | 0.85 | 46.4  | 42.0  | 39.4  | 4.7 | Lock Haven |
| DPA-107                  | -52.2 | -237.0 | 0.04 | 0.000 | 9.96  | 0.089 | 0.0286 | 0.0003 | 0.1898 | 0.0011 | 303.5 | 2.3 | 1.09 | 148.8 | 134.6 | 162.6 |     | Lock Haven |
| DPA-226                  | -71.1 | -215.0 | 0.04 | 0.000 | 9.93  | 0.097 | 0.0279 | 0.0001 | 0.1940 | 0.0009 | 295.3 | 2.0 | 0.34 | 105.7 | 95.7  | 35.9  |     | Alluvium   |
| DPA-227                  | -48.6 | -225.5 |      | 0.000 |       |       |        |        | 0.1860 | 0.0016 | 297.2 | 2.6 |      | n/a   |       | 80.2  |     | Alluvium   |
| DPA-228                  | -50.4 | -211.1 | 0.03 | 0.000 |       |       |        |        | 0.1890 | 0.0011 | 296.1 | 1.7 | 0.64 | 89.6  | 81.0  | 57.5  |     | Lock Haven |
| <i>Wayne county</i>      |       |        |      |       |       |       |        |        |        |        |       |     |      |       |       |       |     |            |
| DPA-52                   | -43.1 | -202.8 | 0.03 | 0.000 | 9.97  | 0.087 | 0.0287 | 0.0003 | 0.1929 | 0.0013 | 305.6 | 2.4 | 0.36 | 62.5  | 56.5  | 22.3  | 4.3 | Catskill   |
| DPA-53                   | -56.5 | -220.9 | 0.04 | 0.000 | 10.00 | 0.098 | 0.0293 | 0.0002 | 0.1768 | 0.0014 | 295.9 | 1.7 | 0.35 | 50.7  | 45.8  | 17.7  | 5.0 | Catskill   |
| DPA-54                   | -45.2 | -197.5 | 0.04 | 0.000 | 9.93  | 0.086 | 0.0286 | 0.0003 | 0.1868 | 0.0011 | 304.5 | 2.4 | 0.77 | 690.0 | 18.9  | 16.0  | 5.4 | Catskill   |
| DPA-241                  | -43.8 | -219.1 | 0.02 | 0.000 | 10.09 | 0.087 | 0.0288 | 0.0003 | 0.1920 | 0.0013 | 308.0 | 1.5 | 0.88 | 229.8 | 207.9 | 202.2 | 2.0 | Catskill   |
| <i>Sullivan county</i>   |       |        |      |       |       |       |        |        |        |        |       |     |      |       |       |       |     |            |
| DPA-200                  |       |        | 0.98 | 0.005 |       |       |        |        |        |        |       |     | 0.15 | 0.23  | 0.2   | 0.03  |     | Lock Haven |
| DPA-201                  | -44.8 | -195.9 | 0.05 | 0.000 | 9.89  | 0.079 | 0.0290 | 0.0003 | 0.1768 | 0.0014 | 296.7 | 3.8 | 0.43 | 6.5   | 5.9   | 2.8   |     | Alluvium   |
| DPA-202                  | -39.8 | -187.7 | 0.06 | 0.000 | 9.92  | 0.079 | 0.0288 | 0.0002 | 0.1929 | 0.0013 | 297.3 | 1.4 | 0.61 | 2.1   | 1.9   | 1.3   |     | Alluvium   |
| DPA-203                  | -54.8 |        | 0.15 | 0.001 |       |       |        |        |        |        |       |     | 0.42 | 68.8  | 62.3  | 29.0  | 2.1 | Alluvium   |
| DPA-204                  |       |        | 1.15 | 0.005 | 9.94  | 0.080 | 0.0287 | 0.0003 | 0.1768 | 0.0010 | 296.6 | 2.3 | 0.17 | 0.31  | 0.3   | 0.04  | 5.0 | Lock Haven |
| DPA-205                  |       |        | 0.91 | 0.004 |       |       |        |        | 0.1929 | 0.0015 | 296.5 | 2.0 | 0.13 | 0.24  | 0.2   | 0.03  | 7.3 | Alluvium   |
| DPA-206                  |       |        | 0.89 | 0.004 |       |       |        |        |        |        |       |     | 0.13 | 0.23  | 0.2   | 0.03  |     | Lock Haven |
| DPA-207                  |       |        | 0.52 | 0.002 |       |       |        |        |        |        |       |     | 0.14 | 0.42  | 0.4   | 0.06  |     | Lock Haven |
| DPA-208                  |       |        | 1.25 | 0.005 | 9.88  | 0.088 | 0.0287 | 0.0003 | 0.1768 | 0.0010 | 297.1 | 2.6 | 0.11 | 0.40  | 0.4   | 0.04  |     | Lock Haven |
| DPA-209                  | -67.8 |        | 0.73 | 0.003 | 9.83  | 0.087 | 0.0283 | 0.0003 | 0.2100 | 0.0017 | 298.1 | 2.0 | 0.14 | 0.37  | 0.3   | 0.05  |     | Lock Haven |
| <i>Lackawanna county</i> |       |        |      |       |       |       |        |        |        |        |       |     |      |       |       |       |     |            |
| DPA-210                  | -64.7 | -331.2 | 0.84 | 0.004 | 9.68  | 0.084 | 0.0285 | 0.0003 | 0.1880 | 0.0011 | 295.4 | 2.3 | 0.13 | 1.21  | 1.1   | 0.16  | 6.2 | Lock Haven |
| DPA-211                  | -66.1 | -326.0 | 0.88 | 0.004 | 9.73  | 0.087 | 0.0291 | 0.0002 | 0.1790 | 0.0012 | 295.5 | 1.7 | 0.14 | 1.01  | 0.9   | 0.14  | 5.8 | Lock Haven |
| DPA-58                   | -53.7 |        | 0.20 | 0.001 |       |       |        |        |        |        |       |     | 0.44 | 30.4  | 27.5  | 13.3  |     | Catskill   |
| <i>New York</i>          |       |        |      |       |       |       |        |        |        |        |       |     |      |       |       |       |     |            |
| <i>Sullivan county</i>   |       |        |      |       |       |       |        |        |        |        |       |     |      |       |       |       |     |            |
| DNY239                   |       |        | 0.89 | 0.004 | 10.05 | 0.098 | 0.0287 | 0.0003 | 0.1899 | 0.0012 | 298.9 | 2.0 | 0.16 | 0.3   | 0.3   | 0.04  |     | Catskill   |
| DNY-240                  |       |        | 0.75 | 0.003 | 9.92  | 0.077 | 0.0289 | 0.0002 | 0.1889 | 0.0013 | 293.1 | 1.9 | 0.13 | 0.2   | 0.2   | 0.03  | 8.9 | Catskill   |
| <i>Delaware county</i>   |       |        |      |       |       |       |        |        |        |        |       |     |      |       |       |       |     |            |
| DNY-236                  | -50.5 | -215.1 | 0.03 | 0.000 | 10.01 | 0.098 | 0.0287 | 0.0002 | 0.1957 | 0.0019 | 302.1 | 2.4 | 0.86 | 122.0 | 110.4 | 105.0 | 2.1 | Catskill   |
| DNY-238                  | -41.6 | -220.0 | 0.02 | 0.000 | 9.98  | 0.100 | 0.0281 | 0.0002 | 0.1984 | 0.0022 | 306.6 | 2.4 | 0.94 | 89.9  | 81.3  | 84.4  | 4.1 | Catskill   |
| DNY-242                  |       |        | 0.13 | 0.001 | 9.94  | 0.097 | 0.0287 | 0.0003 | 0.1901 | 0.0013 | 296.6 | 2.3 | 0.18 | 3.2   | 2.9   | 0.58  |     | Catskill   |
| <i>Broome county</i>     |       |        |      |       |       |       |        |        |        |        |       |     |      |       |       |       |     |            |
| DNY-243                  | -45.8 | -180.7 | 0.03 | 0.000 | 10.08 | 0.098 | 0.0293 | 0.0001 | 0.1939 | 0.0015 | 301.8 | 2.4 | 0.75 | 135.1 | 122.2 | 100.9 |     | Catskill   |
| DNY-244                  |       |        | 0.94 | 0.004 | 9.83  | 0.097 | 0.0284 | 0.0002 | 0.1895 | 0.0013 | 297.1 | 2.2 | 0.18 | 0.2   | 0.2   | 0.04  | 4.8 | Catskill   |
| DNY-245                  | -48.5 | -199.9 | 0.04 | 0.000 | 10.01 | 0.098 | 0.0297 | 0.0003 | 0.1859 | 0.0016 | 297.9 | 2.0 | 0.27 | 45.4  | 41.1  | 12.5  |     | Catskill   |
| DNY-246                  |       |        | 0.18 | 0.001 | 9.98  | 0.100 | 0.0289 | 0.0003 | 0.1910 | 0.0016 | 297.5 | 1.4 | 0.22 | 2.1   | 1.9   | 0.46  |     | Catskill   |

of a previous study (Warner et al., 2012), all data reported here represent a more recent sample collection and analyses including 38 domestic water wells that were not previously collected or analyzed. All samples ( $n = 73$ ) were analyzed for their major gas abundance (e.g., CH<sub>4</sub>, C<sub>2</sub>H<sub>6</sub>, N<sub>2</sub>, O<sub>2</sub>) and noble gas composition (He, Ne, Ar, and their isotopes) according to standard methods reported previously (Darrah et al., 2014). The stable carbon isotopic composition of methane ( $\delta^{13}\text{C-CH}_4$ ) was determined for all samples with [CH<sub>4</sub>] exceeding 0.5 cm<sup>3</sup> STP/L ( $n = 36$ ), while paired stable hydrogen isotopic composition ( $\delta^2\text{H-CH}_4$ ) is available for  $n = 30$  of the samples included in this study.

Before sampling, wells were flowed to remove stagnant water and simultaneously monitored for pH, electrical conductance, and temperature until stable values were obtained. Water samples were collected prior to any treatment systems and were filtered and preserved following USGS protocols (USGS, 2011). The methods for the analysis of inorganic constituents were identical to those reported previously (Warner et al., 2012). Dissolved hydrocarbon gas samples were collected in the field using procedures detailed by Isotech Laboratories (Isotech, 2011), stored on ice until delivery to their facilities, and analyzed for methane, ethane, and propane concentrations and isotopic compositions of methane. Procedures for gas analyses were summarized previously (Osborn et al., 2011; Jackson et al., 2013). Isotech Laboratories used chromatographic separation followed by combustion and dual-inlet isotope ratio mass spectrometry to measure dissolved gas concentrations and  $\delta^{13}\text{C-CH}_4$  (detection limits for C<sub>1</sub>, C<sub>2</sub>, and C<sub>3</sub> were 0.001, 0.0005, and 0.0001 mol%, respectively).

Noble gas samples were collected in refrigeration-grade copper tubes that were flushed in-line with at least 50 volumes of sample water prior to sealing with stainless steel clamps. In the laboratory, the fluid was extracted from the copper tube on a vacuum line and sonicated for ~30 min to ensure complete transfer of dissolved gases to the sample inlet line (Solomon et al., 1995). Major gas components (e.g., N<sub>2</sub>, O<sub>2</sub>, Ar, CH<sub>4</sub>, C<sub>2</sub>H<sub>6</sub>) were measured using an SRS quadrupole mass spectrometer (MS) and an SRI gas chromatograph (GC) (Hunt et al., 2012; Darrah et al., 2013). The isotopic analyses of noble gases were performed using a VG 5400 MS at the University of Rochester Rare Gas Lab following methods reported previously (Darrah and Poreda, 2012; Hunt et al., 2012; Darrah et al., 2013). Standard analytical errors were  $\pm 3\%$  for noble gas concentrations ( $^4\text{He}$ ] (1.45%),  $^{22}\text{Ne}$ ] (1.61%), and  $^{40}\text{Ar}$ ] (1.59%)). Isotopic errors were approximately  $\pm 0.01$  times the ratio of air (or  $1.4 \times 10^{-8}$ ) for  $^3\text{He}/^4\text{He}$  ratio,  $< \pm 0.5\%$  and  $< \pm 1\%$  for  $^{20}\text{Ne}/^{22}\text{Ne}$  and  $^{21}\text{Ne}/^{22}\text{Ne}$ , respectively, and  $< \pm 1\%$  for  $^{38}\text{Ar}/^{36}\text{Ar}$  and  $^{40}\text{Ar}/^{36}\text{Ar}$ , respectively (higher than normal because of interferences from C<sub>3</sub> on mass = 36). Errors for individual samples are shown in Table 2b.

To evaluate the potential for *in-situ* radiogenic production and/or release of  $^4\text{He}$ , we analyzed the [U] and [Th] in Catskill and Lock Haven outcrop samples collected in Susquehanna and Bradford counties. Analyses were conducted by standard methods using inductively coupled plasma mass spectrometry (ICP-MS) (Darrah et al., 2009; Cuoco et al., 2013). Tritium analyses were performed on

43 groundwater samples, including a sample from Salt Spring State Park, to evaluate the contributions from modern meteoric water. Tritium concentrations were measured by the in-growth of  $^3\text{He}$  using a VG 5400 noble gas MS at the University of Rochester by methods reported previously (Solomon et al., 1992, 1995).

### 3.3. Numerical modeling

When combined, noble gases and the composition of gas-phase hydrocarbons (i.e., molecular and stable isotopic compositions) provide powerful tracers of gas migration processes (e.g., Gilfillan et al., 2009; Hunt et al., 2012). Previous work suggests that diffusion, single-phase advection, and/or dual-phase advection may control the movement of fluids and post-genetic modification of natural gases in the Earth's crust (e.g., Prinzhofer and Pernaton, 1997; Lorant et al., 1998; Gilfillan et al., 2009; Pape et al., 2010; Xia and Tang, 2012; Darrah et al., 2014). Herein, we apply numerical models to investigate and constrain the subsurface conditions and viable mechanisms of gas transport to shallow aquifers including: (1) single-phase advection of methane-rich brine (gas dissolved in water); (2) "buoyant" advection of a gas-phase natural gas; (3) two-phase advection (i.e., free gas + brine); and (4) aqueous diffusion of gases. Mechanisms 1 (gray), 2 and 3 (red), and 4 (green) are shown as dashed color-coded lines in Figs. 10 and 11.

All models assume: (1) that the initial ASW composition of shallow drinking-water wells are consistent with recently recharged meteoric water. Note that this assumption is supported by the minor presence of tritium, local meteoric water line-like composition of water isotopes ( $\delta^2\text{H-H}_2\text{O}$  and  $\delta^{18}\text{O-H}_2\text{O}$ ) (Warner et al., 2012), non-detectable methane, low salinity, and ASW-like composition in many samples. Groundwater recharged under these conditions is assumed to have a salinity of zero and to have equilibrated at  $\sim 10^\circ\text{C}$  at an elevation of 600 m (i.e., present day equilibration conditions for shallow groundwater in this area). Under these conditions, the  $^{20}\text{Ne}$  and  $^{36}\text{Ar}$  in ASW are  $171 \times 10^{-6}$  cm<sup>3</sup> STP/L and  $1223 \times 10^{-6}$  cm<sup>3</sup> STP/L, respectively; (2) the starting natural gas composition of migrated hydrocarbon gases are consistent with Marcellus production gas:  $^{20}\text{Ne}/^{36}\text{Ar} = 0.10$ ,  $^4\text{He}/\text{CH}_4 = 350$  ( $\times 10^{-6}$ ),  $\text{C}_2+\text{C}_1 = 0.018$ , and  $\delta^{13}\text{C-CH}_4 = -33\text{‰}$  to  $-28\text{‰}$  generated at an initial reservoir depth of  $\sim 2500$  m and  $\sim 1$  M NaCl. We use a Marcellus-like starting composition because it is the shallowest major hydrocarbon-producing unit in the current study area (Fig. 1) and the inorganic geochemistry (e.g.,  $^{87}\text{Sr}/^{86}\text{Sr}$ ) of shallow brines in this area are consistent with a Marcellus-like source (Warner et al., 2012); and (3) hydrocarbon generation and migration conditions (salinity, geothermal gradient, etc.) are consistent with the conditions of the NAB. Because the evidence for mantle contributions  $> 1\%$  within our current study are limited to a subset of four samples with low salt content and hydrocarbon gas levels, we do not incorporate hydrothermal circulation into our numerical or physical transport models for the hydrocarbon-gas and salt-rich fluids. Similarly, due to a lack of empirical or field-based evidence for oil-phase hydrocarbons in our study, we do

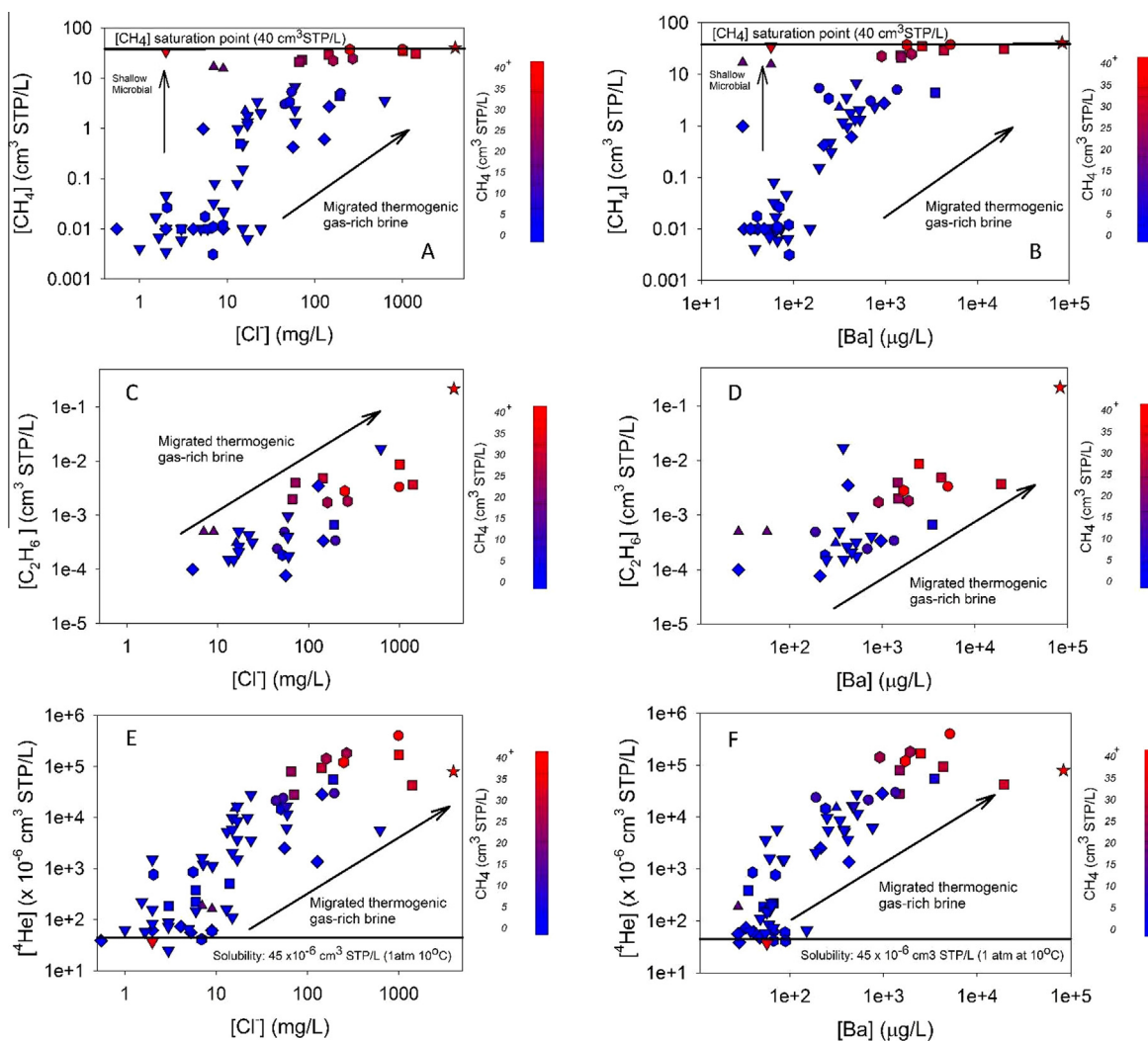


Fig. 3. Variations of  $[\text{CH}_4]$ ,  $[\text{C}_2\text{H}_6]$ , and  $[\text{He}]$  compared to  $[\text{Cl}]$  and  $[\text{Ba}]$  in groundwater (symbol designations shown in Section 3.1) and a natural salt-rich spring (Salt Spring State Park, Montrose, PA shown as a star) located  $\gg 1$  km from active shale gas drilling in PA and NY at the time of sampling. In general,  $\text{CH}_4$ ,  $\text{C}_2\text{H}_6$ , and  ${}^4\text{He}$  concentrations increase with brine components (i.e., Cl and Ba) (or Br, not shown) across the study area. The Cl-rich fluids contain elevated  $\text{Br}^-/\text{Cl}^-$  and Ba/Sr, as well as  ${}^{87}\text{Sr}/{}^{86}\text{Sr}$  consistent with Middle Devonian Formation brines (i.e., Marcellus-like) (Warner et al., 2012). Notice that the increase in  $[\text{CH}_4]$  “rolls over” as methane concentrations approach saturation levels for shallow groundwater. The upper level (saturation = 40 ccSTP/L at 10 °C and 1 atm) for  $[\text{CH}_4]$  demonstrates how groundwater saturation or “bubble point” limits constrain the maximum dissolved gas concentrations in natural conditions. The positive correlations of  $[\text{CH}_4]$ ,  $[\text{C}_2\text{H}_6]$ , and  $[\text{He}]$  with  $[\text{Cl}]$  and  $[\text{Ba}]$  suggest the coherent migration of a gas-rich, saline fluid from deeper formations into Upper Devonian aquifers across the region that has been recently diluted by meteoric water. The coexistence of  $\text{CH}_4$ ,  $\text{C}_2\text{H}_6$ , and  ${}^4\text{He}$  suggests a thermogenic source for the hydrocarbon gases.

not incorporate oil–gas partitioning into our numerical models for the hydrocarbon-gas and salt-rich fluids.

We model Mechanism 1 (single-phase advection; gray trend in Fig. 10) assuming gas and brine migrate as a single-phase fluid (i.e., no free gas-phase is present) and thus does not experience any gas-phase partitioning. In this scenario (i.e.,  $V_{\text{gas}}/V_{\text{liquid}} = 0$ ), the ASW noble gases (e.g.,  ${}^{20}\text{Ne}/{}^{36}\text{Ar}$ ) would not experience any quantifiable fractionation of ASW components in the absence of multiple phases (e.g., gas + water) (Ballentine et al., 2002). However, the migrating fluid would accumulate radiogenic  ${}^4\text{He}$  from the country rock, resulting in an increase in the  ${}^4\text{He}/\text{CH}_4$ .

Mechanisms 2 and 3 (dashed red lines) assume a free gas-phase or dual-phase (i.e., brine + free gas) fluid migrates within a crustal matrix that contains static, capillary bound, or connate pore fluids (e.g., crustal water). In this scenario, gases would partition according to their respective solubilities (Smith and Kennedy, 1982; Ballentine et al., 2002). The Bunsen solubility ( $\beta$ ) constants for the noble gases are determined using Weiss (1971a, 1971b) and Smith and Kennedy (1982), while the partition coefficients ( $\alpha = \beta_x/\beta_y$ ) are calculated following Smith and Kennedy (1982) and Ballentine et al. (2002). Because the timing and thermal history for natural gas migration is uncertain, we model a range of temperature

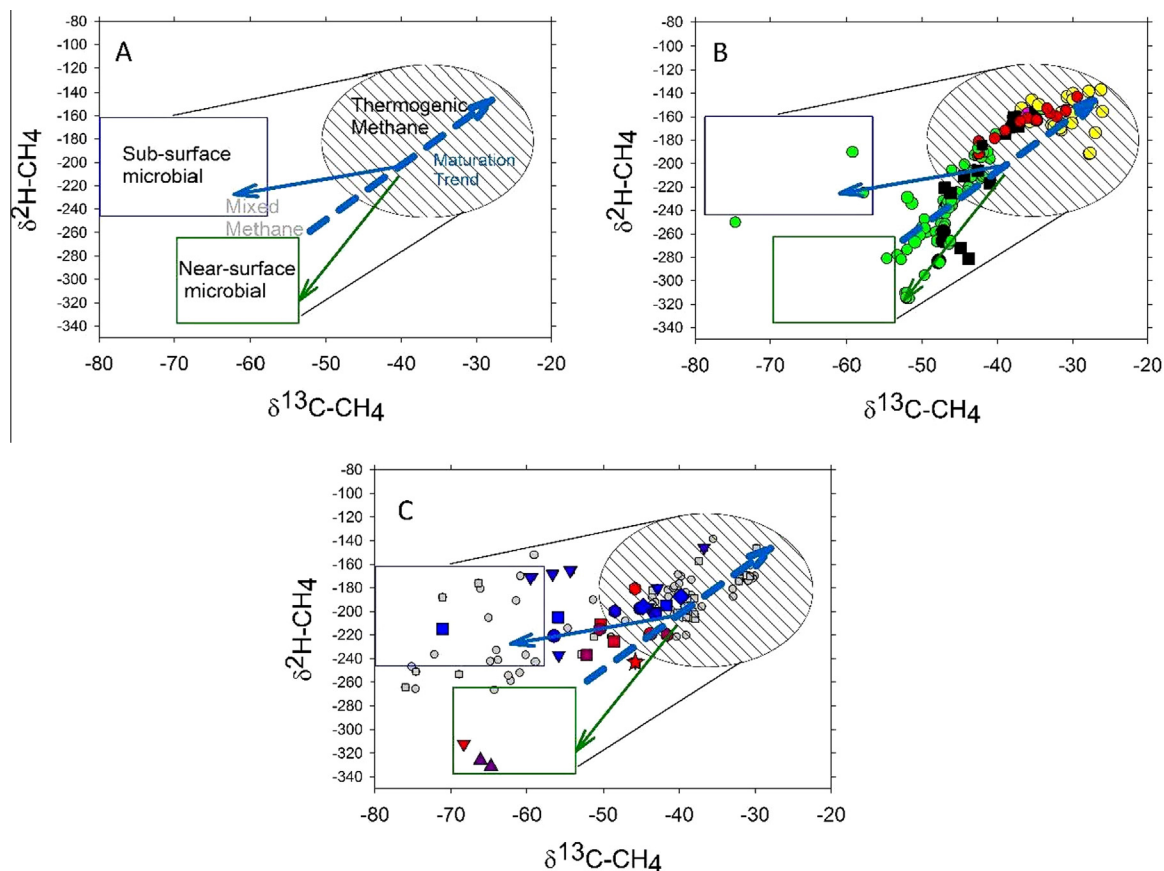


Fig. 4. Hydrogen ( $\delta^2\text{H-CH}_4$ ) versus carbon ( $\delta^{13}\text{C-CH}_4$ ) isotopic compositions of possible natural gas sources (a-top); Ordovician (yellow circles), Silurian (black squares), Marcellus (red circles), and Upper Devonian (green circles) production gases from PA and NY regions of the NAB (e.g., Jenden et al., 1993; Laughrey and Baldassare, 1998; Burruss and Laughrey, 2010; Osborn and McIntosh, 2010) (b-middle); and dissolved methane in shallow groundwater across the region (c-bottom). The conventional interpretation of this plot relates the isotopic composition ( $\delta^2\text{H-CH}_4$  and  $\delta^{13}\text{C-CH}_4$ ) of methane to the thermal maturity of the source (trend of increasing maturity producing heavier  $\delta^2\text{H-CH}_4$  and  $\delta^{13}\text{C-CH}_4$  shown in the thick dashed blue line (a)) (e.g., Schoell, 1983). Gas produced by microbes (green and blue boxes) yield lighter isotopic ratios for  $\text{CH}_4$ , while intermediate values are assumed to represent mixing between thermogenic and biogenic end-members (trends shown with blue and green arrows). The “subsurface” and “near-surface” microbial end-members both have light  $\delta^{13}\text{C-CH}_4$ , but are distinguishable by lighter  $\delta^2\text{H-CH}_4$  in “near-surface” microbial  $\text{CH}_4$ . The Ordovician and Middle-Devonian (Marcellus) production gases in NAB are characterized by “dry thermogenic” composition, while most oil-associated Upper Devonian gases exhibit either a composition along a “mixing” trend between dry thermogenic and sub-surface microbial end-members or alternatively may represent gases formed during the early evolution of hydrocarbon gases associated with oil (b). Isotopic data of methane in groundwater (c) is based on previous publications (marked by gray squares (Revesz et al., 2010) and gray circles (Jackson et al., 2013)) and our new data collected  $\geq 1$  km from shale gas development (colored symbols). The isotopic variations of carbon and hydrogen (i.e.,  $\delta^2\text{H-CH}_4$  and  $\delta^{13}\text{C-CH}_4$ ) follow an apparent mixing relationship between “dry thermogenic” and “subsurface microbial” natural gas. (For interpretation of the references to color in this figure legend, the reader is referred to the web version of this article.)

conditions (a proxy for burial depth), assuming a standard geothermal gradient (i.e.,  $25\text{ }^\circ\text{C/km}$ ). The modeled temperatures range from 0 to  $>200\text{ }^\circ\text{C}$ . Since all groundwater wells were sampled at depths  $<90$  m, Bunsen solubility constants ( $\beta$  values: e.g.,  $\beta_{\text{Ne}}/\beta_{\text{Ar}}$ ) were not corrected for geothermal gradients. The solubility fractionation model adapts the GGS-R model developed for  $\text{CO}_2$  (Gilfillan et al., 2008, 2009; Zhou et al., 2012), and previously adapted for hydrocarbons (Darrah et al., 2014), to evaluate the fractionation of atmospheric (i.e.,  $^{20}\text{Ne}/^{36}\text{Ar}$ ) and crustally-derived components (e.g.,  $^4\text{He}/\text{CH}_4$ ,  $\text{C}_2+\text{C}_1$ , and  $\delta^{13}\text{C-CH}_4$ ).

The two-stage groundwater gas stripping and re-dissolution (GGs-R) model, as outlined in Gilfillan et al. (2008, 2009), Zhou et al., (2012), postulates that trace gas components are extracted from the water phase in equilibrium with a gas phase through “gas stripping.” The nucleation of a separate gas phase in groundwater occurs when the sum of the partial pressures of all dissolved gases (but generally dominated by a few major components such as  $\text{CO}_2$  or  $\text{CH}_4$ ) exceeds the hydrostatic pressure, commonly called the saturation point or “bubble point”. In cases where the partial pressure of dissolved methane is dominant, it controls the partitioning of trace gases (He, Ne,

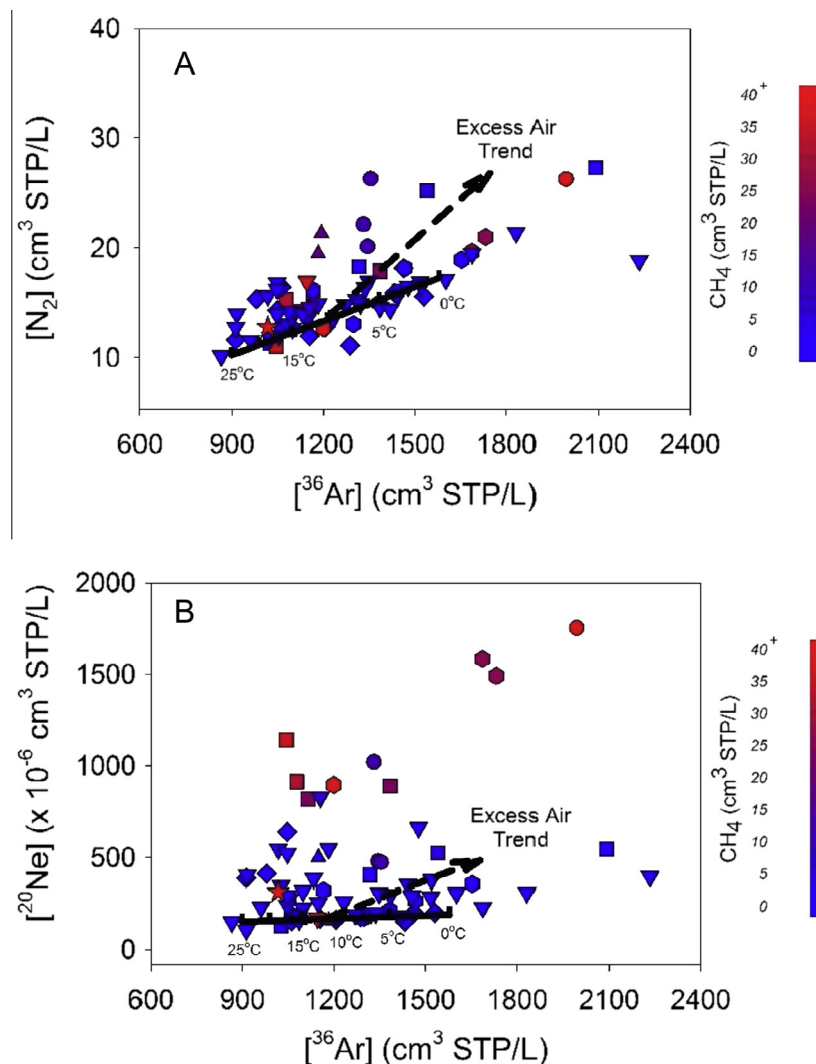


Fig. 5.  $\text{N}_2$  (top) and  $^{20}\text{Ne}$  (bottom) vs.  $^{36}\text{Ar}$  in northeastern PA and southeastern NY at distances  $>1$  km from drilling. In natural groundwater systems, the concentration of atmospheric (ASW) gases (e.g.,  $^{20}\text{Ne}$ ,  $^{36}\text{Ar}$ ,  $\text{N}_2$ ) is determined by their solubility during meteoric recharge. The majority of samples collected  $\gg 1$  km from drilling in PA have  $^{36}\text{Ar}$  and  $\text{N}_2$  that vary within 15% of the temperature-dependent solubility line. A subset of methane-rich samples show a moderate increase in  $[\text{Ne}^{20}]$  discussed below.

Ar) because these trace components alone cannot attain (or sustain) sufficient partial pressures to nucleate or remain in the bubble phase even at the relatively low hydrostatic pressures present near the vadose zone.

Our adaptation of the GGS-R model for hydrocarbons postulates that catagenesis produces sufficiently high natural gas concentrations to generate a free gas-phase or “bubble” leading to the *primary* and later *secondary* migration of hydrocarbon gases. Note that although bubble nucleation could occur through hydrothermal circulation (Ma et al., 2009a,b), there is evidence for  $<1\%$  contribution of mantle-derived helium in hydrocarbon gas and salt-rich samples in our current study. Similarly, there are no reported excess geothermal (heat) anomalies in the current study area. The gas-phase (or two-phase) fluid would then contain crustal and ASW noble gases with the relative partitioning of the trace gas components between the gas and

water phases dependent upon: (a) the respective Bunsen solubility coefficients for each phase ( $\beta x$ , the ratio at equilibrium of the volume of dissolved gas  $x$  (at STP conditions) per unit volume of solution, when the partial pressure of  $x$  is 1 atmosphere) and (b) the *in-situ* volume ratio of gas to water (i.e.,  $V_{\text{gas}}/V_{\text{water}}$ ) (Aeschbach-Heritg et al., 1999; Ballentine et al., 2002; Holocher et al., 2003; Aeschbach-Hertig et al., 2008). This initial stage would significantly enrich the migrated hydrocarbon fluid in  $[\text{Ne}^{20}]$  and increase the  $^{20}\text{Ne}/^{36}\text{Ar}$ . As the gas migrates into overlying groundwater containing gas levels below methane saturation, there is a partial re-dissolution of methane and the previously exsolved components back into groundwater (Gilfillan et al., 2008, 2009). In this scenario, the more soluble trace gas components (e.g.,  $\text{C}_2\text{H}_6 > \text{CH}_4 = ^{36}\text{Ar}$ ) preferentially re-dissolve into the static, capillary bound or connate pore fluids according to their relative partition

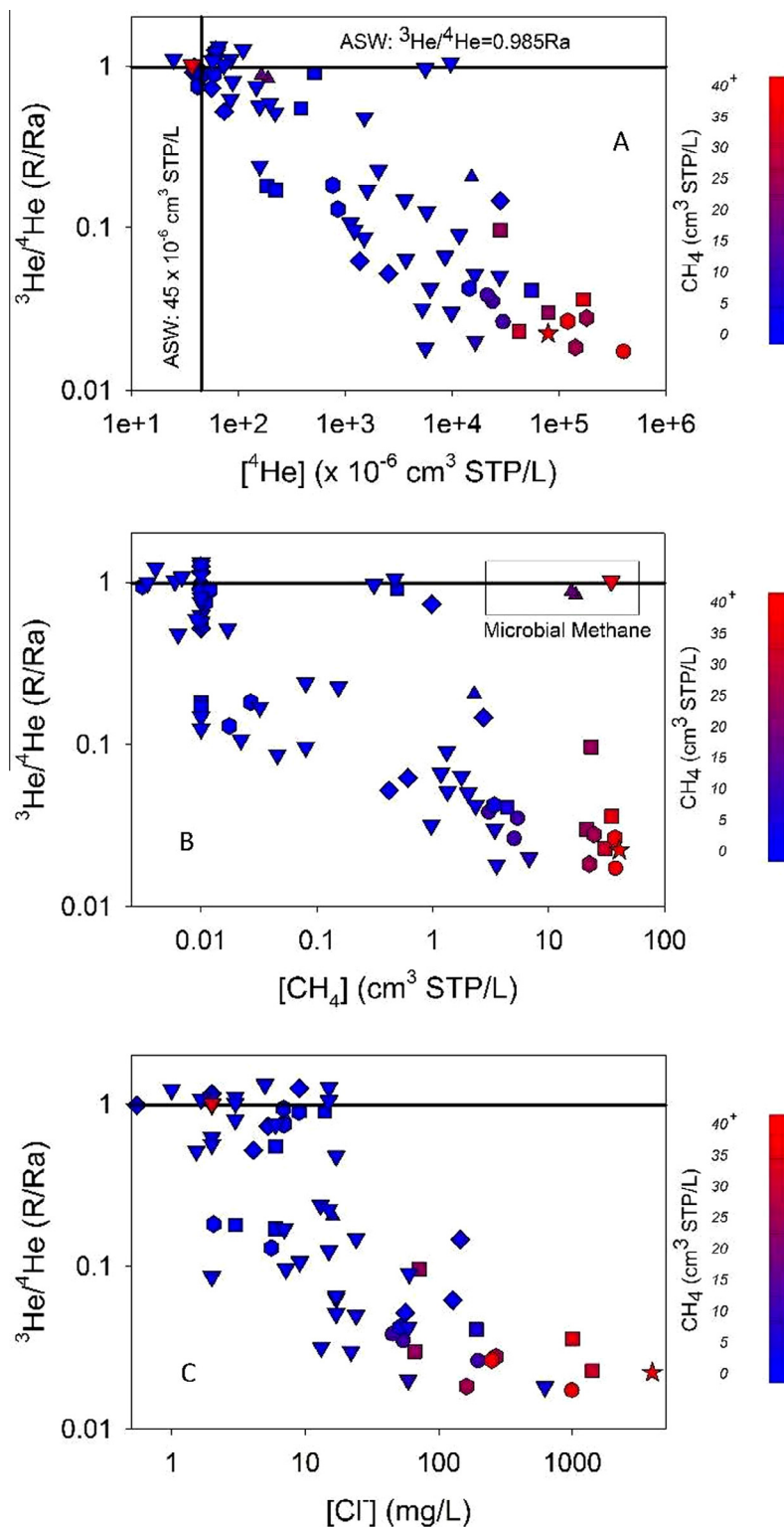


Fig. 6. The helium isotopic composition ( $^3\text{He}/^4\text{He}$ ) shown as the ratio of the sample to the air standard ( $1\text{Ra}$ ) vs.  $[\text{He}]$  (top),  $[\text{CH}_4]$  (middle), and  $[\text{Cl}^-]$  (bottom) in northeastern PA at distances  $>1$  km from drilling. Fresh meteoric water has solubility levels of  $[\text{He}] = 45 \times 10^{-6} \text{ cm}^3 \text{ STP/L}$  and a  $^3\text{He}/^4\text{He}$  near the atmospheric standard ( $0.985\text{Ra}$ ). After groundwater recharge, the  $^3\text{He}/^4\text{He}$  varies as a function of the radiogenic decay of  $^3\text{H}$  to  $^3\text{He}$  and the influx of  $^4\text{He}$  from: (a) radioactive decay of U and Th; (b) intrinsic release of  $^4\text{He}$  that has accumulated in mineral grains within the aquifer; and (c) a flux from exogenous sources. Our data suggest that in the majority of samples the helium has a crustal source, while maximum crustal inputs correspond to the addition of thermogenic natural gas ( $[\text{CH}_4]$  (middle) and increasingly brine-rich components  $[\text{Cl}^-]$  (bottom)). Four samples with low salt and natural gas levels have elevated  $R/Ra$  values with elevated  $\text{He}/\text{Ne}$  likely providing evidence for mantle-derived contributions (discussed further in Fig. 7). Four samples with low  $[\text{He}]$  and  $\text{He}/\text{Ne}$  are related to targeted microbial samples.

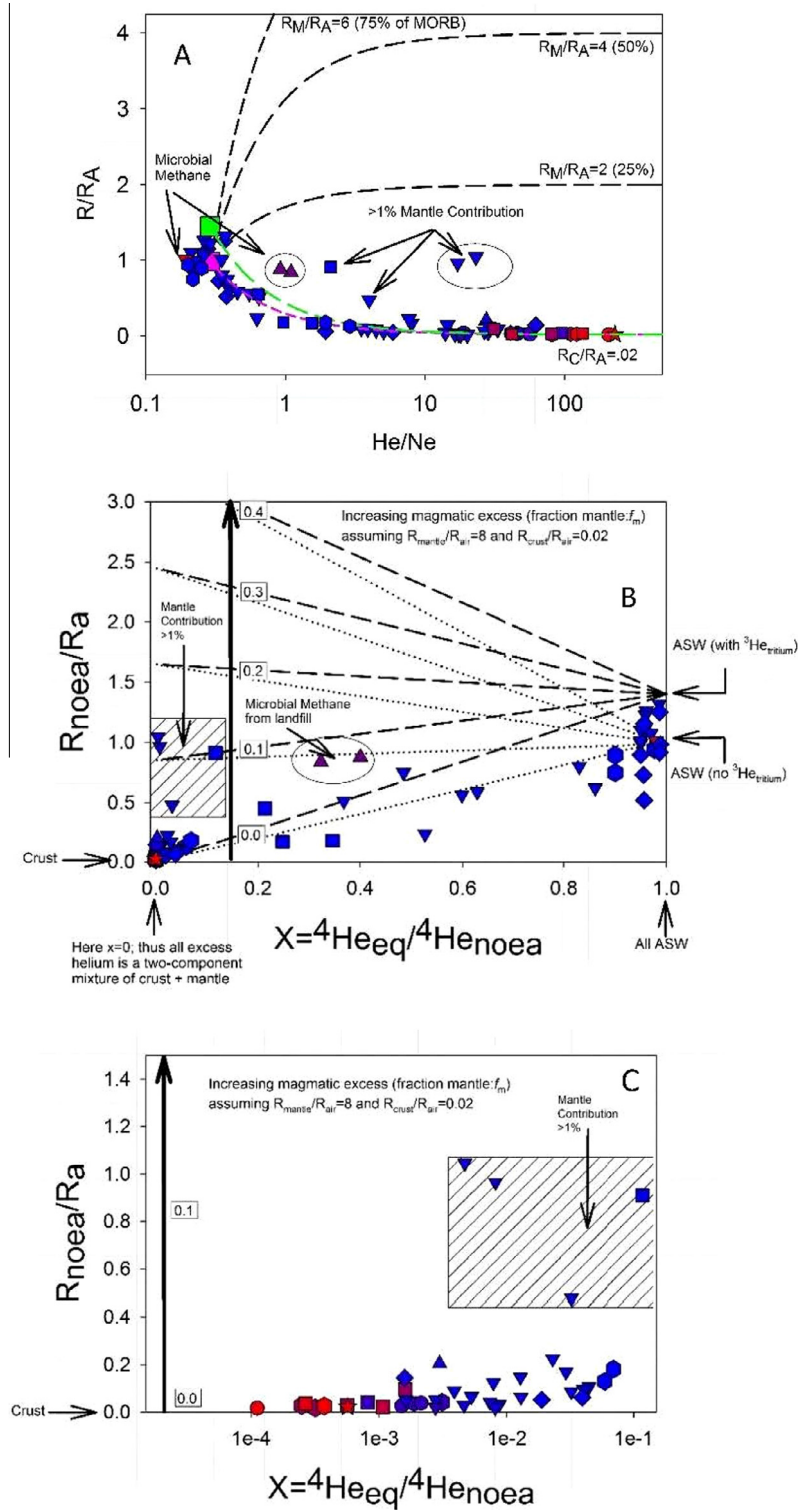


Fig. 7. The  $R/Ra$  vs.  $He/Ne$  (A); the  $R/Ra$  with air-saturated water and excess air removed (i.e., noea: no excess air) ( $R_{noea}/Ra$ ) vs.  $^4He_{eq}/^4He$  (i.e., atmospheric equilibration concentrations of  $^4He$  over measured  $^4He$  minus air-saturated water and excess air) (B); and a zoomed in image of B (C). The majority of groundwater samples in this region, specifically in the hydrocarbon gas-rich and salt-rich end-member, appear to be a two component mixture of ASW and crustal helium (<1% mantle-derived); in these samples the helium isotopic composition for the gas-rich end-member approaches  $0.02Ra$  and tracks an increase in  $[^4He]$  with increased  $[CH_4]$ ,  $[Cl^-]$ , and  $[Ba]$ . By comparison, four samples show  $R/Ra$  values well above crustal production ratios even at elevated  $He/Ne$  and after atmospheric helium is removed; these samples show evidence for between 1.2% and 11.6% mantle-derived helium.

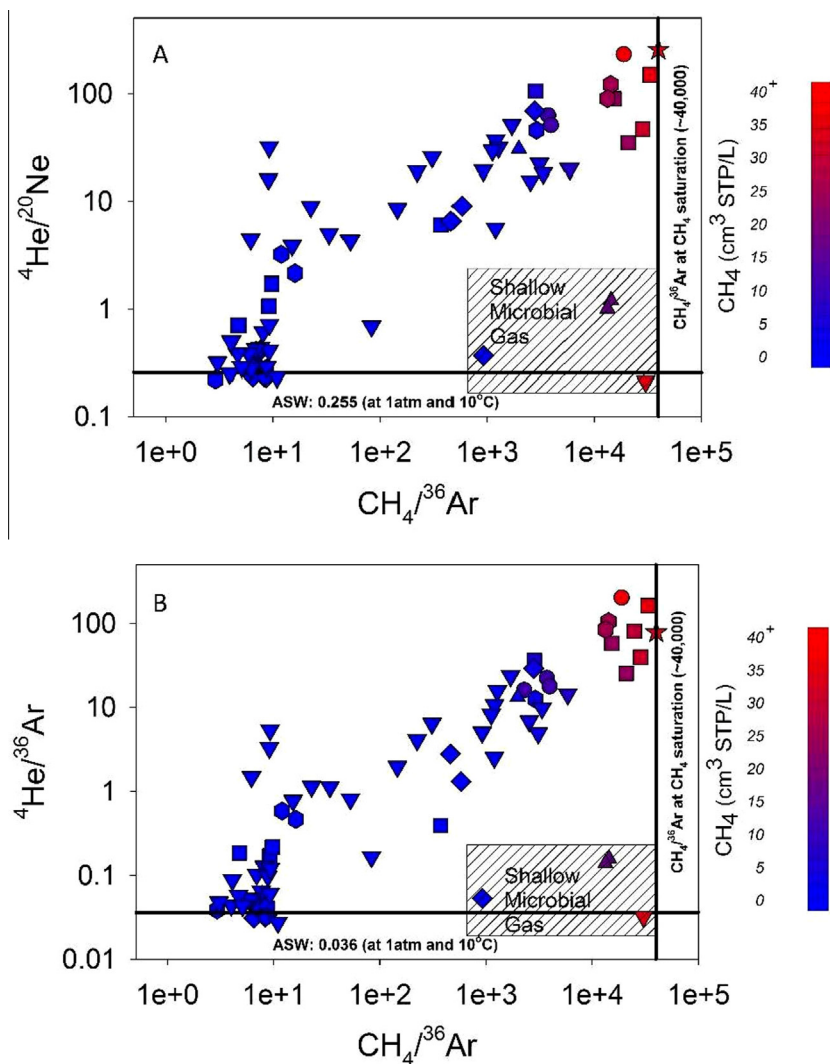


Fig. 8. The  ${}^4\text{He}/{}^{20}\text{Ne}$  vs.  $\text{CH}_4/{}^{36}\text{Ar}$  (top) and  ${}^4\text{He}/{}^{36}\text{Ar}$  vs.  $\text{CH}_4/{}^{36}\text{Ar}$  (bottom) in groundwater samples from the current study. The trends of increasing  ${}^4\text{He}/{}^{36}\text{Ar}$  and  ${}^4\text{He}/{}^{20}\text{Ne}$  vs.  $\text{CH}_4/{}^{36}\text{Ar}$  show a coherent dilution of  ${}^4\text{He}$ -rich and  $\text{CH}_4$ -saturated groundwater (typified by the Salt Spring) by meteoric water with ASW composition (low concentrations of  ${}^4\text{He}$ , Cl, and no  $\text{CH}_4$ ). These findings suggest that hydrocarbon-rich brine components were diluted (mixed) with relatively young meteoric waters in the shallow subsurface. The combination of high  $[\text{CH}_4]$  (i.e., high  $\text{CH}_4/{}^{36}\text{Ar}$ ) and  $[\text{He}]$  (e.g.,  ${}^4\text{He}/{}^{36}\text{Ar}$  and  ${}^4\text{He}/{}^{20}\text{Ne}$ ) enables us to distinguish natural gases targeted for their shallow microbial inputs (e.g., landfills and agricultural fertilizer) from the hypothesized migrated thermogenic gases in the NAB.

coefficients ( $\alpha$ ), while less soluble components (e.g.,  ${}^4\text{He}$  and  ${}^{20}\text{Ne}$ ) preferentially remain in the gas-phase.

In low gas to water conditions (i.e., as  $V_{\text{gas}}/V_{\text{water}}$  approaches 0), trace gases with different solubilities will strongly fractionate as they partition from groundwater into the gas-phase (Gilfillan et al., 2009). In this scenario, the degree of molecular fractionation increases and can approach a maximum fractionation value of the ratio of their respective Bunsen coefficients ( $\beta_X/\beta_Y$ ), termed alpha ( $\alpha$ ) (assuming single stage fractionation; multi-stage fractionation can greatly exceed  $\alpha$ ). For example, the Bunsen coefficient ratio ( $\alpha$ ) for  ${}^{20}\text{Ne}$  vs.  ${}^{36}\text{Ar}$  ( $\beta_{\text{Ne}}/\beta_{\text{Ar}}$ ) is  $\sim 3.7$  at  $10^\circ\text{C}$ , and for  ${}^4\text{He}$  vs.  $\text{CH}_4$  ( $\beta_{\text{He}}/\beta_{\text{CH}_4}$ ) is  $\sim 4.4$  at the same temperature. On the other hand, for components with similar solubilities such as  $\text{CH}_4$  vs.  ${}^{36}\text{Ar}$  ( $\beta_{\text{CH}_4}/\beta_{\text{Ar}}$ ),  $\alpha$  is about 1 at  $10^\circ\text{C}$  (Ballentine et al., 1991; Sherwood Lollar and

Ballentine, 2009) and for  ${}^4\text{He}$  vs.  ${}^{20}\text{Ne}$  ( $\beta_{\text{He}}/\beta_{\text{Ne}}$ )  $\alpha$  is about 1.2 at the same temperature (Weiss, 1971a,b). Thus, these pairs of gases will partition into the gas phase according to the  $V_{\text{gas}}/V_{\text{water}}$ , but will not experience significant molecular or isotopic fractionation relative to each other. As the  $V_{\text{gas}}/V_{\text{water}}$  increases, the amount of dissolved gas that partitions into the gas-phase will increase, while the degree of molecular (or isotopic) fractionation between gases with different solubilities decreases. Thus, in high  $V_{\text{gas}}/V_{\text{water}}$  conditions nearly all of the trace gases will partition into the gas-phase. In this case, even components with relatively large differences in solubility will not experience changes in molecular or isotopic ratios in either the gas or the residual water phases. Our model assumes maximum  $\alpha$  fractionation values because theoretically gas emplacement occurs when relatively low volumes of gas migrate

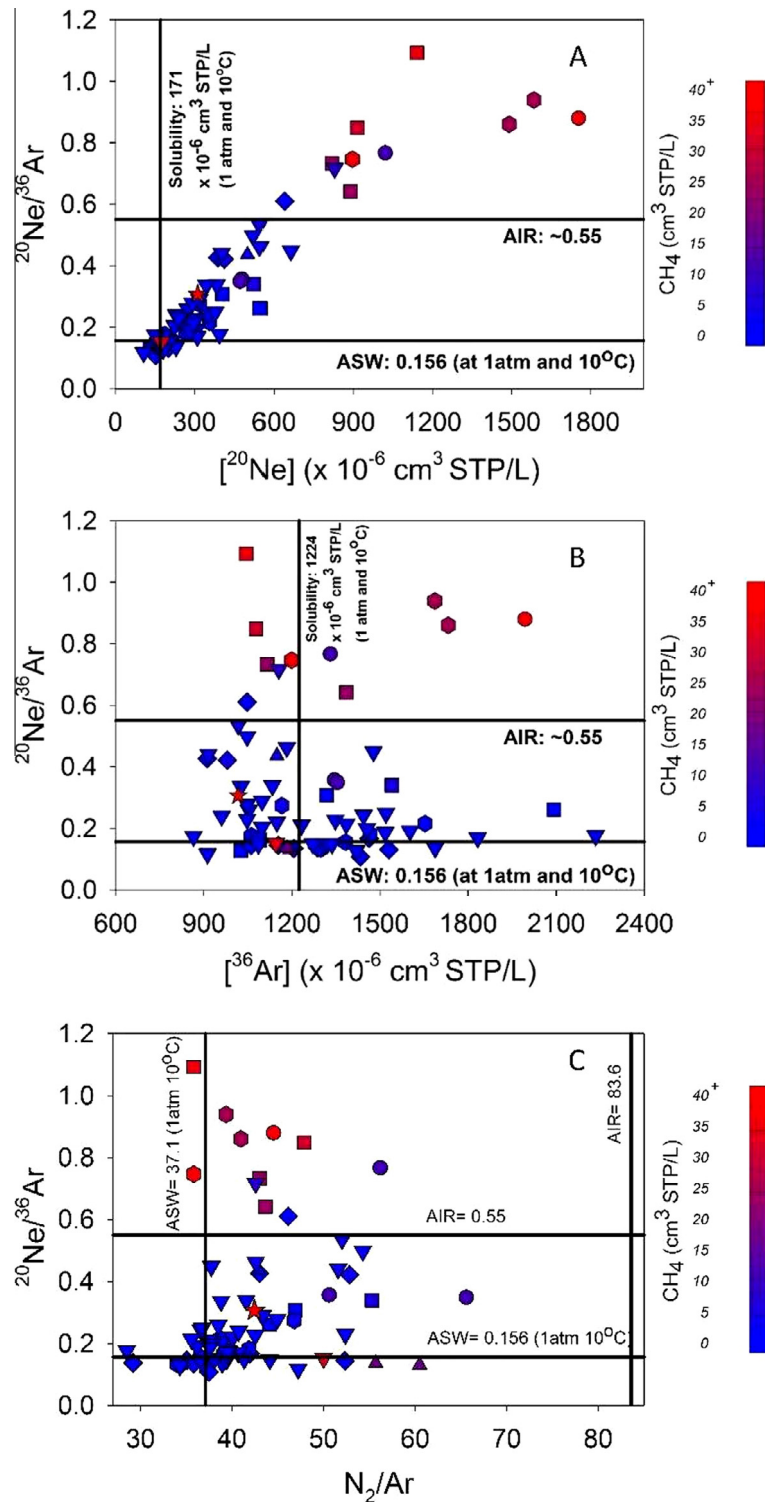


Fig. 9. The  $^{20}\text{Ne}/^{36}\text{Ar}$  vs.  $^{20}\text{Ne}$  (top),  $^{36}\text{Ar}$  (middle), and  $\text{N}_2/\text{Ar}$  (bottom) in groundwater from the present study. The  $^{20}\text{Ne}/^{36}\text{Ar}$  can be a sensitive proxy for gas–water interactions and crustal fluid migration mechanisms. However, the  $^{20}\text{Ne}/^{36}\text{Ar}$  can also be impacted by air contamination and/or the addition of “excess air”. The present dataset shows a strong positive correlation ( $r^2 = 0.849$ ;  $p < 0.01$ ) between  $^{20}\text{Ne}/^{36}\text{Ar}$  and  $^{20}\text{Ne}$  (top), but no significant correlation ( $p > 0.35$ ) with  $^{36}\text{Ar}$  (middle) or  $\text{N}_2/\text{Ar}$  (bottom). These trends suggest that the elevated  $^{20}\text{Ne}/^{36}\text{Ar}$  in the current study relates to a history of gas–water interactions as opposed to excess air. Elevated  $^{20}\text{Ne}$  without increased  $^{36}\text{Ar}$  or  $\text{N}_2/\text{Ar}$  suggests that a highly fractionated (i.e., elevated  $^{20}\text{Ne}/^{36}\text{Ar}$ ) hydrocarbon-rich brine mixes with a young meteoric water close to surface (i.e., otherwise both  $^{20}\text{Ne}/^{36}\text{Ar}$  and  $\text{N}_2/\text{Ar}$  would both be fractionated by the migrational process). The addition of a migrated gas-rich phase with exogenous  $^{20}\text{Ne}$  increases the  $^{20}\text{Ne}$  significantly, but does not alter the  $^{36}\text{Ar}$ .

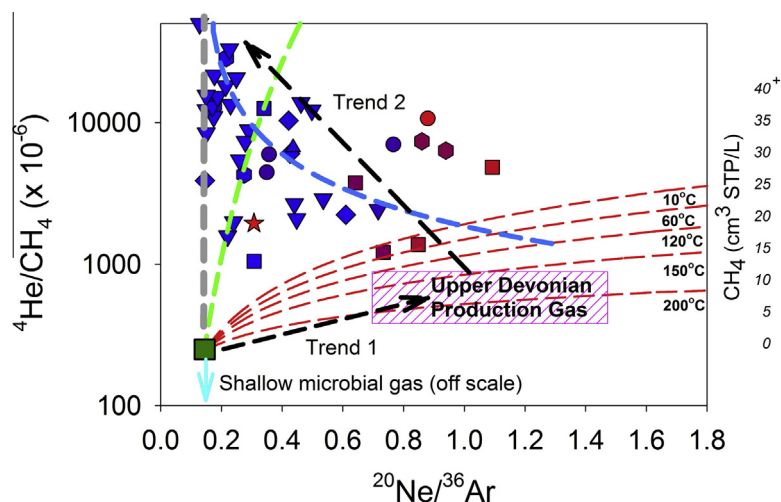


Fig. 10.  $^4\text{He}/\text{CH}_4$  versus  $^{20}\text{Ne}/^{36}\text{Ar}$  in dissolved gas in shallow groundwater samples as compared to Marcellus (solid red box) and Upper Devonian production gases (pink box). Once incorporated into a crustal fluid, the ratios of thermogenic and ASW components can be predictably fractionated by gas–water interactions in the crust (e.g., Gilfillan et al., 2009; Sherwood Lollar and Ballentine, 2009). As a result, dissolved gas components are sensitive tracers for distinguishing different migration processes. We modeled four migration scenarios from a single source of the Marcellus gas: (1) simple 1-phase advection (gray line); (2 and 3) solubility fractionation during the advection of a fluid with a gas phase (i.e., a free-phase gas (2) and a 2-phase fluid (3)), sorted by temperature (red dashed lines); and (4) primary diffusion (green line). The observed  $^{20}\text{Ne}/^{36}\text{Ar}$  and  $^4\text{He}/\text{CH}_4$  data of shallow groundwater are not consistent with any of these three models alone. Consequently, we hypothesize two sequential stages of hydrocarbon-rich brine migration including: (1) transport of the Marcellus gas to UD reservoirs via primary and later secondary (buoyant) migration, during which isotopic fractionation is induced by differential solubility of the gases that generated the NAB UD production gases (Trend 1) and (2) a final secondary diffusion of the UD gas into the shallow UD aquifers, termed tertiary migration (blue dashed line) (Trend 2). The combination of elevated  $^{20}\text{Ne}/^{36}\text{Ar}$  and the correlation between gas components (e.g.,  $\text{CH}_4$ ,  $^4\text{He}$ ,  $^{20}\text{Ne}/^{36}\text{Ar}$ ) and salts (e.g., Cl, Br, Ba) suggests that the initial emplacement occurred by the advection of a 2-phase fluid. (For interpretation of the references to color in this figure legend, the reader is referred to the web version of this article.)

through the water-saturated crust (i.e., low  $V_{\text{gas}}/V_{\text{water}}$ ); note also that our empirical observations require extensive fractionation (near maximum  $\alpha$ ) to accommodate the observed  $^{20}\text{Ne}/^{36}\text{Ar}$  in the methane-rich samples.

The diffusion model (Mechanism 4: dashed green lines) assumes 1-D diffusion of a hydrocarbon-rich brine with Marcellus composition into an overlying static crustal brine that was previously devoid of any thermogenic natural gas components (i.e.,  $\text{CH}_4$ ,  $\text{C}_2\text{H}_6$ ,  $^4\text{He}$ ). The assumed boundary conditions (i.e., a natural gas from the Marcellus diffuses into a brine devoid of any natural gas previously) may be plausible for crustally-derived components (e.g.,  $^4\text{He}$ ,  $[\text{CH}_4]$ ), but clearly represent maximum diffusional constants for the ASW components (e.g.,  $^{20}\text{Ne}$ ,  $^{36}\text{Ar}$ ). The latter results from the fact that the concentration of ASW components were fixed in the past when crustal waters equilibrated with the atmosphere during recharge and should have minimal concentration gradients. These boundary conditions for diffusional fractionation were chosen because they represent the maximum possible fractionation factors for ASW noble gases (i.e.,  $^{20}\text{Ne}$  and  $^{36}\text{Ar}$ ); the importance of which is discussed further below). The relative diffusional fractionation factors ( $\alpha$ ) for various gas components is assumed to be equal to the ratio of the diffusion coefficients for each parameter (i.e.,  $\alpha = D_X/D_Y$ , where  $D_X$  is the diffusional constant for component X and  $D_Y$  is the diffusional constant for component Y). To a first approximation, the diffusional  $\alpha$  for various gas species are equivalent to the ratio of the square roots of their masses.

## 4. RESULTS

### 4.1. Hydrocarbon gases

#### 4.1.1. Hydrocarbon concentrations

Gas-phase hydrocarbons in shallow aquifers may result from *in-situ* microbial or thermogenic production and/or the migration of hydrocarbons from an exogenous source (e.g., Revesz et al., 2010; Osborn et al., 2011). Methane concentrations in groundwater from this sample set range from below detection limits ( $\sim 0.01 \text{ cm}^3 \text{ STP/L}$ ) to  $39.8 \text{ cm}^3 \text{ STP/L}$  (Table 2a). The upper limit is near saturation conditions for methane in fresh water (saturation for  $[\text{CH}_4]$  is  $\sim 32\text{--}40 \text{ cm}^3 \text{ STP/L}$  (e.g., Revesz et al., 2010) at  $P(\text{CH}_4) = 1 \text{ atm}$  at  $10^\circ\text{C}$ ). By comparison, ethane concentrations range from below detection limits ( $\sim 0.001 \text{ cm}^3 \text{ STP/L}$ ) to  $0.271 \text{ cm}^3 \text{ STP/L}$  (Table 2a). Because microbes do not produce significant quantities of ethane or heavier aliphatic hydrocarbons in the subsurface (Bernard, 1978; Schoell, 1980), ethane serves as an indicator of thermogenic gas inputs (e.g., Jackson et al., 2013).

All samples with elevated salt contents (e.g., [Cl], [Ba]) display a concomitant increase in  $[\text{CH}_4]$  and  $[\text{C}_2\text{H}_6]$  (Fig. 3). This trend reinforces the hypothesis for the natural coexistence of  $[\text{CH}_4]$  and brine-rich salts in low lying valleys across the region (Fig. 3 and Table 2a) (Molofsky et al., 2011, 2013; Warner et al., 2012; Darrah et al., 2014; Kravchenko et al., 2014). The general co-variation of  $[\text{CH}_4]$ ,  $[\text{C}_2\text{H}_6]$ , and  $^4\text{He}$  with dissolved salts (i.e., [Cl] and

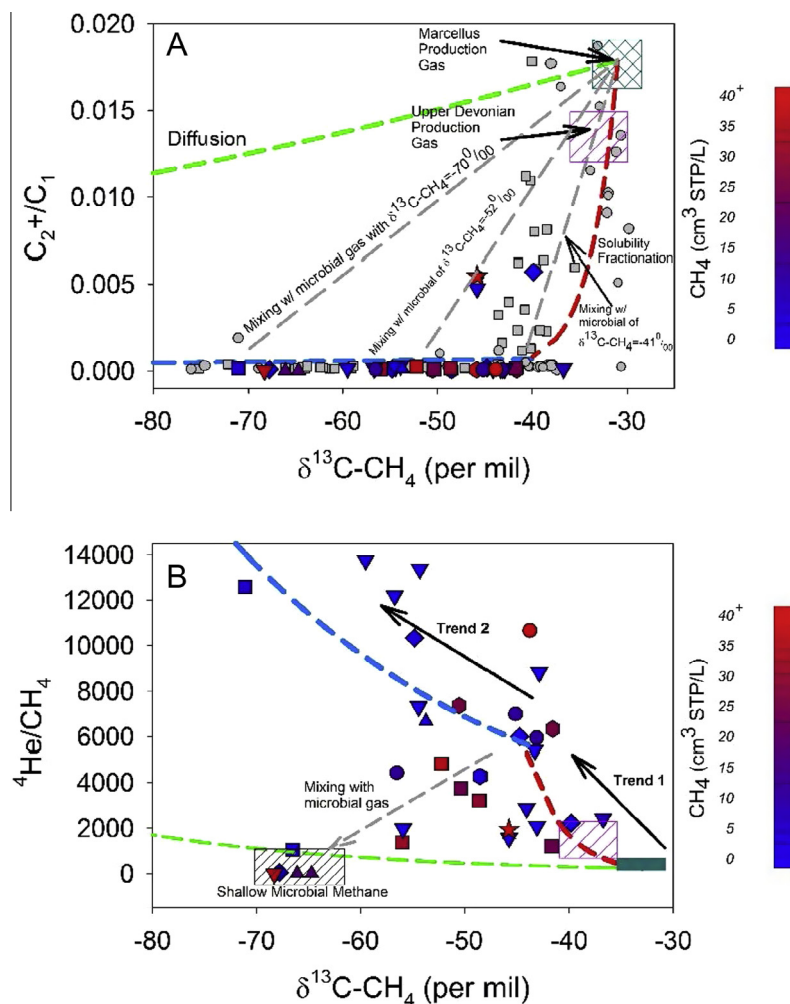


Fig. 11.  $C_2+/C_1$  vs.  $\delta^{13}C-CH_4$  (top) and  $^4He/CH_4$  vs.  $\delta^{13}C-CH_4$  (bottom) in groundwater from the current study area. In the  $C_2+/C_1$  versus  $\delta^{13}C-CH_4$  (top), we compare our data to published data (gray squares (Revesz et al., 2010); gray circles (Jackson et al., 2013)) and values of shallow microbial gas (gray box), Marcellus production gases (red box), and UD production gases (pink box). Notice that many of NAB groundwaters do not plot along a mixing trajectory, even if one assumes a relatively enriched microbial end-member ( $\delta^{13}C-CH_4 = -52$  per mil). In fact, a hypothetical microbial end-member of  $\delta^{13}C-CH_4 = -41$  per mil is required to account for the stable isotopic composition of the majority of the methane-rich samples. Similar results are obtained by assuming mixing occurs between UD production gases and microbial end-members (not shown). By comparison, elevated helium levels in shallow groundwater are produced as natural gases fractionate during migration from a deep, thermogenic source. Thus,  $^4He$  (i.e.,  $^4He/CH_4$ ) provides a powerful externally defined end-member for distinguishing between biogenic and thermogenic natural gas inputs. If mixing were to occur between Marcellus or UD production gases and microbial end-members, the  $^4He/CH_4$  should decrease. Similarly, methane oxidation could increase the  $^4He/CH_4$ , but should lead to an increase in the residual  $\delta^{13}C-CH_4$ . Instead, the opposite trend (more negative  $\delta^{13}C-CH_4$  and increasing  $^4He/CH_4$ ) is observed in a plot of  $^4He/CH_4$  versus  $\delta^{13}C-CH_4$ . A subset of samples that do diverge from this trend and show paired decreases in  $^4He/CH_4$  and  $\delta^{13}C-CH_4$  (dashed gray arrow denoted as “mixing with microbial methane”) were targeted specifically for their microbial sources (e.g., landfill). These samples have low  $^4He$  (consistent with air-saturated water) and  $^4He/CH_4$  orders of magnitude lower than production gases or other samples in the study. Together, these data suggest that a post-genetic alteration process other than microbial alteration may affect the  $C_2+/C_1$ ,  $^4He/CH_4$ , and  $\delta^{13}C-CH_4$  relative to the original source composition (i.e., Marcellus gas). When combined with noble gas data, it appears that the concave curve typified by the rapid depletion of  $C_2$  relative to  $C_1$  in the  $C_2+/C_1$  versus  $\delta^{13}C-CH_4$ , previously interpreted as post-genetic fractionation by “diffusional fractionation” (Prinzhofer and Pernaton, 1997), may instead reflect solubility fractionation (red line) during the advection of a dual-phase (water and gas) fluid consistent with Fig. 10. In combination with Fig. 4, these data suggest that a subset of the “subsurface microbial” end-member may also include some migrated thermogenic natural gas in the NAB. (For interpretation of the references to color in this figure legend, the reader is referred to the web version of this article.)

[Ba]) likely demonstrates a common origin and migration process for natural gas and dissolved inorganic solutes, consistent with hydrocarbon-rich brines observed elsewhere (Eisenlohr et al., 1994; Schlegel et al., 2011; Warner et al.,

2012, 2014). The exceptions to this trend are (a) those methane-rich waters that have a microbial source as defined by low  $\delta^{13}C-CH_4$  and  $\delta^2H-CH_4$  and a lack of ethane and radiogenic  $^4He$  (explored further below) and (b) a subset

of samples <1 km from drilling reported elsewhere that have multiple lines of evidence suggesting the presence of fugitive gas contamination related to shale gas development (Osborn et al., 2011; Jackson et al., 2013; Darrah et al., 2014). Although only [Cl] and [Ba] are shown in Fig. 3, previous work on the other inorganic constituents (e.g., Br<sup>-</sup>/Cl<sup>-</sup>, <sup>87</sup>Sr/<sup>86</sup>Sr, Ba/Sr) of these high salinity waters (i.e., [Cl] > 20 mg/L) indicated that the salt components are consistent with the addition of deep, Mid-Devonian (Marcellus-like) formational brines into shallow groundwater (Warner et al., 2012). Based on these considerations, and the fact that the shallowest hydrocarbon source rock in this study area is the Marcellus, we suggest that a Marcellus source for these fluids is plausible.

Groundwater transport plays a fundamental role in hydrocarbon gas migration and physically controls the migration of gases from and within hydrocarbon reservoirs (Cathles, 1990; Ballentine et al., 1991; Ballentine and O’Nions, 1994). Fig. 3 also reveals how the conditions of gas saturation in water regulate the concentrations of methane in groundwater from the region. In Fig. 3a and b, notice that the [CH<sub>4</sub>] “roll over” (i.e., stop increasing) as they approach the saturation level (“bubble point”) of methane (32–40 cm<sup>3</sup> STP/L) in fresh water at 1 atm and 10 °C for a water in equilibrium with a methane partial pressure of 1 atm (P(CH<sub>4</sub>) = 1 atm) and normal levels of air-saturated water gases (predominantly N<sub>2</sub>), whereas [Cl] and [Ba] continue to increase (Fig. 3a and b). The “roll over” in methane results from the fact that conservative inorganic tracers (e.g., Cl, Br, etc.) remain well below their respective saturation levels in water, while the levels of CH<sub>4</sub> (or other major gases) are limited by their saturation levels (i.e., “bubble point”).

In order to prevent gas loss or significant two-phase partitioning, which commonly occurs when using simple plastic or glass screw-top containers or the inverted bottle method, we collected the groundwater samples using gas-tight copper tube samplers in-line with the domestic wells prior to any pressure tanks or treatment systems. Thus, this upper “roll over” limit for [CH<sub>4</sub>] in shallow aquifers >1 km from drilling is not an artifact of sampling, as is the case for the other sampling techniques listed above, and is regulated by the saturation or bubble point for methane in water at or near P(CH<sub>4</sub>) = 1 atm.

#### 4.1.2. Stable isotopic composition of hydrocarbon gases

The stable isotopic compositions of methane (i.e., δ<sup>2</sup>H-CH<sub>4</sub> and δ<sup>13</sup>C-CH<sub>4</sub>) provide additional insight into the origin of methane-rich crustal fluids present in Middle and Upper Devonian formations (Fig. 4a). The conventional interpretation of Fig. 4a relates the isotopic composition of methane to the degree of thermal maturity. Thermogenic gases fall along the thermal maturation trend (dashed blue arrow in 4a), whereas biogenic gases plot as two distinct “light” δ<sup>13</sup>C-CH<sub>4</sub> end-members predominantly distinguished by their δ<sup>2</sup>H-CH<sub>4</sub>; shallow “near-surface” microbial gases (green box) have significantly lower δ<sup>2</sup>H-CH<sub>4</sub> signatures than “subsurface microbial” gases (solid blue box; Fig. 4a) (Schoell, 1980, 1988).

The majority of production gas data from Ordovician (yellow circles), Silurian (black squares), and Middle Devonian (Marcellus, red circles) sequences in PA and NY are consistent with thermally mature, “dry thermogenic” methane with δ<sup>13</sup>C-CH<sub>4</sub> of -28 to -40‰ and clearly fall along the “thermal maturation line” (Fig. 4a and b) (data from Jenden et al., 1993; Burruss and Laughrey, 2010; Osborn and McIntosh, 2010). By comparison, many oil-associated Silurian production gases (black squares) from PA (Laughrey and Baldassare, 1998) and oil-associated Upper Devonian production gases (green circles) from NY (Jenden et al., 1993; Osborn and McIntosh, 2010), range between -44‰ to -55‰. These samples fall along a trend that can be interpreted as either a mixture between thermogenic gases that plot along the thermal “maturation trend” and “near-surface microbial” end-members or the thermally immature end-member of oil-associated hydrocarbon gases.

The stable isotope trends for dissolved CH<sub>4</sub> in the majority of groundwater samples also fall along an apparent “mixing” trend between a “dry thermogenic end-member”, similar to Marcellus production gases (e.g., Jenden et al., 1993; Laughrey and Baldassare, 1998; Baldassare et al., 2012), and microbial inputs (Schoell, 1980, 1983; Jenden et al., 1993) (Fig. 4c). By comparison to the production gases from this region, the majority of groundwater samples appear to plot along a mixing line between the production gases and the “subsurface” microbial end-member. Importantly, all groundwater samples in the present study have isotopic compositions that plot along the “mixed” gas trend, with the exception of four samples intentionally targeted for their “surficial” microbial production (i.e., near a landfill and/or manure leachate ponds, with low levels of ethane, <sup>4</sup>He, Ba, and Cl) as reported in Darrah et al. (2014) (Fig. 4c).

## 4.2. Non-combustible gases

### 4.2.1. Major dissolved gases

The concentrations of dissolved atmospheric (ASW) gases (i.e., <sup>20</sup>Ne, <sup>36</sup>Ar, N<sub>2</sub>) can also help to elucidate the interactions that occur between natural gas and water (Solomon et al., 1992; Holocher et al., 2002, 2003; Aeschbach-Hertig et al., 2008; Gilfillan et al., 2009). Groundwater samples from the current study display N<sub>2</sub> ([N<sub>2</sub>] = 15.8 cm<sup>3</sup> STP/L) and Ar ([Ar] = 0.38 cm<sup>3</sup> STP/L) concentrations that vary within 12% and 3% of ASW values (13.9 and 0.37 cm<sup>3</sup> STP/L, respectively) on average, assuming Henry’s Law solubility equilibration conditions at atmospheric pressure (1 atm), 10 °C, and ~600 m of elevation (average elevation in the study area) (Table 2a and Fig. 5a). The majority of samples have [N<sub>2</sub>] and [Ar] that plot within 15% of the temperature-dependent ASW solubility line (see ticked line in Fig. 5a and b).

Although some background groundwater samples showed minor “bubble enrichment” or “excess air” entrainment common in pumped groundwater globally (Heaton and Vogel, 1981; Aeschbach-Hertig et al., 2008), these ranges reflect normal equilibration between the atmosphere and meteoric water during groundwater recharge (Weiss,

1971a,b). These findings were as expected for a typical shallow aquifer groundwater sample. Importantly, this relationship is maintained independent of the methane concentration, which suggests the addition of methane did not result in any major two-phase effects (gas–liquid interactions), such as partitioning of the atmospheric components into a separate gas-phase that altered the ASW [N<sub>2</sub>] or [Ar] (e.g., “stripping”) as reported in Darrah et al. (2014) (Table 2a and Fig. 5). The most obvious deviations from ASW composition include concomitantly elevated levels of <sup>4</sup>He, <sup>20</sup>Ne, CH<sub>4</sub>, and C<sub>2</sub>H<sub>6</sub>, which all correspond to increasing salt content (e.g., [Cl], [Ba]) (Table 2a; Figs. 3 and 5b).

#### 4.2.2. Noble gas geochemistry

**4.2.2.1. Potential for mantle contributions?.** The isotopic composition (e.g., <sup>3</sup>He/<sup>4</sup>He, <sup>20</sup>Ne/<sup>22</sup>Ne, <sup>21</sup>Ne/<sup>22</sup>Ne, or <sup>40</sup>Ar/<sup>36</sup>Ar) and relative abundance of ASW (i.e., <sup>20</sup>Ne/<sup>36</sup>Ar) and crustal (i.e., [<sup>4</sup>He], <sup>4</sup>He/CH<sub>4</sub>, <sup>4</sup>He/<sup>20</sup>Ne, or <sup>4</sup>He/<sup>36</sup>Ar) gas components can often help to identify the source, mixtures, history of migration, and interactions that occur between fluids (e.g., gas and water) in the Earth’s crust (e.g., Ma et al., 2005; Castro et al., 2009; Gilfillan et al., 2009; Dubacq et al., 2012; Zhou et al., 2012; Darrah et al., 2014). Here, we attempt to use these parameters to determine whether the hydrocarbon gases, diluted brines, and elevated helium contents result from the migration of an exogenous fluid or if these components are native to Upper Devonian aquifers and to determine the physical mechanisms by which the exogenous fluids (e.g., hydrocarbon gases and salts) may have migrated to shallow aquifers. Nonetheless, mantle-derived fluids may contribute to the mixture of noble gases (Poreda et al., 1986; Ballentine and Sherwood Lollar, 2002; Castro et al., 2009) and complicate the interpretation of diagnostic isotopic ratios in some hydrocarbon-producing basins (e.g., Michigan Basin, Hugoton Panhandle, Sacramento Basin). For example, in normal crustal fluids (i.e., those lacking mantle contributions), the abundance and isotopic composition of ASW noble gases are established during the recharge of groundwater and altered by the addition of crustal gases or gas–water interactions (e.g., gas-phase partitioning, diffusion). Thus, isotopic variations in ASW noble gases provide information that may distinguish between various mechanisms of gas–water interaction and/or fluid migration (Gilfillan et al., 2008, 2009; Sherwood Lollar and Ballentine, 2009). By comparison, elevated <sup>20</sup>Ne/<sup>36</sup>Ar values may result from isotopic fractionation during gas–liquid partitioning or from the contribution of mantle-derived neon (i.e., <sup>20</sup>Ne/<sup>36</sup>Ar = 0.5–1.6, or <sup>20</sup>Ne/<sup>22</sup>Ne and <sup>21</sup>Ne/<sup>22</sup>Ne = 12.8 and 0.04, respectively) (e.g., Farley and Poreda, 1993; Gilfillan et al., 2009; Ma et al., 2009a; Darrah et al., 2013). Therefore before employing these diagnostic noble isotopic ratios, we must first evaluate the proportion of mantle contributions in our study area.

In magmatic or geothermal systems, elevated <sup>3</sup>He/<sup>4</sup>He ratios (above radiogenic production values) provide unequivocal evidence for the presence of mantle-derived fluids in crustal and hydrological systems (Craig et al.,

1978; Ballentine et al., 2002). However, in shallow groundwater systems, the use of <sup>3</sup>He/<sup>4</sup>He ratios alone is complicated by uncertainty in the original composition of mantle-derived fluids, mixing with radiogenic fluids (elevated [<sup>4</sup>He] and low <sup>3</sup>He/<sup>4</sup>He) during transport and storage in the crust, mixing with air-saturated components both in the crust and in shallow aquifers, and the potential addition of tritogenic <sup>3</sup>He (i.e., note that all ground water samples in this study had measurable <sup>3</sup>H levels).

Various approaches have been used to apportion the abundance of mantle-derived components in shallow aquifers (Craig et al., 1978; Poreda et al., 1986; Hilton, 1996; Ballentine et al., 2002; Saar et al., 2005; Crossey et al., 2009; Karlstrom et al., 2013). Here, we evaluate mantle contributions in three ways: (1) evaluating the relative distribution of <sup>3</sup>He/<sup>4</sup>He to non-air-like gas components (e.g., He/Ne or He/Ar). We use He/Ne because of the similarity in solubility between He and Ne. The mixing models assume ASW:  $R/Ra = 0.985$ , He/Ne = 0.233; ASW with 10 tritium units (10 T.U.):  $R/Ra = 1.4$ , He/Ne = 0.233; crustal:  $R/Ra = 0.02Ra$ , He/Ne = 1000; and mantle-derived component:  $R/Ra = 2–8Ra$  for 25–100% mantle fraction and He/Ne = 1000 (Figs. 6 and 7) (Craig et al., 1978; Hilton, 1996; Crossey et al., 2009); (2) three component mixing (air-saturated water-derived He and excess helium from crustal and mantle-derived components) including heavier noble gases (Ne, Ar) following methods reported in Saar et al., (2005) (Fig. 6) and (3) neon isotopic compositions (Table 2b).

Consistent with both the noble gas isotope data (e.g., He, Ne, and Ar isotopes) from Ordovician, Silurian, and Devonian production gases (Hunt et al., 2012) and the archetypal salt-decollement-controlled tectonic framework from the plateau region of the NAB (Frey, 1973), the noble gas compositions of the majority of groundwater samples in this region, specifically in the hydrocarbon gas-rich and salt-rich end-member, do not display evidence for any resolvable (>1%) mantle contributions. The helium isotopic composition for the gas-rich end-member approaches 0.02*Ra* with highly elevated He/Ne (>50) and tracks an increase in [<sup>4</sup>He] with increased [CH<sub>4</sub>], [Cl<sup>-</sup>], and [Ba] (Fig. 6). Similarly, by correcting the  $R/Ra$  and [<sup>4</sup>He] values by removing the air-saturated water and excess <sup>3</sup>He and <sup>4</sup>He ( $R_{noea}/Ra$ ) components following the methods of Saar et al., (2005), we find that the majority of samples with elevated hydrocarbon gas and salt contents plot along the purely crustal mixing end-member. Finally, the isotopic ratios of Ne (<sup>20</sup>Ne/<sup>22</sup>Ne (9.90 ± 0.099) and <sup>21</sup>Ne/<sup>22</sup>Ne (0.0288 ± 0.0003)) and ASW Ar components <sup>38</sup>Ar/<sup>36</sup>Ar (0.190 ± 0.006) have atmospheric composition within analytical errors. By comparison, these samples have variable [<sup>40</sup>Ar\*] inputs with a maximum enrichment of ~5% above air (<sup>40</sup>Ar/<sup>36</sup>Ar = ~310) (Table 2b), reflecting radiogenic inputs of argon from crustal minerals.

While we interpret these observations as an absence of mantle contributions in the majority of samples, both the  $R/Ra$  vs. He/Ne and  $R_{noea}/Ra$  vs. <sup>4</sup>He<sub>eq</sub>/4He<sub>noea</sub> plots demonstrate the presence of six samples (DPA-105, 210, 211, 216, 217, and 219) with  $R/Ra$  values well above crustal

production values ( $0.02Ra$ ). Two of these samples (DPA-210 and 211) were collected adjacent to municipal landfills. Thus, we hypothesize that these samples likely have elevated  $R/Ra$  values from the presence of elevated tritium ( $^3H$ ) in the municipal landfills. Conversely, samples DPA-105, 216, 217, and 219 have  $R/Ra$  values above crustal production ratios with  $He/Ne$  ranging from 1.14 to 23.17 without obvious additional anthropogenic sources for  $^3He$  (i.e., tritium). For these reasons, we conclude that these four samples likely contain resolvable mantle contributions ranging from 1.2% to 11.6%. While these four samples display resolvable mantle contributions, it should be noted that these samples all have low methane concentrations ( $[CH_4] = 0.01\text{--}0.49$  ccSTP/L), low levels of salt ( $[Cl] = 14\text{--}17$  mg/L), marginally elevated  $[Ne]$  relative to the hydrocarbon gas- and salt-rich end-member ( $^{20}Ne/^{36}Ar = 0.21\text{--}0.34$ ), and neon isotopic values within  $1\sigma$  of ASW. For these reasons, we suggest that mantle contributions do not quantitatively impact our noble gas interpretations for the majority of samples with elevated hydrocarbon gases and salt, which suggests that the variations in ASW noble gases likely result from fluid interactions in the crust. Because the hydrocarbon-producing formations within our study area do not have a history of oil production, we focus on the impact of post-genetic modification of hydrocarbon natural gases during water–rock interactions in the crust and/or microbial activity.

It should be noted that our observations in produced gases and shallow groundwater from the NAB do not reveal the same frequency of mantle-derived contributions as is observed in deep crustal brines from the neighboring Michigan Basin. The Michigan Basin has a distinctly different tectonic and geological history despite the presence of nominally similar stratigraphic formations. For example, the Michigan Basin experienced significant rifting, basaltic intrusions, and the onset of geothermal advection starting in the Cretaceous (Ma et al., 2005, 2009a,b; Castro et al., 2009). By comparison, the Devonian sequences of the NAB represent an archetypal fold-thrust belt system whose tectonic history is controlled by continental-continental collision that led to deformation exclusively in stratigraphic sequences above the Salina decollement (Frey, 1973; Scanlin and Engelder, 2003). In fact, the most proximal rift basins to our study area are on the opposite side of the Appalachian Structural Front. Thus, Triassic rifts were not necessarily expected to contribute mantle components to this region (i.e., >150 km away from the rift areas). Future work should examine the spatial distribution of samples with evidence of mantle-derived gases in the NAB in order to evaluate the feasibility of magmatic sources and/or tectonic pathways for mantle-derived fluid migration.

**4.2.2.2. Helium.** Combined elevated  $[^4He]$  and  $He/Ne$  and low  $^3He/^4He$  unambiguously indicate that the  $CH_4$ -rich end-member in groundwater from UD aquifers is dominated by an exogenous crustal/radiogenic source (i.e., a source of helium external to the present aquifer lithologies) (Figs. 6 and 7). Helium concentrations in our dataset range from ASW values ( $\sim 45 \times 10^{-6}$  cm<sup>3</sup> STP/L) up to 0.4 cm<sup>3</sup>

STP/L ( $\sim 400,000 \times 10^{-6}$  cm<sup>3</sup> STP/L). With the exception of four apparent outliers (DPA-105, 216, 217, and 219), which show quantifiable mantle contributions, the majority of samples have  $^3He/^4He$  ratios that decrease from  $1.32Ra$  (ASW values plus contributions from the in-growth of tritogenic  $^3He$  (Table 2b)) to a uniformly crustal isotopic composition of  $0.02Ra$  with increasing  $[^4He]$ ,  $[CH_4]$ , and  $[Cl]$  (Fig. 6 and Table 2a).

With the exception of the four outliers with quantifiable mantle contributions, the  $[^4He]$  in groundwater samples from shallow UD aquifers in this study reflect a combination of: (1) atmospheric inputs, (2) *in-situ* production of  $^4He$  from  $\alpha$ -decay of U-Th, (3) the release of  $^4He$  that previously accumulated in detrital grains, and (4) the flux from exogenous sources (Solomon et al., 1996; Zhou and Ballentine, 2006). We use the  $[U]$  and  $[Th]$  of Lock Haven and Catskill aquifer rocks (Table 3) to estimate the potential *in-situ* production of  $[^4He]$ . Using average measured values of  $[U]$  (2.2 ppm) and  $[Th]$  (6.8 ppm) (Table 3) for these aquifer rocks, we find an estimate of steady-state production and accumulation for  $[^4He]$  of  $<2.6 \times 10^{-9}$  cm<sup>3</sup> STP/L of water/yr.

Additionally, crustal minerals may accumulate  $^4He$  over geologic time and release it into groundwater at rates exceeding steady-state production by  $\sim 100$ -fold for periods of at least 10,000 yr (Solomon et al., 1996; Hunt, 2000; Sheldon et al., 2003). Other work in the NAB has found  $^4He$  accumulation in shallow aquifers to be consistent with the modeled  $^4He$  release from Paleozoic quartz (assuming 30% porosity, measured quartz diffusion coefficients, a 1-D radial diffusion model, and the measured average initial  $[^4He]$  of  $6 \times 10^{-5}$  cm<sup>3</sup> STP/g of mineral grains from the Lock Haven and Catskill aquifers) (Hunt, 2000). Based

Table 3  
Uranium  $[U]$  and thorium  $[Th]$  concentrations of aquifer lithologies and UCC.

| Element           | U (mg/kg) | Th (mg/kg) |
|-------------------|-----------|------------|
| <i>Sample</i>     |           |            |
| <i>Lock Haven</i> |           |            |
| LH-1              | 2.4       | 6.5        |
| LH-2              | 2.5       | 6.2        |
| LH-3              | 2.5       | 6.7        |
| LH-4              | 3.4       | 8.2        |
| LH-5              | 2.0       | 6.2        |
| Average:          | 2.6       | 9.7        |
| <i>Catskill</i>   |           |            |
| CAT-1             | 1.0       | 5.1        |
| CAT-2             | 2.3       | 6.4        |
| CAT-3             | 2.1       | 5.7        |
| CAT-4             | 1.6       | 6.4        |
| CAT-5             | 1.4       | 5.1        |
| CAT-6             | 1.5       | 4.7        |
| Average:          | 1.7       | 7.9        |
| <i>Alluvium</i>   |           |            |
| ALV-1             | 3.0       | 8.6        |
| ALV-2             | 3.2       | 8.1        |
| Average:          | 1.7       | 7.9        |
| UCC               | 2.8       | 10.7       |
| Model value       | 2.2       | 6.8        |

on these estimates, the calculated maximum release within these shallow UD aquifer lithologies of the NAB is  $\sim 0.5 \times 10^{-6} \text{ cm}^3 \text{ STP/L/yr}$ .

The  $[\text{}^4\text{He}]$  that we observed (up to  $0.4 \text{ cm}^3 \text{ STP/L}$ ) in methane-rich and high salinity samples greatly exceeds the viable combined concentrations from  $[\text{}^4\text{He}]_{\text{ASW}}$ , the maximum  $[\text{}^4\text{He}]_{\text{in-situ}}$  production, and the release from  ${}^4\text{He}$  that previously accumulated in grains within Catskill and Lock Haven aquifers. Thus, even if the shallow groundwater sampled from UD aquifers (<90 m below land surface) had an average residence time of 1000 yr, the *in-situ* release and accumulation of  ${}^4\text{He}$  would account for  $< \sim 1\%$  of the observed  $[\text{}^4\text{He}]$  in methane-rich and high salinity samples (Table 2a) (methods as reported in (Solomon et al., 1996)). While the age of 1000 yr is entirely arbitrary, it likely overestimates the true age, given the relatively high levels of precipitation and recharge in this area and the consistent presence of tritium (with a half-life of 12.3 yr) observed in groundwater from this study. For example, groundwater from this study had  $[\text{}^3\text{H}] = 3.92$  tritium units (T.U.) on average, with a total range from 0.1 to 11.7 tritium units. Even the Salt Spring had 2.5 T.U., confirming a mixture between young meteoric water and old thermogenic hydrocarbon-rich diluted brines in the shallow subsurface. To put this into perspective, even if the true groundwater residence time is  $\sim 13,000$  yr, the maximum contributions from the release of accumulated  $[\text{}^4\text{He}]$  would still be  $< \sim 10\%$  of the values observed in the methane-rich samples. The true age of the groundwater appears less than 13,000 yr since reported water stable isotope data ( $\delta^2\text{H-H}_2\text{O}$  and  $\delta^{18}\text{O-H}_2\text{O}$ ) from these samples are consistent with the modern post-glacial meteoric water line (Warner et al., 2012), suggesting post-glacial (post-Pleistocene) meteoric groundwater recharge. Therefore, we conclude that the excess  $[\text{}^4\text{He}]$  we have observed in groundwater from UD aquifers cannot be derived solely by *in-situ* production or release within the Catskill or Lock Haven aquifers. Instead, the observed  $[\text{}^4\text{He}]$  requires the migration of an exogenous source into these shallow aquifers. Based on the correlations between  ${}^4\text{He}$ ,  $\text{CH}_4$ , and salts and the lack of resolvable mantle-derived components ( $> 1\%$ ) in the majority of samples, we suggest that hydrocarbon-rich brine is the most likely source of exogenous  ${}^4\text{He}$  in this area.

**4.2.2.3. Fluid interactions in the crust.** Methane, ethane, and radiogenic  ${}^4\text{He}$  (produced by the decay of U and Th) dominate thermogenic natural gases, while  ${}^{20}\text{Ne}$  and  ${}^{36}\text{Ar}$  are sourced predominantly from the atmosphere, and thus only enter natural gas reservoirs through the interaction with formation water (e.g., Gilfillan et al., 2009). Because  $\text{CH}_4$  and  ${}^{36}\text{Ar}$  ( $\beta_{\text{CH}_4}/\beta_{\text{Ar}} = 1$  at  $10^\circ\text{C}$ , STP) as well as  ${}^4\text{He}$  and  ${}^{20}\text{Ne}$  ( $\beta_{\text{He}}/\beta_{\text{Ne}} = 1.2 \times$  at  $10^\circ\text{C}$ , STP) each have similar respective solubility constants, the  $\text{CH}_4/{}^{36}\text{Ar}$  and  ${}^4\text{He}/{}^{20}\text{Ne}$  ratios allow a direct comparison of the proportion of thermogenic and ASW components. For example, the  $\text{CH}_4/{}^{36}\text{Ar}$  provides a sensitive tracer of the gas–water ratio (the percentage of the methane and atmospheric component in the mixture) irrespective of any gas–fluid partitioning that may have occurred.

Because the saturation (i.e., bubble point) of methane increases with depth, while  ${}^{36}\text{Ar}$  is fixed by ASW contributions at recharge, the  $\text{CH}_4/{}^{36}\text{Ar}$  can provide information about the depth of groundwater equilibration in some cases. In our study area, the  $\text{CH}_4/{}^{36}\text{Ar}$  ranges from  $\sim 0$  (i.e., 100% atmospheric gases) to  $\text{CH}_4/{}^{36}\text{Ar} = \sim 3.80 \times 10^4$ . By comparison, the calculated saturation conditions (i.e., bubble point) for methane (i.e.,  $P(\text{CH}_4) = 1 \text{ atm}$ ) in a shallow aquifer recharging at 600 m and  $10^\circ\text{C}$  are  $\text{CH}_4/{}^{36}\text{Ar} = \sim 4.0 \times 10^4$  (Fig. 8). Only the Salt Spring sample (Montrose, PA) has a  $\text{CH}_4/{}^{36}\text{Ar}$  above saturation ( $4.01 \times 10^4$ ), which indicates equilibration at greater depths with a methane-rich source at pressures above  $P(\text{CH}_4) = 1 \text{ atm}$ .

Across the study area, the ratios of thermogenic to ASW components (e.g.,  $\text{CH}_4/{}^{36}\text{Ar}$ ,  ${}^4\text{He}/{}^{20}\text{Ne}$ ,  ${}^4\text{He}/{}^{36}\text{Ar}$ ) show a strong positive correlation ( $r^2 > 0.768$ ;  $p < 0.01$ ) with each other and diluted brine components (i.e.,  $[\text{Cl}^-]$ ,  $[\text{Br}]$ ,  $[\text{Ba}]$ ) (Figs. 3 and 8). Interestingly, these trends consistently fall along a two-component mixing line between the Salt Spring and meteoric ASW ( $\text{CH}_4/{}^{36}\text{Ar} = \sim 0$ ,  ${}^4\text{He}/{}^{20}\text{Ne} = 0.3$ ,  ${}^4\text{He}/{}^{36}\text{Ar} = 0.045$ ) (Fig. 8). These results suggest that naturally present salt- and gas-rich groundwater samples  $> 1 \text{ km}$  from natural gas drill sites in our study area likely result from variable additions of a thermogenic hydrocarbon gas-rich brine (dominated by methane with minor ethane and other crustal components, e.g.,  ${}^4\text{He}$ ) to tritium-active, and hence, relatively recent meteoric water (dominated by ASW components, e.g.,  $\text{N}_2$ ,  ${}^{36}\text{Ar}$ ) in shallow groundwater conditions.

Because isotopic ratios of atmospheric components in shallow groundwater are largely consistent globally, with only minor variations that result from salinity, temperature, and elevation (atmospheric pressure) (Ballentine et al., 2002), the isotopic ratios of ASW gases (in the absence of mantle contributions) provide additional insight into the history of gas–water interactions and post-genetic modification processes (Gilfillan et al., 2009; Dubacq et al., 2012; Zhou et al., 2012; Darrah et al., 2014). Similarly, the relative concentration of exogenous  ${}^4\text{He}$  in crustal fluids (e.g.,  ${}^4\text{He}/\text{CH}_4$ ) results from a combination of the  ${}^4\text{He}$  released within the original thermogenic natural gas source (e.g., the Marcellus Formation) and the fractionation that occurs during fluid migration processes (Ballentine et al., 2002; Ballentine and Sherwood Lollar, 2002; Hunt et al., 2012; Darrah et al., 2014). For example, both diffusion and gas-phase partitioning (gas and water separation) enrich the lighter trace gases in fluids that migrate away from the source (e.g., increased  ${}^4\text{He}/\text{CH}_4$  and  ${}^{20}\text{Ne}/{}^{36}\text{Ar}$ ). As a result, the  ${}^4\text{He}/\text{CH}_4$  and  ${}^{20}\text{Ne}/{}^{36}\text{Ar}$  of crustal fluids (specifically groundwater) are particularly useful for fingerprinting the source of natural gas and evaluating the process of gas migration (e.g., diffusion or solubility fractionation).

The  ${}^{20}\text{Ne}/{}^{36}\text{Ar}$  records other important clues about the transport mechanisms by which the hydrocarbon-rich brine reached the surface. Groundwater samples in the gas-rich end-member of our study area have  ${}^{20}\text{Ne}/{}^{36}\text{Ar}$  above ASW equilibrium ( $\sim 0.156$ ) (Fig. 9). Although elevated  ${}^{20}\text{Ne}/{}^{36}\text{Ar}$  can result from the addition of “excess air,” an increase in the excess air content should increase both

[ $^{20}\text{Ne}$ ] and [ $^{36}\text{Ar}$ ], while only increasing the  $^{20}\text{Ne}/^{36}\text{Ar}$  to approximately 0.55 ( $^{20}\text{Ne}/^{36}\text{Ar}$  in air). Instead, our data include numerous samples with  $^{20}\text{Ne}/^{36}\text{Ar} > 0.55$ , where the increase of neither [ $^{20}\text{Ne}$ ] nor  $^{20}\text{Ne}/^{36}\text{Ar}$  correlates with either [ $^{36}\text{Ar}$ ] or  $\text{N}_2/\text{Ar}$  (Fig. 9). Instead, this increase in  $^{20}\text{Ne}/^{36}\text{Ar}$  relates almost exclusively to an increase of [ $^{20}\text{Ne}$ ] concomitantly with [ $\text{CH}_4$ ], [ $^4\text{He}$ ], and dissolved salts ([Cl] and [Br]) suggesting that the elevated [ $^{20}\text{Ne}$ ] may be exogenous Ne associated with the hydrocarbon-rich brine (plausible mechanisms discussed below). Because there is no correlation between  $^{20}\text{Ne}/^{36}\text{Ar}$  and  $\text{N}_2/\text{Ar}$ , or a statistically meaningful difference ( $p > 0.3$ ) in the concentration of ASW components (e.g., [ $\text{N}_2$ ], [Ar], or  $\text{N}_2/\text{Ar}$ ) according to methane concentration, we suggest that mixing between young meteoric water and the migrated brine (typified by the Salt Spring) occurs near the surface (Figs. 5 and 9). If instead the hydrocarbon-rich brine had mixed with shallow meteoric waters deeper in the crust and then migrated, both the thermogenic natural gas and ASW components (i.e.,  $\text{N}_2/\text{Ar}$  vs.  $^{20}\text{Ne}/^{36}\text{Ar}$ ) should coherently fractionate during the formation of a gas-phase.

The thermogenic components ( $^4\text{He}$  and  $\text{CH}_4$ ) show similar patterns of extensive molecular and isotopic fractionation. All groundwater samples in the study area (except four that were targeted for their shallow microbial source and four samples with evidence of mantle-derived contributions) display [ $^4\text{He}$ ] dominated by an exogenous crustal source and a  $^4\text{He}/\text{CH}_4$  that greatly exceeds ( $p < 0.01$ ) the value measured for the hydrocarbon production gases from either the Marcellus or UD in the NAB (Table 2a and Fig. 10; Hunt et al., 2012). These highly elevated  $^4\text{He}/\text{CH}_4$  values likely reflect significant post-genetic modification of natural gases in the groundwaters from our dataset.

## 5. DISCUSSION

The correlations between exogenous  $^4\text{He}$ , excess atmospheric  $^{20}\text{Ne}$ , thermogenic hydrocarbon gases (i.e.,  $\text{CH}_4$ ,  $\text{C}_2\text{H}_6$ ), diagnostic isotope ratios (e.g.,  $^{20}\text{Ne}/^{36}\text{Ar}$ ,  $^4\text{He}/\text{CH}_4$ , and  $\delta^{13}\text{C}-\text{CH}_4$ ), and salts (i.e., Cl and Ba) suggest that a common process coherently regulates their presence within shallow aquifers in the NAB (Figs. 3, 6 and 8). Here, we examine several hypothetical scenarios that may account for these geochemical observations.

### 5.1. Potential fluid migration mechanisms

Previous investigations into the inorganic geochemical fingerprints (e.g., Br/Cl and  $^{87}\text{Sr}/^{86}\text{Sr}$ ) and stable isotope geochemistry of methane-rich groundwater samples in the NAB suggest that hydrocarbon-rich brines may have migrated from the Marcellus Formation to modern day shallow aquifers on yet undetermined time scales (Warner et al., 2012). Further, gas geochemistry data from the present study suggest that hydrocarbon- and salt-rich fluids in this study area exhibit clear evidence of an exogenous source.

In light of the Marcellus-like inorganic chemistry and the lack of other major hydrocarbon-generating units superior to the Marcellus within the eastern part of the NAB

(Lash and Engelder, 2011), we assume an initial natural gas composition consistent with Marcellus production gases, recognizing that the fluids that migrated to UD formations may have left the Marcellus before they reached the “maximum” thermal maturities observed in Marcellus production gases today (i.e., hydrocarbon may have been emplaced into UD reservoirs while the basin was still subsiding and therefore would exhibit a lower thermal maturity at the time of initial hydrocarbon migration). Using this starting composition, we employ numerical models to determine the viable crustal fluid migration mechanisms that can account for these geochemical observations in the NAB.

We hypothesize that four migration mechanisms can potentially accommodate hydrocarbon transport from the Marcellus Formation to the overlying UD aquifers: (1) advection of a single-phase methane-rich Marcellus brine (gas dissolved in water); (2) “buoyant” advection of a single (“free”) gas-phase natural gas (without dissolved ions); (3) the advection of a two-phase fluid (i.e., free gas + brine); and (4) aqueous diffusion of gases and solutes within a static single-phase methane-rich brine (i.e., primary diffusion). Model parameters are discussed in detail in Section 3.3. For the model fit, we focus on three key tracers:  $^{20}\text{Ne}/^{36}\text{Ar}$ ,  $^4\text{He}/\text{CH}_4$ , and [Cl].

#### 5.1.1. Mechanisms of hydrocarbon emplacement

The correlation between  $^4\text{He}$ ,  $\text{CH}_4$ ,  $\text{C}_2\text{H}_6$ , and dissolved ions (i.e., Cl and Ba), in combination with a Marcellus-type signature for dissolved inorganic constituents (e.g., Br/Cl and  $^{87}\text{Sr}/^{86}\text{Sr}$ ) (Warner et al., 2012), suggests a common mechanism of migration for both natural gas and dissolved salts (Figs. 3, 5, 8–10). As a result, we suggest that primary and secondary hydrocarbon migration in the NAB *do not* occur by the “buoyant” advection of a single (“free”) gas-phase (Mechanism 2).

The advection of a single-phase fluid (i.e., gas dissolved in brine) (Mechanism 1) would not permit quantitative fractionation of the dissolved atmospheric gases (i.e.,  $^{20}\text{Ne}/^{36}\text{Ar}$ ) by phase partitioning, but could increase the relative [ $^4\text{He}$ ] by a combination of helium accumulation from the country rock and/or hydrocarbon oxidation (gray trend in Fig. 10). Because the increase in  $^{20}\text{Ne}$  does not correspond with increases in  $^{36}\text{Ar}$  (Fig. 9), and several samples have  $^{20}\text{Ne}/^{36}\text{Ar} > 0.55$ , we suggest that the elevated  $^{20}\text{Ne}/^{36}\text{Ar}$  in the gas-rich end-member likely results from mixing of ASW noble gases and a fluid with a highly fractionated  $^{20}\text{Ne}/^{36}\text{Ar}$ . As a result, we can also preclude Mechanism 1.

Mechanisms 3 (two-phase advection of gas + brine) and 4 (aqueous diffusion) could fractionate the noble gas composition (e.g.,  $^{20}\text{Ne}/^{36}\text{Ar}$ ,  $^4\text{He}/\text{CH}_4$ ) and enrich the less soluble/lower molecular weight species (i.e.,  $^4\text{He} > ^{20}\text{Ne} > ^{36}\text{Ar}$ ) in the fluids that were emplaced in the UD traps. However, because the degree of fractionation ( $\alpha$ ) differs for each of these mechanisms, we can differentiate the two processes.

Neither Mechanism 3 nor 4 uniquely fits all of the data (e.g.,  $^4\text{He}/\text{CH}_4$  vs.  $^{20}\text{Ne}/^{36}\text{Ar}$ ) from groundwater samples in our study (Figs. 10 and 11). However, because the

$^{20}\text{Ne}/^{36}\text{Ar}$  of both UD production gases (up to  $\sim 1.4$ ) and the methane-rich groundwater end-member in overlying UD formations (up to 1.09) exceed the maximum values obtained by the diffusion model (Mechanism 4) and “excess” air (Fig. 9), we suggest that Mechanism 3 must be an integral component in the emplacement of Marcellus natural gases into the overlying conventional UD hydrocarbon reservoirs, which now constitute modern-day UD aquifers.

The formation of a dual-phase fluid requires that the partial pressure of natural gas overcomes the combined hydrostatic and lithostatic pressure (i.e., overburden pressure) in order to nucleate and sustain a gas phase. Theoretically, tectonically-driven, burial-induced catagenesis would be the most likely mechanism that could generate sufficient  $\text{CH}_4$  pressures to nucleate and sustain a dual-phase fluid at 2–6 km depth (approximate maximum burial depth of the Marcellus in this region (Evans, 1995)) within the crust. We hypothesize that the  $^{20}\text{Ne}/^{36}\text{Ar}$  fractionation observed during Mechanism 3 would occur in two phases: (1) during *primary migration* (e.g., catagenesis, in which less soluble components (e.g.,  $^4\text{He}$ ,  $^{20}\text{Ne}$ ) fractionate into the gas-phase) as hydrocarbons leave the source rock and (2) during *secondary migration* (e.g., during buoyant migration the more soluble components ( $^{36}\text{Ar}$ ,  $\text{CH}_4$ ) would redissolve back into the water and further enrich the ongoing gas in less soluble components ( $^4\text{He}$ ,  $^{20}\text{Ne}$ )) (Gilfillan et al., 2009; Zhou et al., 2012; Darrah et al., 2014). Thus, the elevated  $^{20}\text{Ne}/^{36}\text{Ar}$  observed in these samples is likely the remnant of a scenario in which a relatively low volume of Marcellus-sourced, super-saturated hydrocarbon gas-rich brine migrated through a relatively large volume of crustal liquid (i.e., low  $V_{\text{gas}}/V_{\text{water}}$ ). One important piece of data that is not consistent with this interpretation is the extent of excess in  $^4\text{He}/\text{CH}_4$  relative to the solubility fractionation model (discussed below in Section 5.1.2).

Other scenarios, such as the multi-stage dissolution re-equilibration of a static hydrocarbon-rich fluid, equilibration with oil/hydrocarbon liquids, or contributions from mantle-derived fluids could also account for the elevated  $^{20}\text{Ne}/^{36}\text{Ar}$  (e.g., Zhou et al., 2012). However, it is difficult to envision a scenario that would allow multiple-stage re-equilibration of a static hydrocarbon-gas and brine that would also produce the coherent behavior of the dissolved inorganic ions (i.e., Cl, Br, Ba) and gas components.

In an attempt to constrain the conditions of hydrocarbon-rich brine migration, we model the temperature-dependent fractionation of  $^{20}\text{Ne}/^{36}\text{Ar}$  and  $^4\text{He}/\text{CH}_4$  from 10 to 200 °C. This range includes shallow groundwater conditions (temperature = 10 °C), a modern Marcellus geothermal gradient (assuming 25 °C/km), and past periods of higher thermal conditions (conodont alteration index (CAI):  $>4$ ; vitrinite reflectance ( $R_o$ ):  $>3$  implies temperatures approaching at least 200 °C, possibly during maximum burial of Middle Devonian sequences) (Fig. 10). The proposed temperature-dependent solubility fractionation model implies the advection of a two-phase, hydrocarbon gas-rich brine under temperature conditions exceeding  $\sim 120$  °C (Fig. 10). These temperature estimates are consistent with a conceptual model for geological

emplacement of hydrocarbons during secondary migration, possibly related to the Alleghanian Orogeny (Oliver, 1986; Bethke and Marshak, 1990; Cathles, 1990), and are consistent with temperatures derived from CAI and vitrinite reflectance.

#### 5.1.2. Redistribution of hydrocarbons into modern aquifers by tertiary migration?

Although both UD production gases and methane-rich groundwater samples have highly elevated  $^{20}\text{Ne}/^{36}\text{Ar}$  (above  $\sim 0.55$ ), consistent with solubility fractionation during transport and emplacement, there are several clear geochemical distinctions between the two sample types. Most importantly, numerical modeling for the advection of a dual-phase fluid does not produce sufficient fractionation to account for the highest  $^4\text{He}/\text{CH}_4$  observed in the UD groundwater, even in the hydrocarbon gas-rich end-member. Additionally, as compared to UD produced gases, the UD groundwater shows progressively increasing  $^4\text{He}/\text{CH}_4$  with decreasing  $^{20}\text{Ne}/^{36}\text{Ar}$ , which is opposite to the trend to that would be expected for an additional stage of solubility fractionation during transport (Fig. 10).

One might anticipate that microbial activity in the shallow aquifer could alter the  $^4\text{He}/\text{CH}_4$  values. However, the UD groundwaters from this study show a trend of increasingly more negative  $\delta^{13}\text{C}-\text{CH}_4$  with increasing  $^4\text{He}/\text{CH}_4$  values (Fig. 11). This trend is opposite to what one would expect for the addition of microbial methane by methanogenesis (either *in-situ* or via mixing with an external microbial source), which should decrease the  $^4\text{He}/\text{CH}_4$  (Fig. 11). Alternatively, methane oxidation could increase the  $^4\text{He}/\text{CH}_4$ , but this trend would also enrich the  $\delta^{13}\text{C}-\text{CH}_4$  in the residual gas (e.g., Kessler et al., 2006; Pape et al., 2010), which is also the opposite of what is observed in the current data set (discussed further below) (Fig. 11).

One alternative *ad hoc* interpretation that can account for the correlation between highly elevated  $^4\text{He}/\text{CH}_4$  and decreasing  $\delta^{13}\text{C}-\text{CH}_4$  is a secondary mechanism of post-genetic modification. Although solubility fractionation is not consistent with the data trends (i.e., the  $^4\text{He}/\text{CH}_4$  increases as the  $^{20}\text{Ne}/^{36}\text{Ar}$  decreases), the diffusion of hydrocarbon gases from gas-charged UD stratigraphic or structural traps into modern meteoric groundwater could account for the direction of both  $^4\text{He}/\text{CH}_4$  (increasing) and  $\delta^{13}\text{C}-\text{CH}_4$  (more negative) trends.

The general trends of fractionation are consistent with tertiary migration, which could occur by recent diffusion of natural gas and brine from UD conventional traps into modern, circulating groundwater. In this scenario, diffusion would fractionate gases approximately according to the ratio of the square root of their molecular masses and can account for the highest  $^4\text{He}/\text{CH}_4$ , assuming an elevated  $^4\text{He}/\text{CH}_4$  starting composition consistent with UD production gases. We hypothesize that the fact that these UD production gases already experienced post-genetic fractionation (increased  $^4\text{He}/\text{CH}_4$ ) during emplacement may help the UD groundwater achieve exceptionally high  $^4\text{He}/\text{CH}_4$  in this setting. Nonetheless, some component of methane oxidation (e.g., Kessler et al., 2006; Pape et al., 2010) could aid this process (Figs. 10 and 11).

Therefore, we hypothesize that the most parsimonious explanation for the observed data in shallow groundwaters from UD aquifers is a three-step evolution: (1) the formation of a two-phase hydrocarbon-rich brine, likely during early Marcellus catagenesis (*primary* hydrocarbon migration), that enriched the  $^4\text{He}/\text{CH}_4$  and  $^{20}\text{Ne}/^{36}\text{Ar}$ ; (2) *secondary* hydrocarbon migration of a two-phase fluid from the source rocks to conventional traps, which further enriched the  $^4\text{He}/\text{CH}_4$  and  $^{20}\text{Ne}/^{36}\text{Ar}$  in the migrated phase; followed by (3) *tertiary migration* in which natural gas previously emplaced in conventional structural or stratigraphic traps within UD lithologies diffuses into flowing UD

groundwaters, equilibrates with modern meteoric water, and experiences variable amounts of additional alteration by methanogenic or methanotrophic activity (Fig. 12).

This proposed tertiary migration process may have been enhanced when post-glacial uplift and denudation stimulated neotectonic fracturing in existing stratigraphic and structural traps or re-opened previously mineralized fractures. Based on the upper limit of  $[\text{CH}_4]$  and  $\text{CH}_4/^{36}\text{Ar}$  (at methane saturation in shallow groundwater), it appears that the flux of natural gas is limited by the saturation of methane at shallow hydrostatic pressures consistent with a scenario in which hydrodynamic flow sufficiently restricts

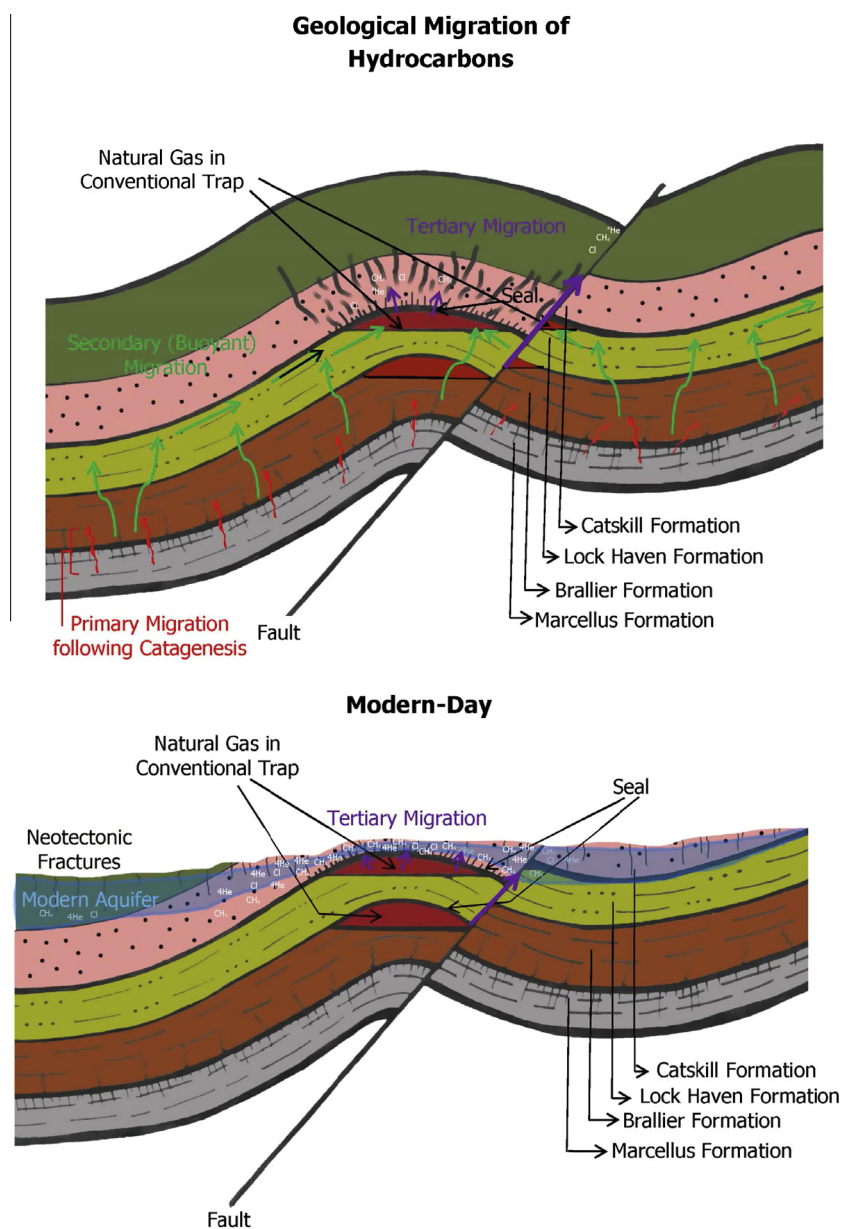


Fig. 12. Conceptual model of primary, secondary, and tertiary hydrocarbon migration mechanisms in the northern Appalachian Basin. Primary and secondary hydrocarbon migration mechanisms likely occurred by the advection of a two-phase fluid following the Alleghanian Orogeny, while tertiary migration of hydrocarbons likely occurs via diffusion and continues today. Notice how the rate and magnitude of tertiary migration would increase following neo-tectonic fracturing in the modern geological setting.

buoyant gas migration in the subsurface. The relative trends of the hypothesized tertiary migration are shown along the dashed blue line in Figs. 10 and 11. The starting composition for these proposed secondary diffusion trends are arbitrarily set amid the range of UD production gases for illustrative purposes.

In our estimation, the two areas of greatest concern for our 3-step model include: (a) the large scale of stable isotope fractionation ( $\sim 25$  per mil shift in  $\delta^{13}\text{C-CH}_4$ ) required to shift from a Marcellus starting composition to the lightest  $\delta^{13}\text{C-CH}_4$  observed in groundwater samples, specifically across relatively short geological distances ( $< 2$  km) and (b) scatter in the data, particularly for the proposed third stage of tertiary migration.

One *ad hoc* consideration is that the level of stable isotope fractionation could become more feasible if the shallow sources of hydrocarbon-rich brine represent the migration of an earlier generation of less thermally mature (i.e., lighter  $\delta^{13}\text{C-CH}_4$ ) natural gas. Hypothetically, a best fit line of the mixing model could provide some insight into the thermal maturity of the migrated component. The mixing model suggest that a  $\delta^{13}\text{C-CH}_4 = \sim -41\%$  is required to provide a reasonable estimate for the starting composition of methane. Theoretically, this earlier stage of Marcellus-sourced gas migrated into stratigraphic and structural traps in UD formations during earlier stages of basin burial. This argument would still be consistent with both the noble gas (elevated  $^4\text{He}/\text{CH}_4$  and  $^{20}\text{Ne}/^{36}\text{Ar}$ ) and dissolved ion data (Cl, Br, Ba, and  $^{87}\text{Sr}/^{86}\text{Sr}$  (Warner et al., 2012)), and could introduce a source of natural gas to the shallow UD formations with a significantly lighter  $\delta^{13}\text{C-CH}_4$  than present Marcellus produced gases. If this earlier generation of natural gas migration occurred, it would minimize the need for extensive stable isotope fractionation by solubility fractionation and diffusion alone. In support of this argument, we note that modern Marcellus production gases from the region have carbon isotope reversals ( $\delta^{13}\text{C-CH}_4 > \delta^{13}\text{C-C}_2\text{H}_6$ ), whereas many UD production gases from the area, which are originally sourced from the Marcellus, and the most enriched  $\delta^{13}\text{C-CH}_4$  values observed  $> 1$  km from drill sites in this study do not have carbon isotope reversals ( $\delta^{13}\text{C-CH}_4 < \delta^{13}\text{C-C}_2\text{H}_6$ ) (Jenden et al., 1993; Osborn et al., 2011; Jackson et al., 2013; Molofsky et al., 2013; Darrah et al., 2014). Obviously, the hypothesis of molecular and isotopic fractionation during late stage diffusion must be tested in other basins, but it is interesting to note that it can account for the general trends in both noble gas and  $\delta^{13}\text{C-CH}_4$  data.

Given the variability across a  $\sim 7500$  km<sup>2</sup> study area, the scatter in data may reflect geospatial variations in the initial source components, variable distances of secondary migration prior to emplacement (i.e., the depths to the Marcellus and distance to the Appalachian structural front are not constant throughout the basin), or natural migration pathways in this tectonically complex region (Figs. 1 and 2). It should be noted, however, that there was no significant correlation between  $[\text{CH}_4]$ ,  $^4\text{He}/\text{CH}_4$ , or  $^{20}\text{Ne}/^{36}\text{Ar}$  with latitude, longitude, sampling depth, or the aquifer formation (all  $p > 0.30$ ). Instead, spatial data suggests that the clearest controls on hydrocarbon-gas, salt, and exogenous [ $^4\text{He}$ ]

relate to the proximity to valley bottoms that reside in the eroded core of anticlines, which suggests hydrodynamic control of hydrocarbon gas-rich, thermogenic brines in groundwater discharge areas (Fig. 13).

## 5.2. Integration of noble gas and hydrocarbon molecular and isotopic data in shallow aquifers

### 5.2.1. Hydrocarbon stable isotopic composition

The noble gas data and numerical models presented above provide a conceptual framework for naturally occurring hydrocarbons in modern shallow UD aquifers and conventional UD production formations in the NAB. However, this conceptual model for hydrocarbon-rich brine migration must be tested for consistency with other traditional hydrocarbon molecular and isotopic techniques. For example, based on the conceptual model established above, we might anticipate multiple stages of post-genetic modification during primary, secondary, and tertiary migration. The migrated thermogenic natural gas could also be altered by the addition of shallow microbial methane or methane oxidation.

Typically, one would test these hypotheses by comparing the relative molecular hydrocarbon ratios and stable isotopic compositions to differentiate distinct sources of thermogenic and microbial  $\text{CH}_4$  (Bernard, 1978). Although  $\text{C}_1/\text{C}_2+$  versus  $\delta^{13}\text{C-CH}_4$  is often used for this purpose, we plot the hydrocarbon ratio  $\text{C}_2+/\text{C}_1$  versus  $\delta^{13}\text{C-CH}_4$  because the empirical mass-balance mixing calculation approximates a straight line independent of the  $[\text{CH}_4]$  in either source (Fig. 11a).

Fig. 11a demonstrates that very few samples appear to fall along a simple two-component mixing trend between the Marcellus-type end-member and microbial inputs, although these mixing proportions could be altered by the assumed isotopic value in the microbial end-member. For example, if  $\delta^{13}\text{C-CH}_4$  of  $-70\%$  were chosen, the majority of samples appear to have significantly more enriched  $\delta^{13}\text{C-CH}_4$  than the mixing trend, while mixing is more feasible for a higher proportion of samples if a relatively heavy microbial end-member ( $\delta^{13}\text{C-CH}_4 = -52\%$ ) is assumed (Fig. 11a). Nonetheless, one must assume a microbial end-member of  $\delta^{13}\text{C-CH}_4 = -41\%$ , which is a significantly more enriched  $\delta^{13}\text{C-CH}_4$  than has been reported for microbial gases to date, to account for the best fit of a two-component mixture that accounts for the majority of samples in the methane-rich end-member. While previous work interpreted the molecular and isotopic composition of dissolved  $\text{CH}_4$  in UD groundwater samples as sourced from complex and variable three-component mixtures of multiple thermogenic gases (Middle and Upper Devonian) and biogenic methane (Laughrey and Baldassare, 1998; Revesz et al., 2010; Osborn et al., 2011), a viable third component has not been identified. Instead, most of the data plot along a trajectory of strong depletion of  $\text{C}_2$  relative to  $\text{C}_1$  with progressively lighter  $\delta^{13}\text{C-CH}_4$  composition, which is a pattern that was previously ascribed to fractionation during “diffusional migration” (e.g., Prinzhofer and Pernaton, 1997) (Fig. 11a).

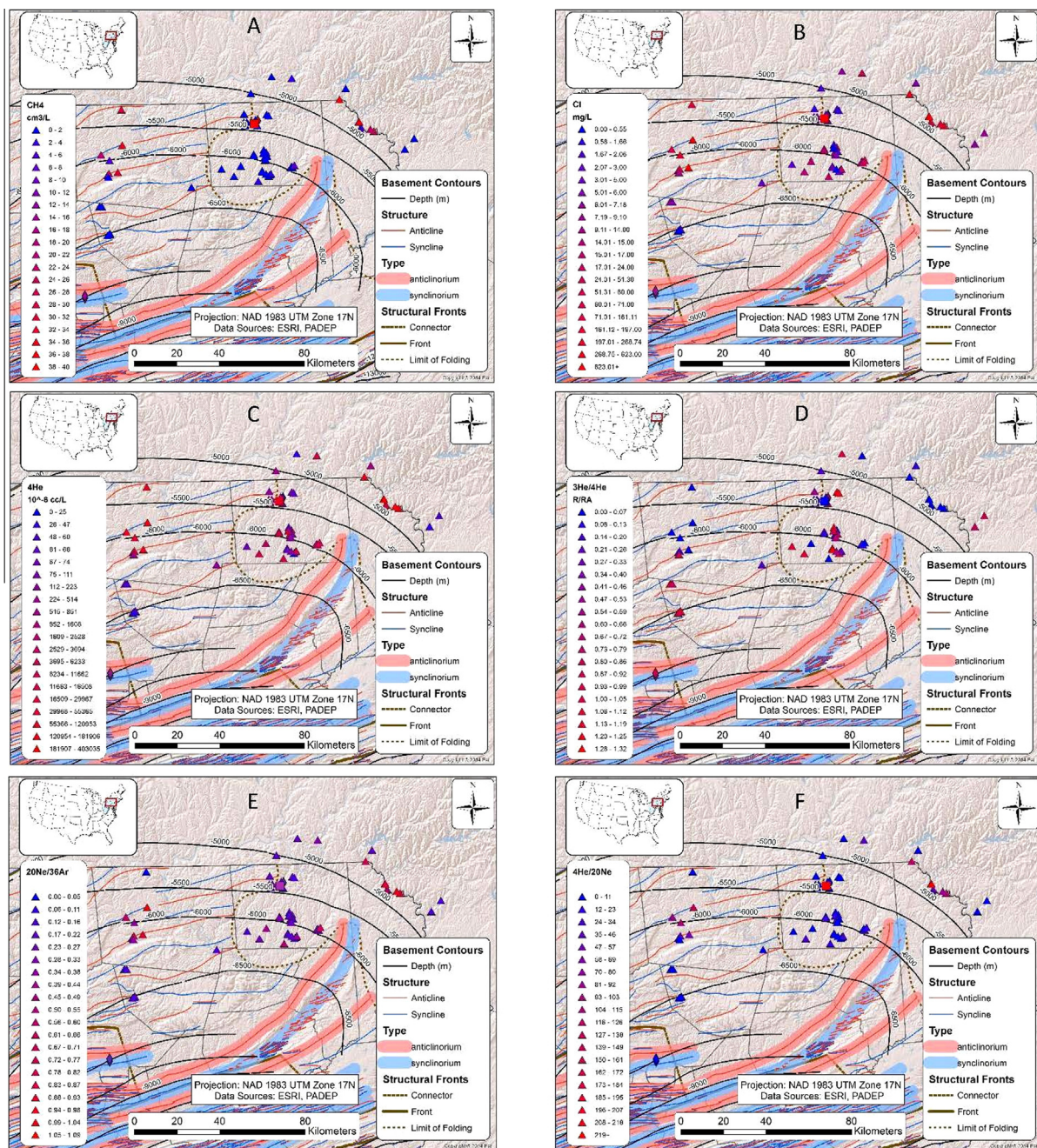


Fig. 13. Spatial distribution of key parameters, including  $[\text{CH}_4]$  (A);  $[\text{Cl}^-]$  (B);  $[\text{He}]$  (C);  $R/Ra$  (D);  $^{20}\text{Ne}/^{36}\text{Ar}$  (E); and  $^4\text{He}/^{20}\text{Ne}$  (F) across the study area. While we do not observe any statistically significant variations in these parameters according to well depth, aquifer stratigraphy, distance from the Appalachian Structural Front (a proxy for maximum burial depth and thermal maturity), latitude, or longitude, we do confirm previous observations (Warner et al., 2012; Molofsky et al., 2013; Llewellyn et al., 2015) of elevated hydrocarbon gases, salts, and exogenous  $[\text{He}]$  in some valley bottoms.

Because noble gases provide an externally defined end-member to calculate hydrocarbon mixing, combining both noble gas and stable isotope tracers may provide additional insight into the argument of mixing between thermogenic and biogenic methane (Stolper et al., 2014, 2015) versus post-genetic modification. For example, thermogenic gases are rich in radiogenic  $^4\text{He}$ , while recently formed microbial

gases in shallow aquifers should be nearly devoid of  $^4\text{He}$ . By comparison, our groundwater samples are extremely rich in helium and the decreases in  $\text{C}_2/\text{C}_1$  and  $\delta^{13}\text{C}-\text{CH}_4$  correspond to an increase in  $^4\text{He}/\text{CH}_4$  values (Fig. 11b). Although we cannot completely exclude the presence of an extremely old, high  $[\text{He}]$ , microbial gas end-member, we suggest that the concomitant presence of “light”

$\delta^{13}\text{C-CH}_4$ , highly exogenous  $[\text{}^4\text{He}]$ , elevated  $^4\text{He}/\text{CH}_4$  and elevated  $^{20}\text{Ne}/^{36}\text{Ar}$  may suggest a role for some component of fractionation during the combined processes of primary, secondary, and tertiary hydrocarbon migration, rather than exclusively mixing of thermogenic and biogenic natural gases (Craig, 1968; Prinzhofer and Huc, 1995; Prinzhofer and Pernaton, 1997). In combination, these results suggest that we must consider the potential role that post-genetic alteration may play in altering the molecular and stable isotope composition of some natural gases in UD formations of the NAB.

Although post-genetic modification of the molecular and isotopic composition of hydrocarbon gases was previously reported (e.g., Craig, 1968; Prinzhofer and Huc, 1995), the viability of this fractionation process was often overlooked because diffusion is not considered a viable transport mechanism at crustal-scales (i.e., kilometers). As a result, many workers do not consider the influence of post-genetic modification when determining the source of methane in shallow aquifers. However, by combining the molecular and isotopic composition of hydrocarbons with noble gas geochemistry, one may potentially differentiate between post-genetic modification and mixing between microbial and thermogenic sources.

It is important to note that these conclusions may appear to contradict some previous reports, which minimize the potential for fractionation by diffusion in laboratory experiments or within production formations (e.g., Fuex, 1980; Xia and Tang, 2012). However, in contrast to previous models, which suggest that “diffusional migration” accounts for the rapid depletion of  $\text{C}_2+\text{C}_1$  (Pernaton et al., 1996; Prinzhofer and Pernaton, 1997; Lorant et al., 1998), our noble gas data (specifically the  $^{20}\text{Ne}/^{36}\text{Ar}$ ) suggest that the solubility-controlled fractionation during the advection of a two-phase fluid controls the alteration of production gases during crustal fluid migration (i.e., secondary hydrocarbon migration). In fact, we do not observe significant evidence for diffusional fractionation during hydrocarbon emplacement (i.e., filling of unconventional UD production reservoirs during migration from the Marcellus) (Figs. 10 and 11).

However, our data do suggest that diffusion may induce measurable post-genetic modification of hydrocarbon gases in the shallow crust. Thus, while our results question the importance of diffusion during the emplacement of hydrocarbons (primary or secondary migration) into conventional traps, they do indicate that post-genetic fractionation during tertiary hydrocarbon migration, presumably following uplift, denudation, and neotectonic fracturing, may significantly alter the hydrocarbon isotopic composition of natural gas found within shallow aquifers, such as the methane-rich end-member in shallow UD aquifers.

Paired  $\delta^{13}\text{C-CH}_4$  and noble gas analyses provide an additional externally-defined component by which to evaluate gas source and migration. If verified in other basins, our findings limit the need to evoke complex, hypothetical, three-component mixtures between multiple thermogenic gases and “sub-surface” microbial gas to account for the concave curve displayed in Fig. 11a in the NAB or other petroliferous basins (Revesz et al., 2010; Baldassare, 2011;

Baldassare et al., 2012). For example, it is unknown if this trend relates to intense neotectonic fracturing and post-glacial unloading that permits interactions between meteoric water and previously emplaced hydrocarbon-rich brines or if this is a common feature in various tectonic settings globally. Future work should evaluate these fractionation trends associated with primary and secondary hydrocarbon migration as well as subsequent processes (i.e., tertiary migration) that transport hydrocarbons from conventional traps into shallow overlying formations in sedimentary basins with diverse tectonic histories in order to validate this framework for unconventional energy basins in different geographic areas.

### 5.2.2. Differentiating microbial and migrated gases

Noble gas data, combined with hydrocarbon elemental and isotopic data presented above, suggest that the previously hypothesized “subsurface microbial” component, commonly interpreted as an end-member in crustal mixing arrays, may include a subset of samples that have experienced some degree of post-genetic fractionation during crustal fluid migration. While these results potentially suggest a paucity of microbial methane in a subset of UD groundwater samples from the NAB, we targeted four samples with anticipated microbial origins (i.e., near a landfill and agricultural manure deposits) to evaluate these trends. Although these anticipated microbial samples are indistinguishable from many other groundwater samples in the revised Bernard plot (Fig. 11a), they are easily distinguishable by both stable and noble gas isotopes. Microbial gases in our study had significantly lower  $[\text{}^4\text{He}]$  (shown as  $^4\text{He}/^{20}\text{Ne}$  and  $^4\text{He}/^{36}\text{Ar}$  in Fig. 8) and lighter  $\delta^2\text{H-CH}_4$  (consistent with “near-surface” microbial in the Schoell plot; Fig. 4c) than our inferred migrated end-member (previously termed “subsurface microbial”) despite an overlapping range of  $\delta^{13}\text{C-CH}_4$ .

Thus, we suggest that at least one externally-defined variable is required to uniquely determine the relative proportions of mixing (e.g., Poreda and Craig, 1992) in fluids with stable isotope patterns consistent with the “subsurface microbial” field. The relative contributions of crustal noble gases (e.g.,  $^4\text{He}$ ) provide an appropriate external variable, which when paired with methane stable isotopes or ASW noble gas isotopes (e.g.,  $^4\text{He}/\text{CH}_4$ ,  $^4\text{He}/^{36}\text{Ar}$  or  $^4\text{He}/^{20}\text{Ne}$ ), can easily distinguish mixtures of microbial and thermogenic gases (Fig. 8). In the four samples with microbial inputs, the ASW noble gases are consistent with Henry’s Law equilibration between groundwater and the atmosphere, whereas the remaining samples show a thermogenic gas trend with highly elevated  $[\text{}^4\text{He}]$  that increases with  $[\text{CH}_4]$  (Fig. 8).

## 6. CONCLUSIONS

Our data confirm a subset of groundwater samples in shallow aquifers in the northern Appalachian Basin (NAB) contain naturally (i.e., unrelated to shale gas development) present methane, predominantly in valley bottoms. The radiogenic  $[\text{}^4\text{He}]$  (up to  $0.4\text{ cm}^3\text{ STP/L}$ ) and associated increases in  $[\text{}^4\text{He}]$ ,  $[\text{CH}_4]$ ,  $[\text{Ba}]$ , and  $[\text{Cl}]$

indicate an exogenous origin for hydrocarbon gas and salt-rich components in modern UD aquifers of the NAB. The geochemistry of the methane-rich groundwater (elevated  $^4\text{He}/\text{CH}_4$ ,  $^{20}\text{Ne}/^{36}\text{Ar}$ ,  $\delta^{13}\text{C}-\text{CH}_4$ , Cl) combined with numerical modeling suggests that natural gases in UD aquifers are the product of three sequential stages of fluid migration and post-genetic alteration during: (1) primary migration out of Marcellus source rocks by the advection of a two-phase fluid leading to an initial stage of fractionation; (2) secondary migration and emplacement of Middle-Devonian natural gases into conventional structural or stratigraphic traps in the Brallier, Lock Haven, and Catskill Formations; and finally (3) tertiary migration in which natural gases diffuse from previously competent UD structural or stratigraphic traps or healed fractures into shallow UD aquifers and equilibrate with meteoric groundwater. These first two stages likely relate to episodic crustal fluid migration associated with burial resulting from the Alleghanian Orogeny, while the third mechanism likely continues today. This model contrasts with previous hypotheses (Prinzhofer and Huc, 1995; Prinzhofer and Pernaton, 1997) for hydrocarbon fractionation by molecular diffusion (i.e., diffusional migration) alone. Instead, our results suggest that post-genetic modification during the advection of a two-phase fluid contributes to the observed differential depletion of  $\text{C}_2/\text{C}_1$ , and elevated  $^{20}\text{Ne}/^{36}\text{Ar}$ . Future research should work to improve our understanding of the timing and pathways of each stage of fluid migration.

The integration of noble gas data with hydrocarbon chemistry of shallow groundwaters in the NAB suggests that a previously termed “subsurface microbial” component may also encompass a subset of thermogenic methane that has experienced significant post-genetic modification during crustal fluid migration. We propose that adding independent verification of the potential alteration by post-genetic modification (i.e., exogenous  $^4\text{He}$ ,  $^4\text{He}/\text{CH}_4$ ,  $^4\text{He}/^{20}\text{Ne}$ , and  $^{20}\text{Ne}/^{36}\text{Ar}$ ) can differentiate these two subsets. Finally, these results suggest that the use of hydrocarbon molecular composition and stable isotopes as indicators for tracing the source of gases in groundwater (e.g., investigations of suspected stray gas incidents) can benefit from being paired with noble gas elemental and isotopic data including [ $^4\text{He}$ ],  $^4\text{He}/\text{CH}_4$ ,  $^{20}\text{Ne}/^{36}\text{Ar}$ , etc.

#### ACKNOWLEDGEMENTS

We acknowledge financial support from NSF EAGER (EAR-1249255), NSF SusChem (EAR-1441497), the Nicholas School of the Environment (NSOE) and from Fred and Alice Stanback to the NSOE. We thank Robyn E. Hannigan (UMass Boston), Frank Schwartz (OSU), Gautam Mitra (U. Rochester), and Ron Perkins (Duke) for stimulating discussions on the geology and geochemistry of the northern Appalachian Basin. We thank Dr. Karlis Muehlenbachs (U. Alberta) and Dr. Michael A. Lebo for a constructive review of earlier versions of this manuscript. We thank Amanda Carey (U. Rochester), Jon Karr (Duke), Gary Dwyer (Duke), Alissa White (Duke), William K. Eymold (OSU) for their assistance in sample collection and analysis.

#### REFERENCES

- Aeschbach-Heritg W., Peeters F., Beyerle U. and Kipfer R. (1999) Interpretation of dissolved atmospheric noble gases in natural waters. *Water Resour. Res.* **35**, 2779–2792.
- Aeschbach-Hertig W., El-Gamal H., Wieser M. and Palcsu L. (2008) Modeling excess air and degassing in groundwater by equilibrium partitioning with a gas phase. *Water Resour. Res.* **44**, W08449.
- Allen P. A. and Allen J. R. (1990) *Basin Analysis: Principles and Applications*. Blackwell Science Ltd, Oxford, UK.
- Baldassare F. (2011) *The Origin of Some Natural Gases in Permian through Devonian Age Systems in the Appalachian Basin and the Relationship to Incidents of Stray Gas Migration, Technical Workshops for Hydraulic Fracturing Studies*. US EPA, Washington, DC.
- Baldassare F. J., McCaffrey M. and Harper J. (2012) *A geochemical context for stray gas investigations in the N.*
- Baldassare F. J., McCaffrey M. A. and Harper J. A. (2014) A geochemical context for stray gas investigations in the northern Appalachian Basin: Implications of analyses of natural gases from Neogene-through Devonian-age strata. *AAPG Bull.* **98**, 341–372.
- Ballentine C. J. and O’Nions R. K. (1994) The use of He, Ne, and Ar isotopes to study hydrocarbon related fluid provenance, migration, mass balance in sedimentary basins. In *Geofluids: Origin, Migration, and Mass Balance in Sedimentary Basins*, vol. 78 (ed. J. Parnell), pp. 347–361.
- Ballentine C. J. and Hall C. M. (1999) Determining paleotemperature and other variables by using an error-weighted, nonlinear inversion of noble gas concentrations in water. *Geochim. Cosmochim. Acta* **63**, 2315–2336.
- Ballentine C. J. and Burgess R. (2002) Production, release and transport of noble gases in the continental crust. In *Noble Gases in Geochemistry and Cosmochemistry* (eds. D. Porcelli, C. J. Ballentine and R. Wieler), pp. 481–538.
- Ballentine C. J. and Sherwood Lollar B. (2002) Regional groundwater focusing of nitrogen and noble gases into the Hugoton-Panhandle giant gas field, USA. *Geochim. Cosmochim. Acta* **66**, 2483–2497.
- Ballentine C. J., Onions R. K., Oxburgh E. R., Horvath F. and Deak J. (1991) Rare-gas constraints on hydrocarbon accumulation, crustal degassing, and groundwater-flow in the Pannonian Basin. *Earth Planet. Sci. Lett.* **105**, 229–246.
- Ballentine C. J., Burgess R. and Marty B. (2002) Tracing fluid origin, transport and interaction in the crust. In *Noble Gases in Geochemistry and Cosmochemistry* (eds. D. Porcelli, C. J. Ballentine and R. Wieler), pp. 539–614.
- Bernard B. B. (1978) *Light Hydrocarbons in Marine Sediments*. Texas A&M University, College Station, TX.
- Bethke C. M. and Marshak S. (1990) Brine migrations across North America – the plate-tectonics of groundwater. *Annu. Rev. Earth Planet. Sci.* **18**, 287–315.
- Blackmer G. C., Omar G. I. and Gold D. P. (1994) Post-Alleghanian unroofing history of the Appalachian Basin, Pennsylvania, from apatite fission-track analysis and thermal models. *Tectonics* **13**, 1259–1276.
- Bofinger V. M. and Compston W. (1967) A reassessment of age of Hamilton Group in New York and Pennsylvania and role of inherited radiogenic Sr-87. *Geochim. Cosmochim. Acta* **31**, 2353–2357.
- Burruss R. C. and Laughrey C. D. (2010) Carbon and hydrogen isotopic reversals in deep basin gas: evidence for limits to the stability of hydrocarbons. *Org. Geochem.* **41**, 1285–1296.

- Castro M. C., Ma L. and Hall C. M. (2009) A primordial, solar He–Ne signature in crustal fluids of a stable continental region. *Earth Planet. Sci. Lett.* **279**, 174–184.
- Cathles L. M. (1990) Scales and effects of fluid-flow in the upper crust. *Science* **248**, 323–329.
- Clayton C. (1991) Carbon isotope fractionation during natural gas generation from kerogen. *Mar. Pet. Geol.* **8**, 232–240.
- Craig H. (1953) The geochemistry of the stable carbon isotopes. *Geochim. Cosmochim. Acta* **3**, 53–92.
- Craig H. (1968) Isotope separation by carrier diffusion. *Science* **159**, 93–96.
- Craig H., Lupton J. E. and Horibe Y. (1978) A mantle component in circum Pacific volcanic glasses: Hakone, the Marianas, and Mt. Lassen. In *Terrestrial Rare Gases* (eds. E. C. Alexander and M. Ozima). Japan Science Societies Press, Tokyo, Japan.
- Crossey L. J., Karlstrom K. E., Springer A. E., Newell D., Hilton D. R. and Fischer T. (2009) Degassing of mantle-derived CO<sub>2</sub> and He from springs in the southern Colorado Plateau region–neotectonic connections and implications for groundwater systems. *Geol. Soc. Am. Bull.* **121**, 1034–1053.
- Cuoco E., Tedesco D., Poreda R. J., Williams J. C., De Francesco S., Balagizi C. and Darrah T. H. (2013) Impact of volcanic plume emissions on rain water chemistry during the January 2010 Nyamuragira eruptive event: implications for essential potable water resources. *J. Hazard. Mater.* **244**, 570–581.
- Darrah T. H. and Poreda R. J. (2012) Evaluating the accretion of meteoritic debris and interplanetary dust particles in the GPC-3 sediment core using noble gas and mineralogical tracers. *Geochim. Cosmochim. Acta* **84**, 329–352.
- Darrah T. H., Prutsman-Pfeiffer J. J., Poreda R. J., Campbell M. E., Hauschka P. V. and Hannigan R. E. (2009) Incorporation of excess gadolinium into human bone from medical contrast agents. *Metallomics* **1**, 479–488.
- Darrah T. H., Tedesco D., Tassi F., Vaselli O., Cuoco E. and Poreda R. J. (2013) Gas chemistry of the Dallol region of the Danakil depression in the Afar region of the northern-most East African Rift. *Chem. Geol.* **339**, 16–29.
- Darrah T. H., Vengosh A., Jackson R. B., Warner N. R. and Poreda R. J. (2014) Noble gases identify the mechanisms of fugitive gas contamination in drinking-water wells overlying the Marcellus and Barnett Shales. *Proc. Natl. Acad. Sci. U.S.A.* **111**, 14076–14081.
- Darrah T. H., Jackson R. B., Vengosh A., Warner N. R. and Poreda R. J. (2015) Noble gases: a new technique for fugitive gas investigation in groundwater. *Groundwater* **53**, 23–28.
- Davis D. M. and Engelder T. (1985) The role of salt in fold-and-thrust belts. *Tectonophysics* **119**, 67–88.
- Drollette B. D., Hoelzer K., Warner N. R., Darrah T. H., Karatum O., O'Connor M. P., Nelson R. K., Fernandez L. A., Reddy C. M., Vengosh A., Jackson R. B., Elsner M. and Plata D. R. (2015) Elevated levels of diesel-range organic compounds in groundwater near Marcellus gas operations are derived from surface activities. *Proc. Natl. Acad. Sci. U.S.A.*, [www.pnas.org/cgi/doi/10.1073/pnas.1511474112](http://www.pnas.org/cgi/doi/10.1073/pnas.1511474112).
- Dubacq B., Bickle M. J., Wigley M., Kampman N., Ballentine C. J. and Sherwood Lollar B. (2012) Noble gas and carbon isotopic evidence for CO<sub>2</sub>-driven silicate dissolution in a recent natural CO<sub>2</sub> field. *Earth Planet. Sci. Lett.* **341**, 10–19.
- Eisenlohr B. N., Tompkins L. A., Cathles L. M., Barley M. E. and Groves D. I. (1994) Mississippi valley-type deposits – products of brine expulsion by eustatically induced hydrocarbon generation – an example from northwestern Australia. *Geology* **22**, 315–318.
- Engelder T. (2008) Structural geology of the Marcellus and other Devonian gas shales: geological conundrums involving joints, layer-parallel shortening strain, and the contemporary tectonic stress field. In *AAPG-SEG Eastern Section Meeting Field Trip Guide. AAPG-SEG Eastern Section Meeting* (ed. AAPG).
- Engelder T. (2012) Capillary tension and imbibition sequester frack fluid in Marcellus gas shale. *Proc. Natl. Acad. Sci. U.S.A.* **109**, E3625.
- Engelder T. and Whitaker A. (2006) Early jointing in coal and black shale: evidence for an Appalachian-wide stress field as a prelude to the Alleghanian orogeny. *Geology* **34**, 581–584.
- Engelder T., Lash G. G. and Uzcategui R. S. (2009) Joint sets that enhance production from Middle and Upper Devonian gas shales of the Appalachian Basin. *AAPG Bull.* **93**, 857–889.
- Evans M. A. (1995) Fluid inclusions in veins from the Middle Devonian shales – a record of deformation conditions and fluid evolution in the Appalachian Plateau. *Geol. Soc. Am. Bull.* **107**, 327–339.
- Fail R. T. (1997a) A geologic history of the north-central Appalachians. 1. Orogenesis from the mesoproterozoic through the taconic orogeny. *Am. J. Sci.* **297**, 551–619.
- Fail R. T. (1997b) A geologic history of the north-central Appalachians. 2. The Appalachian basin from the Silurian through the Carboniferous. *Am. J. Sci.* **297**, 729–761.
- Farley K. A. and Poreda R. J. (1993) Mantle neon and atmospheric contamination. *Earth Planet. Sci. Lett.* **114**, 325–339.
- Frey M. G. (1973) Influence of Salina salt on structure in New York-Pennsylvania part of the Appalachian Plateau. *Am. Assoc. Pet. Geol. Bull.* **57**, 1027–1037.
- Fuex A. N. (1980) Experimental evidence against an appreciable isotopic fractionation of methane during migration. *Phys. Chem. Earth* **12**, 725–732.
- Gilfillan S. M., Ballentine C. J., Holland G., Blagburn D., Sherwood Lollar B., Stevens S., Schoell M. and Cassidy M. (2008) The noble gas geochemistry of natural CO<sub>2</sub> gas reservoirs from the Colorado Plateau and Rocky Mountain provinces, USA. *Geochim. Cosmochim. Acta* **72**, 1174–1198.
- Gilfillan S. M. V., Sherwood Lollar B., Holland G., Blagburn D., Stevens S., Schoell M., Cassidy M., Ding Z. J., Zhou Z., Lacrampe-Couloume G. and Ballentine C. J. (2009) Solubility trapping in formation water as dominant CO<sub>2</sub> sink in natural gas fields. *Nature* **458**, 614–618.
- Heaton T. H. E. and Vogel J. C. (1981) Excess air in groundwater. *J. Hydrol.* **50**, 201–216.
- Heilweil V. M., Grieve P. L., Hynek S. A., Brantley S. L., Solomon D. K. and Risser D. W. (2015) Stream measurements locate thermogenic methane fluxes in groundwater discharge in an area of shale-gas development. *Environ. Sci. Technol.* **49**, 4057–4065.
- Hilton D. R. (1996) The helium and carbon isotope systematics of a continental geothermal system: results from monitoring studies at Long Valley caldera (California, U.S.A.). *Chem. Geol.* **127**, 269–295.
- Holland G., Sherwood Lollar B., Li L., Lacrampe-Couloume G., Slater G. F. and Ballentine C. J. (2013) Deep fracture fluids isolated in the crust since the Precambrian era. *Nature* **497**, 357.
- Holocher J., Peeters F., Aeschbach-Hertig W., Hofer M., Brennwald M., Kinzelbach W. and Kipfer R. (2002) Experimental investigations of the formation of excess air in quasi-saturated porous media. *Geochim. Cosmochim. Acta* **66**, 4103–4117.
- Holocher J., Peeters F., Aeschbach-Hertig W., Kinzelbach W. and Kipfer R. (2003) Kinetic model of gas bubble dissolution in groundwater and its implications for the dissolved gas composition. *Environ. Sci. Technol.* **37**, 1337–1343.
- Hunt A. G. (2000) *Diffusion a Release of Helium-4 from Mineral Phases as Indicators of Groundwater Age and Depositional History*. Dept. of Earth and Environmental Sciences, University of Rochester, Rochester, NY, USA.

- Hunt A. G., Darrah T. H. and Poreda R. J. (2012) Determining the source and genetic fingerprint of natural gases using noble gas geochemistry: a northern Appalachian Basin case study. *AAPG Bull.* **96**, 1785–1811.
- Isotech (2011) *Collection of Groundwater Samples from Domestic and Municipal Water Wells for Dissolved Gas Analysis*. Isotech Laboratories, Champaign, IL.
- Jackson R. B., Vengosh A., Darrah T. H., Warner N. R., Down A., Poreda R. J., Osborn S. G., Zhao K. and Karr J. D. (2013) Increased stray gas abundance in a subset of drinking water wells near Marcellus shale gas extraction. *Proc. Natl. Acad. Sci. U.S.A.* **110**, 11250–11255.
- Jenden P. D., Drazan D. J. and Kaplan I. R. (1993) Mixing of thermogenic natural gases in the Northern Appalachian Basin. *AAPG Bull.* **77**, 980–998.
- Karlstrom K. E., Crossey L. J., Hilton D. R. and Barry P. H. (2013) Mantle He-3 and CO<sub>2</sub> degassing in carbonic and geothermal springs of Colorado and implications for neotectonics of the Rocky Mountains. *Geology* **41**, 495–498.
- Kerr R. A. (2010) Natural gas from shale bursts onto the scene. *Science* **328**, 1624–1626.
- Kessler J. D., Reeburgh W. S. and Tyler S. C. (2006) Controls on methane concentration and stable isotope ( $\delta^2\text{H-CH}_4$  and  $\delta^{13}\text{C-CH}_4$ ) distributions in the water columns of the Black Sea and Cariaco Basin. *Global Biogeochem. Cycles* **20**.
- Kravchenko J., Darrah T. H., Miller R. K., Lysterly H. M. and Vengosh A. (2014) A review of the health impacts of barium from natural and anthropogenic exposure. *Environ. Geochem. Hlth.* **36**, 797–814.
- Lash G. G. and Engelder T. (2009) Tracking the burial and tectonic history of Devonian shale of the Appalachian Basin by analysis of joint intersection style. *Geol. Soc. Am. Bull.* **121**, 265–277.
- Lash G. G. and Engelder T. (2011) Thickness trends and sequence stratigraphy of the Middle Devonian Marcellus Formation, Appalachian Basin: implications for Acadian foreland basin evolution. *AAPG Bull.* **95**, 61–103.
- Lash G., Loewy S. and Engelder T. (2004) Preferential jointing of Upper Devonian black shale, Appalachian Plateau, USA: evidence supporting hydrocarbon generation as a joint-driving mechanism. *Geol. Soc. Lond.* **231**, 129–151.
- Laughrey C. D. and Baldassare F. J. (1998) Geochemistry and origin of some natural gases in the Plateau province, central Appalachian basin, Pennsylvania and Ohio. *AAPG Bull.* **82**, 317–335.
- Lerche I., Yu Z., Tgorudbakken B. and Thomsent R. O. (1997) Ice loading effects in sedimentary basins with reference to the Barents Sea. *Mar. Pet. Geol.* **14**, 227–338.
- Llewellyn G. T. (2014) Evidence and mechanisms for Appalachian Basin brine migration into shallow aquifers in NE Pennsylvania, U.S.A. *Hydrogeol. J.* **22**, 1055–1066.
- Llewellyn G. T., Dorman F., Westland J. L., Yoxtheimer D., Grieve P., Sowers T., Humston-Fulmer E. and Brantley S. L. (2015) Evaluating a groundwater supply contamination incident due to Marcellus Shale gas development. *Proc. Natl. Acad. Sci. U.S.A.* **112**(20), 6325–6330.
- Lohman S. W. (1937) *Groundwater in northeastern Pennsylvania*, 312.
- Lohman S. W. (1939) *Groundwater in northcentral Pennsylvania*, 219.
- Lorant F., Prinzhofer A., Behar F. and Huc A. Y. (1998) Carbon isotopic and molecular constraints on the formation and the expulsion of thermogenic hydrocarbon gases. *Chem. Geol.* **147**, 249–264.
- Ma L., Castro M. C., Hall C. M. and Walter L. M. (2005) Cross-formational flow and salinity sources inferred from a combined study of helium concentrations, isotopic ratios, and major elements in the Marshall aquifer, southern Michigan. *Geochem. Geophys. Geosyst.* **6**.
- Ma L., Castro M. C. and Hall C. M. (2009a) Atmospheric noble gas signatures in deep Michigan Basin brines as indicators of a past thermal event. *Earth Planet. Sci. Lett.* **277**, 137–147.
- Ma L., Castro M. C. and Hall C. M. (2009b) Crustal noble gases in deep brines as natural tracers of vertical transport processes in the Michigan Basin. *Geochem. Geophys. Geosyst.* **10**.
- Milici R. C. and Witt W. D. (1988) The Appalachian Basin. In *The Geology of North America, Denver, CO* (ed. G. S. o. America), pp. 427–469.
- Milkov A. V. (2011) Worldwide distribution and significance of secondary microbial methane formed during petroleum biodegradation in conventional reservoirs. *Org. Geochem.* **42**, 184–207.
- Molofsky L. J., Connor J. A., Farhat S. K., Wylie A. S. and Wagner T. (2011) Methane in Pennsylvania water wells unrelated to Marcellus shale fracturing. *Oil Gas J.* **109**, 54–59.
- Molofsky L. J., Connor J. A., Wylie A. S., Wagner T. and Farhat S. K. (2013) Evaluation of methane sources in groundwater in northeastern Pennsylvania. *Groundwater* **51**, 333–349.
- Oliver J. (1986) Fluids expelled tectonically from orogenic belts – their role in hydrocarbon migration and other geologic phenomena. *Geology* **14**, 99–102.
- Osborn S. G. and McIntosh J. C. (2010) Chemical and isotopic tracers of the contribution of microbial gas in Devonian organic-rich shales and reservoir sandstones, northern Appalachian Basin. *Appl. Geochem.* **25**, 456–471.
- Osborn S. G., Vengosh A., Warner N. R. and Jackson R. B. (2011) Methane contamination of drinking water accompanying gas-well drilling and hydraulic fracturing. *Proc. Natl. Acad. Sci. U.S.A.* **108**, 8172–8176.
- Oxburgh E. R., O’Nions R. K. and Hill R. I. (1986) Helium isotopes in sedimentary basins. *Nature* **324**, 632–635.
- Pape T., Bahr A., Rethemeyer J., Kessler J. D., Sahling H., Hinrichs K. U., Klapp S. A., Reeburgh W. S. and Bohrmann G. (2010) Molecular and isotopic partitioning of low-molecular-weight hydrocarbons during migration and gas hydrate precipitation in deposits of a high-flux seepage site. *Chem. Geol.* **269**, 350–363.
- Pernaton E., Prinzhofer A. and Schneider F. (1996) Reconsideration of methane isotope signature as a criterion for the genesis of natural gas – influence of migration on isotopic signatures. *Revue De L Institut Francais Du Petrole* **51**, 635–651.
- Poreda R. J. and Craig H. (1992) He and Sr isotopes in the Lau Basin Mantle – depleted and primitive mantle components. *Earth Planet. Sci. Lett.* **113**, 487–493.
- Poreda R. J., Jenden P. D., Kaplan I. R. and Craig H. (1986) Mantle helium in Sacramento Basin natural-gas wells. *Geochim. Cosmochim. Acta* **50**, 2847–2853.
- Prinzhofer A. A. and Huc A. Y. (1995) Genetic and post-genetic molecular and isotopic fractionations in natural gases. *Chem. Geol.* **126**, 281–290.
- Prinzhofer A. and Pernaton E. (1997) Isotopically light methane in natural gas: bacterial imprint or diffusive fractionation? *Chem. Geol.* **142**, 193–200.
- Rast N. (1989) The evolution of the Appalachian chain. In *The Geology of North America – An overview* (eds. A. W. Bally and A. R. Palmer). Geological Society of America, pp. 347–358.
- Revez K. M., Breen K. J., Baldassare A. J. and Burruss R. C. (2010) Carbon and hydrogen isotopic evidence for the origin of combustible gases in water-supply wells in north-central Pennsylvania. *Appl. Geochem.* **25**, 1845–1859.
- Rice D. D. and Claypool G. E. (1981) Generation, accumulation, and resource potential of biogenic gas. *AAPG Bull.* **65**, 5–25.

- Ryder R. T., Aggen K. L., Hettinger R. D., Law B. E., Miller J. J., Nuccio V. F., Perry W. J., Prensky S. E., SanFilipo J. R. and Wandry C. J. (1996) Possible continuous-type (unconventional) gas accumulation in the Lower Silurian “Clinton” sands, Medina Group, and Tuscarora Sandstone in the Appalachian basin: a progress report of 1995 activities. *United States Geological Survey USGS Open-File Report*, 96–42.
- Saar M. O., Castro M. C., Hall C. M., Manga M. and Rose T. P. (2005) Quantifying magmatic, crustal, and atmospheric helium contributions to volcanic aquifers using all stable noble gases: implications for magmatism and groundwater flow. *Geochem. Geophys. Geosyst.* **6**, 1–18.
- Sak P. B., McQuarrie N., Oliver B. P., Lavdovsky N. and Jackson M. S. (2012) Unraveling the central Appalachian fold-thrust belt, Pennsylvania: the power of sequentially restored balanced cross sections for a blind fold-thrust belt. *Geosphere* **8**, 685–702.
- Scanlin M. A. and Engelder T. (2003) The basement versus the no-basement hypotheses for folding within the Appalachian plateau detachment sheet. *Am. J. Sci.* **303**, 519–563.
- Schlegel M. E., Zhou Z., McIntosh J. C., Ballentine C. J. and Person M. A. (2011) Constraining the timing of microbial methane generation in an organic-rich shale using noble gases, Illinois Basin, USA. *Chem. Geol.* **287**, 27–40.
- Schoell M. (1980) The hydrogen and carbon isotopic composition of methane from natural gases of various origins. *Geochim. Cosmochim. Acta* **44**, 649–661.
- Schoell M. (1983) Genetic characterization of natural gases. *AAPG Bull.* **67**, 2225–2238.
- Schoell M. (1988) Multiple origins of methane in the earth. *Chem. Geol.* **71**, 1–10.
- Selley R. C. (1998) *Elements of Petroleum Geology*. Academic Press, London, UK.
- Sheldon A. L., Solomon D. K., Poreda R. J. and Hunt A. (2003) Radiogenic helium in shallow groundwater within a clay till, southwestern Ontario. *Water Resour. Res.* **39**.
- Sherwood Lollar B. and Ballentine C. J. (2009) Insights into deep carbon derived from noble gases. *Nat. Geosci.* **2**, 543–547.
- Sherwood Lollar B., Onions R. K. and Ballentine C. J. (1994) Helium and neon isotope systematics in carbon dioxide-rich and hydrocarbon-rich gas reservoirs. *Geochim. Cosmochim. Acta* **58**, 5279–5290.
- Siegel D. I., Azzolina N. A., Smith B. J., Perry A. E. and Bothun R. L. (2015) Methane concentrations in water wells unrelated to proximity to existing oil and gas wells in northeastern Pennsylvania. *Environ. Sci. Technol.* **49**, 4106–4112.
- Smith S. P. and Kennedy B. M. (1982) The solubility of noble gases in water and in NaCl brine. *Geochim. Cosmochim. Acta* **47**, 503–515.
- Solomon D. K., Poreda R. J., Schiff S. L. and Cherry J. A. (1992) Tritium and He-3 as groundwater age tracers in the Borden aquifer. *Water Resour. Res.* **28**, 741–755.
- Solomon D. K., Poreda R. J., Cook P. G. and Hunt A. (1995) Site characterization using H-3/He-3 groundwater ages, Cape Cod, MA. *Ground Water* **33**, 988–996.
- Solomon D. K., Hunt A. and Poreda R. J. (1996) Source of radiogenic He-4 in shallow aquifers: implications for dating young groundwater. *Water Resour. Res.* **32**, 1805–1813.
- Stolper D. A., Lawson M., Davis C. L., Ferreira A. A., Santos Neto E. V., Ellis G. S., Lewan M. P., Martini A. M., Tang Y., Schoell M., Sessions A. L. and Eiler J. M. (2014) Formation temperature of thermogenic and biogenic methane. *Science* **344** (6181), 1500–1503.
- Stolper D. A., Martini A. M., Clog M., Douglas P. M., Shusta S. S., Valentine D. L., Sessions A. L. and Eiler J. M. (2015) Distinguishing and understanding thermogenic and biogenic sources of methane using multiply substituted isotopologues. *Geochim. Cosmochim. Acta* **161**, 219–247.
- Straeten C. A. V., Brett C. E. and Sageman B. B. (2011) Mudrock sequence stratigraphy: a multi-proxy (sedimentological, paleobiological and geochemical) approach, Devonian Appalachian Basin. *Palaeogeogr. Palaeoclimatol. Palaeoecol.* **304**, 54–73.
- Taylor L. (1984) *Groundwater Resources of the Upper Susquehanna River Basin, Pennsylvania: Water Resources Report 58 Pennsylvania Department of Environmental Resources-Office of Parks and Forestry – Bureau of Topographic and Geologic Survey*, p. 136.
- Taylor S. R. and McLennan S. M. (1995) The geochemical evolution of the continental crust. *Rev. Geophys.* **33**, 241–265.
- Tour J. M., Kittrell C. and Colvin V. L. (2010) Green carbon as a bridge to renewable energy. *Nat. Mater.* **9**, 871–874.
- USGS (2011) *National Field Manual for the Collection of Water-Quality Data*. U.G. Survey, Washington, DC.
- Vengosh A., Jackson R. B., Warner N., Darrah T. H., Kondash A., Gibbs A. and Gibbs B. (2014) A critical review of the risks to water resources from unconventional shale gas development and hydraulic fracturing in the United States. *Environ. Sci. Technol.* **48**, 8334–8348.
- Vidic R. D., Brantley S. L., Vandenbossche J. M., Yoxheimer D. and Abad J. D. (2013) Impact of shale gas development on regional water quality. *Science* **340**.
- Warner N. R., Jackson R. B., Darrah T. H., Osborn S. G., Down A., Zhao K. G., White A. and Vengosh A. (2012) Geochemical evidence for possible natural migration of Marcellus Formation brine to shallow aquifers in Pennsylvania. *Proc. Natl. Acad. Sci. U.S.A.* **109**, 11961–11966.
- Warner N. R., Darrah T. H., Jackson R. B., Millot R., Kloppman W. and Vengosh A. (2014) New tracers identify hydraulic fracturing fluids and accidental releases from oil and gas operations. *Environ. Sci. Technol.* <http://dx.doi.org/10.1021/es5032135>.
- Weiss R. (1971a) Effect of salinity on the solubility of argon in water and seawater. *Deep-Sea Res.* **17**, 721.
- Weiss R. (1971b) Solubility of helium and neon in water and seawater. *J. Chem. Eng. Data* **16**, 235.
- Whiticar M. J., Faber E. and Schoell M. (1985) Hydrogen and carbon isotopes of C-1 to C-5 alkanes in natural gases. *AAPG Bull.* **69**, 316.
- Whiticar M. J., Faber E. and Schoell M. (1986) Biogenic methane formation in marine and fresh-water environments – CO<sub>2</sub> reduction vs acetate fermentation isotope evidence. *Geochim. Cosmochim. Acta* **50**, 693–709.
- Williams J. H. (2010) *Evaluation of Well Logs for Determining the Presence of Freshwater, Saltwater, and Gas above the Marcellus Shale in Chemung, Tioga, and Broome Counties, New York*. USGS Scientific Investigations Report, 5224.
- Williams J. H., Taylor L. E. and Low D. J. (1998) *Hydrogeology and groundwater quality of the glaciated valleys of Bradford, Tioga, and Potter Counties, Pennsylvania*, 68.
- Xia X. Y. and Tang Y. C. (2012) Isotope fractionation of methane during natural gas flow with coupled diffusion and adsorption/desorption. *Geochim. Cosmochim. Acta* **77**, 489–503.
- Zhou Z. and Ballentine C. J. (2006) He-4 dating of groundwater associated with hydrocarbon reservoirs. *Chem. Geol.* **226**, 309–327.
- Zhou Z., Ballentine C. J., Schoell M. and Stevens S. H. (2012) Identifying and quantifying natural CO<sub>2</sub> sequestration processes over geological timescales: the Jackson Dome CO<sub>2</sub> deposit, USA. *Geochim. Cosmochim. Acta* **86**, 257–275.